UNIVERSITÀ DI PISA

University of Pisa
Faculty of Engineering

Corso di Laurea Magistrale in Ingegneria Aerospaziale

Limit Cycle Analysis for Spacecraft with Pulsed Thrusters

Supervisor:

Prof. Giovanni Mengali

Candidate:

Alessandro Cattabiani

Academic Year 2011/2012

A Nino, per ieri
A Cinzia, per oggi

Abstract

Throughout the last decades, attitude control systems with switching actuators and discrete sensors have been used in satellites subjected to slowly varying disturbances. Sun sensors are usually employed. Such sensors are discrete and, typically, slower than actuators. Several types of on-off thrusters are employed as actuators, such as hydrazine, cold-gas and pulse plasma thrusters. These thrusters are typically affected by switching constraints. Due to these constraints and the disturbances, the system shall operate in limit cycle conditions. Two types of limit cycles can occur:

- *Saturation limit cycles.*
- *Disturbance limit cycles.*

Our purpose is the development of a controller design method which avoids *saturation limit cycles* - that are very expensive in terms of fuel consumption - and produces a *disturbance limit cycle* which meets amplitude and bandwidth requirements. A reference scenario will be presented and simulations will be performed to test potential outcomes.

The first part of the thesis will study the methods used to predict limit cycles. Particular emphasis will be given to the *classical describing function* theory. After that, we will develop the new *dual-input describing function* theory which can deal with slowly varying disturbances. In order to address strange behaviors the *classical Tsypkin method* will be presented and the *hybrid Tsypkin-dual-input describing function* method, which takes into account disturbances, will be applied to our case.

In the second part, we will focus on the design methods of the controller. The *Kharitonov approach*, which is robust and uses the *classical describing function* theory, will be studied in detail. In the end we will introduce the new *dual-input Kharitonov approach*, developed by using the *dual-input describing function* theory and capable of dealing with slowly varying disturbances.

Sommario

Negli ultimi decenni é aumentato l'impiego di attuatori nonlineari on-off nel controllo dell'assetto dei satelliti soggetti a disturbi lentamente variabili. Per determinare l'assetto del satellite sono solitamente usati sensori solari. Le frequenze a cui operano questi rilevatori sono tipicamente inferiori alle frequenze a cui operano gli attuatori. Tali attuatori sono di norma razzi ad idrazina, a gas freddo o a plasma pulsante. Il problema presentato dall'utilizzo di questi attuatori é legato alle limitazioni concernenti la spinta generata e la frequenza a cui essi possono operare. A causa della nonlinearitá degli attuatori e dei disturbi questi sistemi operano tipicamente in condizioni di ciclo limite. Questi sistemi possono presentare due tipi di cicli limite:

- *Saturation limit cycles.*
- *Disturbance limit cycles.*

Scopo di questa tesi é lo sviluppo di un algoritmo per la scelta di un controllore che escluda la presenza di *saturation limit cycles*, poiché portano il satellite a consumare molto carburante, e che costringa il sistema ad operare in un ben preciso *disturbance limit cycle*, che soddisfi i requisiti di banda passante e di ampiezza. Per testare i risultati saranno conodotte simulazioni su uno scenario di riferimento.

La prima parte di questa tesi si occuperá dello studio e della determinazione dei cicli limite. Per prima cosa sará presentato lo stato dell'arte con un analisi dei principali pregi e difetti di ogni metodo. Sará studiata in dettaglio la *classical describing function theory* dal momento che sará largamente utilizzata nella seconda parte. Successivamente sará sviluppata la nuova *dual-input describing function theory*, che permette lo studio di sistemi soggetti a disturbi lentamente variabili. Per esaminare alcuni strani comportamenti del sistema sará studiato in dettaglio anche il *classical Tsypkin method* e il suo naturale sviluppo *hybrid Tsypkin-dual-input describing function method*, che é la sua generalizzazione per studiare sistemi soggetti a disturbi.

La seconda parte della tesi si occuperá invece della determinazione vera e propria di un algoritmo per la scelta di un controllore che soddisfi i requisiti

di banda passante e di ampiezza. Come per la prima parte della tesi, sará presentato in primis lo stato dell'arte con un un'analisi dei pregi e dei difetti di ogni algoritmo. Successivamente, sará studiato in dettaglio il *Kharitonov approach*, in particolare, che permette la determinazione di un controllore robusto, utilizza la *classical describing function theory* e tiene conto dei requisiti di ampiezza e banda passante. Partendo dall'analisi di questo metodo ne sará poi sviluppata la generalizzazione per sistemi soggetti a disturbi lentamente variabili, ossia il *dual-input Kharitonov approach.*

Acknowledgments

A Dragoni, senza il quale mi sarei laureato nel doppio del tempo
A Cinzia che ha avuto la pazienza di ascoltarmi quando brancolavo nel buio
A Tatiana e Vomere, amici veri, componenti di un trio che spero non si perda nel tempo
A Marco, compagno di avventure
Ai miei amici e alla mia famiglia per aver creduto in me

Contents

List of Figures

List of Tables

Notation

Symbol	Meaning
$\triangleq$	Definition
$\Leftrightarrow$	If and only if
$\min_{s,x}\{f(s,x,y)\}$	Minimum of the function f over the variables $\{s,x\}$
$\max_{s,x}\{f(s,x,y)\}$	Maximum of the function f over the variables $\{s,x\}$
$\lvert f(s)\rvert$	Absolute value of f
$\lvert f(s)\rvert_{s\to x}$	Operator that substitute the variable s with the variable x in the function $f(s)$
$\lVert H\rVert$	Magnitude of a transfer function
$[a,b)$	Group that contains the segment between a and b. a is included and b is not depending on the parenthesis
$(\cdot)$	Generic variable
j	Imaginary unit
b	Bias of the limit cycle
A	Amplitude of the limit cycle
ω	Frequency of the limit cycle
$\underline{a}$	Generic signal
$\vec{a}$	Generic vector or array
$\dot{\underline{a}}$	Time derivative of the signal $\underline{a}$
H	Generic block, transfer function or matrix
N	Nonlinear block

Symbol	**Meaning**
$N(\cdot)$	Describing function of the nonlinear block
$h_{altitude}$	Average orbit altitude
M	Average total mass
J	Average moment of inertia
Arm	Arm
max_{thrust}	Max thrust of one thruster
τ	Generic delay
τ_{on}	Delay when the actuator is switching on
τ_{off}	Delay when the actuator is switching off
$AOCS$	Sampling frequency of the lead network and the sensor
APE	Absolute pointing error

Chapter 1

Introduction

Throughout the last decades, attitude control systems with switching actuators have been used in satellite and launching systems. Some studies have been performed in: [2], [12], [13], [15]. In the attitude stabilization phase, such systems typically have been operated in limit cycle conditions. As actuators, several types of on-off thrusters are employed, such as hydrazine, cold-gas and pulse plasma thrusters as described in [6]. These thrusters are typically affected by switching constraints, as depicted in [15], which have been a cause of concern about the degradation of the performance of the system. Non-conventional analysis and design problems arise when actuators are subject to switching-time restrictions. Certain conditions ensure that limit cycles exist. When these conditions do not hold, quasi-periodic-like behavior or chaos motion could arise.

Part I

Problem description

Chapter 2

Block diagram

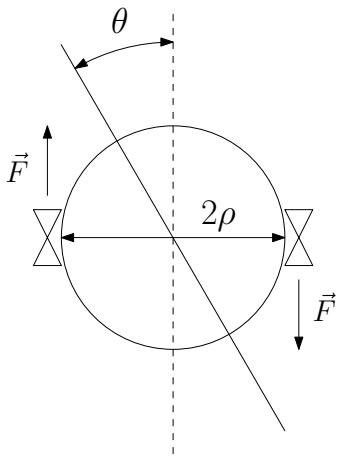

Figure 2.1: Simple rigid body.

Consider a simple rigid body[1] subjected to torque disturbances that should be controlled to achieve appropriate performance requirements. The body attitude $\underline{\theta}$ is controlled using a set of small thrusters which are on-off actuators with switching-time and thrust-restrictions. Figure 2.1 shows a simplified representation of the system. Usually the design requirement is to stabilize, in steady state, the system in a *well shaped* limit cycle that meets accuracy and bandwidth requirements. All the factors above shall be considered and studied during limit cycle analysis and design.

The system can be modeled in a feedback diagram as shown in figure 2.2.

We need to underline that the controller and the sensor are approximated as continuous blocks in this modelization. This assumption shall be checked

[1]E.g. satellite or rocket in the upper atmosphere.

when results are extrapolated. This approximation holds if the bandwidth is at least ten times smaller than the sampling frequencies of the controller and the sensor. Usually the sampling frequency of the controller is of some order of magnitude greater than that of the sensor thus the sampling frequency of the sensor adds a restriction about the closed loop bandwidth.

2.1 Input signals

2.1.1 $\underline{r}$

This is the reference signal. We can set:

$$\underline{r} = 0 \tag{2.1}$$

without loss of generality. The origin of the coordinates is the Earth pointing vector and it is usually the target of the control system. If this would not be the case, a simple rotation of the reference axis can bring the system to the case of equation 2.1. We need to underline that we have implicitly assumed the reference as a constant or a slowly varying signal with respect to the rest of the system.

2.1.2 $\underline{d}$

This is the disturbance signal. The system is intrinsically nonlinear thus it means that the principle of superposition of the effects can not be applied (at least to the modulator block). A structured modelization of the inputs shall be done.

There are four main sources of disturbance for a spacecraft:

- Gravity gradient of the Earth.
- Solar pressure.
- Geomagnetic field.
- Aerodynamic drag.

Gravity gradient of the Earth

Every non-symmetrical object of finite dimensions in orbit is subject to a gravitational torque because of the variation in the Earth's gravitational force over the object. This gravity-gradient torque results from the inverse square

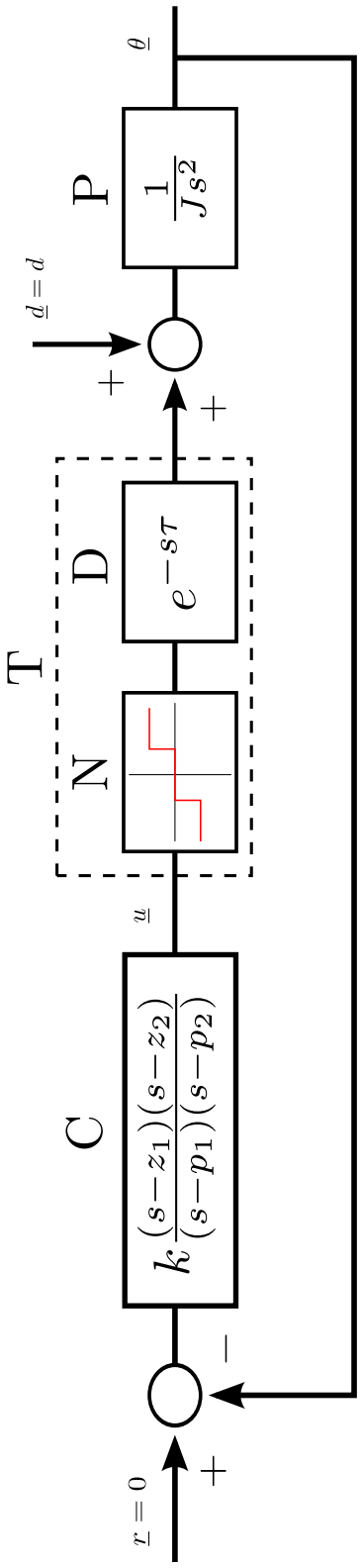

Figure 2.2: Block diagram of the controlled system.

gravitational force field; there would be no gravitational torque in a uniform gravitational field. The following equation is valid:

$$d_{gg} \propto \frac{1}{r^3} \tag{2.2}$$

where:

- d_{gg} is the disturbance produced by the gravity gradient.
- r is the distance between the center of mass of the Earth and of the spacecraft.

The general reference scenario is a linear combination of two opposite cases:

- The spacecraft must be maintained oriented to the Earth. In this case the disturbance is a bias.
- The spacecraft must be maintained oriented to a fixed point of the celestial sphere. In this case the disturbance is a sine wave[2].

Thus the disturbance could be modelled as:

$$d_{gg} = b'_{gg} + A_{gg} \sin(\omega_{gg} t) \tag{2.3}$$

where:

- b'_{gg} is a constant offset.
- A_{gg} is the amplitude of the sine wave.
- ω_{gg} is an angular frequency. It is strictly related to the orbital period T_{rE}. In the worst case it is:

$$\omega_{gg} \propto \frac{1}{T_{rE}} = 0.01\text{Hz} \tag{2.4}$$

- t is the time.

The frequency of the system is leaded by the sensors and the switching-time restrictions of the actuators. It is:

$$f_s \geq 1\text{Hz}. \tag{2.5}$$

The frequency of the disturbance is at least of two orders of magnitude lower than the frequency of the system. Thus the sine wave could be treated as a bias and the disturbance becomes:

$$d_{gg} = b_{gg} \tag{2.6}$$

where:

[2]E.g. a star.

- b_{gg} is a constant offset that is the sum of the previous bias and the value of the sine wave.

Solar pressure

Radiation incident on a spacecraft's surface produces a force which results in a torque about the spacecraft's center of mass. The surface is subjected to radiation pressure equal to the difference between the incident and reflected momentum flux. Because the solar radiation varies as the inverse square of the distance from the Sun, the solar radiation pressure is essentially altitude independent for spacecraft in Earth orbit. Depending on the geometry of the spacecraft and its attitude with respect to the sun it can produce a disturbance torque d_{sp}. It is strictly related to the attitude target and the exposure of the spacecraft to the sun light during the mission. It can be modelled as:

$$d_{sp} = b'_{sp} + \sum_{i=1}^{n} A_{sp_i} \sin\left(\omega_{sp_i} t\right) \tag{2.7}$$

where:

- b'_{sp} is a bias disturbance.
- n is the appropriate number of sine waves necessary to describe the torque during the mission.
- A_{sp_i} is the amplitude of the generic sine wave.
- ω_{sp_i} is the generic angular frequency. Each one, as the gravity gradient, is strictly related orbital period.

As we did for the gravity gradient disturbance we can approximate disturbance to a bias that is a sum of the sine waves and the bias. This is possible due to the difference of at least two orders of magnitude between the frequency of the control system and the frequencies of the sine waves. Thus the disturbance can be modelled as follows:

$$d_{sp} = b_{sp} \tag{2.8}$$

where:

- b_{sp} is a constant offset that is the sum of the previous bias and the sine waves.

Geomagnetic field

Geomagnetic disturbance torque results from the interaction between the spacecraft's residual magnetic field and the geomagnetic field. The signal shape heavily depends on the orbit of the particular mission and on the attitude target of the mission. Without loss of generality we can write:

$$d_{gf} = b'_{gf} + \sum_{i=1}^{n} A_{gf_i} \sin\left(\omega_{gf_i} t\right) \tag{2.9}$$

where:

- b'_{gf} is a bias disturbance.
- n is the appropriate number of sine waves necessary to describe the torque moment during the mission.
- A_{gf_i} is the amplitude of the generic sine wave.
- ω_{gf_i} is the generic angular frequency. Each one, as the gravity gradient, is proportional to the orbital period.

As we did for the previous disturbances we can approximate the geomagnetic disturbance to a bias that is a sum of the sine waves and the bias. It can be done due to the difference of at least two orders of magnitude between the frequency of the control system and the frequencies of the sine waves. Thus the disturbance can be modelled as follow:

$$d_{gf} = b_{gf} \tag{2.10}$$

where:

- b_{gf} is a constant offset that is the sum of the previous bias and the sine waves.

Aerodynamic drag

The interaction of the upper atmosphere with a satellite's surface produces a torque about its center of mass. For spacecraft below approximately 400km, the aerodynamic torque is the dominant environmental disturbance torque. Following the same line of reasoning of the *gravity gradient disturbance* we can model the aerodynamic drag as:

$$d_{ad} = b'_{ad} + A_{ad} \sin\left(\omega_{ad} t\right) \tag{2.11}$$

where:

- b'_{gg} is a constant offset.
- A_{ad} is the amplitude of the sine wave.
- ω_{ad} is an angular frequency. It is strictly related to the angular frequency of revolution around the Earth.
- t is the time.

The frequency of the disturbance is at least of 2 orders of magnitude lower than the frequency of the system. Thus the sine wave could be treated as a bias and the disturbance became:

$$d_{ad} = b_{ad} \tag{2.12}$$

where:

- b_{ad} is a constant offset that is the sum of the previous bias and the sine wave.

Remarks

Every source of disturbance has been modeled and approximated as a bias due to the difference in the order of magnitude between the sine waves of the disturbances and the frequency of the control system. Usually one of these disturbances is predominant as is shown in figure 2.3. Thus we can simply neglect others and consider it as a simple bias.

2.2 Blocks

2.2.1 The controller C

In order to achieve performance, accuracy and bandwidth requirements a lead-lag network is added to the loop. This choice will be discussed in detail in subsection 5.2.4.

The controller and the sensors are intrinsically discrete but they will be approximated as continuous. Results shall meet the previously described bandwidth requirement. It is introduced by the modelization; if it can not be met, a discrete study shall be performed.

The equation 2.13 shows the transfer function of the lead network controller. The input is the angle $\underline{\theta}$ and the output is the torque commanded $\underline{u}$:

$$C = k\frac{(s - z_1)}{(s - p_1)}\frac{(s - z_2)}{(s - p_2)} \tag{2.13}$$

where:

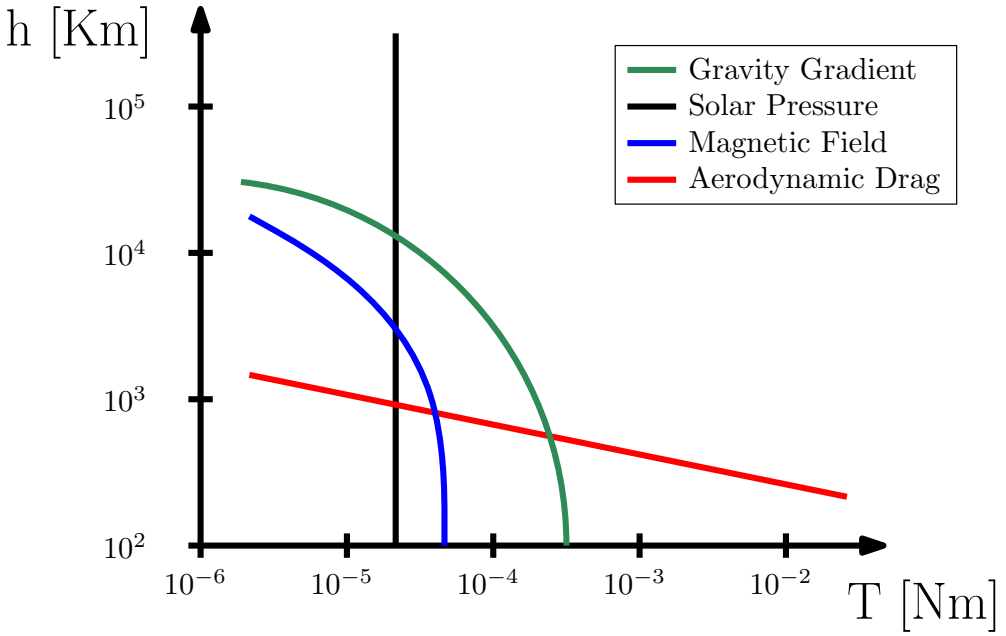

Figure 2.3: Dependency of the magnitude of the disturbances over altitude.

- $k\frac{(s-z_1)}{(s-p_1)}$ is the lead part of the network.
- $\frac{(s-z_2)}{(s-p_2)}$ is the lag part of the network.

By definition, the following set of inequalities is valid:

$$\begin{cases} p_1 < z_1 < 0 & (2.14) \\ z_2 < p_2 < 0. & (2.15) \end{cases}$$

2.2.2 The actuator T

In this block the on-off actuator is modeled. This set of thrusters is intrinsically nonlinear and presents build-up dynamics. These two effects are considered in the modulator block N and in the delay block D.

The modulator N

The modulator block models nonlinearities of the on-off actuators. In particular it takes into account[3]:

[3]The possible hysteresis will be assumed small in respect of the dead zone h, thus, it will be neglected.

- Saturation.
- Dead-zone.

The on-off actuators have switching-time restrictions. As stated in [16], these constraints produce a restriction on the possible limit cycle achievable by the system:

$$f \leq \frac{1}{2\left(\tau_{on} + \tau_{off}\right)}. \tag{2.16}$$

The input is the torque commanded by the controller $\underline{u}$ and the output is the torque provided by the actuators. This block has no transfer function due to the nonlinear behavior; figure 2.4 shows the relation between input and output that describes the block.

- m is the maximum torque given by the actuators.
- h is the dead-zone.

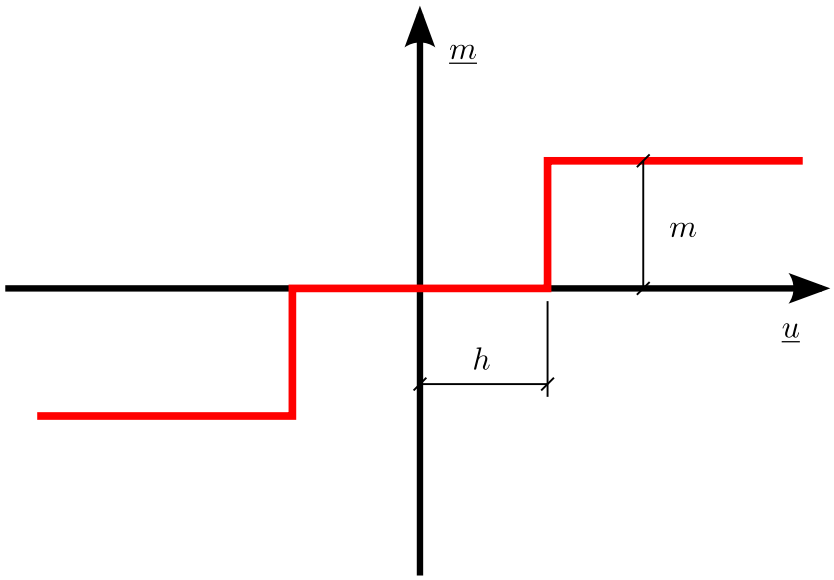

Figure 2.4: Modulator behavior. Input-output relation.

The delay *D*

This block represents the delay generated by the thruster build-up dynamics. The transfer function is:

$$e^{-s\tau} \tag{2.17}$$

where τ is the maximum between the maximum switch-on delay and the maximum switch-off delay.

2.2.3 The plant P

This is the plant block. The attitude is controlled by couples of thrusters. This means that the input of this block is the torque produced by the actuators and the output is the angle $\underline{\theta}$. The transfer function is:

$$P = \frac{1}{Js^2} \tag{2.18}$$

where:

- J is the moment of inertia of the spacecraft.

2.3 The transfer function

In order simplify the study of the system without loss of generality we can consider the disturbance $\underline{d}$ as input and $\underline{u}$ instead of $\underline{\theta}$ as output. The signal $\underline{\theta}$ can be always found using the transfer function[4] between $\underline{u}$ and $\underline{\theta}$:

$$\underline{u} = -C\underline{\theta} = k\frac{(s-z_1)(s-z_2)}{(s-p_1)(s-p_2)}\underline{\theta} \tag{2.19}$$

keeping in mind that:

$$N = N(\underline{u}), \tag{2.20}$$

the transfer function is:

$$\begin{aligned} \underline{u} &= -\frac{PC}{1+MDPC}\underline{d} = -\frac{\frac{k(s-z_1)(s-z_2)}{Js^2(s-p_1)(s-p_2)}}{1+N(\underline{u})e^{-s\tau}\frac{k(s-z_1)(s-z_2)}{Js^2(s-p_1)(s-p_2)}}\underline{d} = \\ &= -\frac{k(s-z_1)(s-z_2)}{Js^2(s-p_1)(s-p_2)+N(\underline{u})e^{-s\tau}k(s-z_1)(s-z_2)}\underline{d}. \end{aligned} \tag{2.21}$$

Considering that the disturbance is a constant offset d:

$$\underline{u} = -\frac{kd(s-z_1)(s-z_2)}{Js^2(s-p_1)(s-p_2)+N(\underline{u})e^{-s\tau}k(s-z_1)(s-z_2)s}. \tag{2.22}$$

[4]Using the feedback line that is composed by linear blocks only.

Chapter 3

The reference scenario

3.1 Spacecraft data

In order to test the validity of the results, that are very general, we need to simulate a specific reference scenario. Simulations will be performed with the program MATLAB® SIMULINK®. The table 3.1 states the specific data of the reference scenario.

Spacecraft data			
Average orbit altitude	$h_{altitude}$	200	km
Average total mass	M	870	kg
Average moment of inertia	MoI	400	kgm^2
Arm	l	0.5	m
Thrust of one thruster	T_{max}	0.1	N
Delay when the actuator is switching on	τ_{on}	0.1	s
Delay when the actuator is switching off	τ_{off}	0.1	s
Sampling frequency of the sensor	$AOCS$	10	Hz

Table 3.1: Data of the reference scenario.

3.2 Requirements

The requirement is to stabilize the system in a limit cycle with an amplitude smaller than the absolute pointing error.

As we stated in 2.2, in order to obtain a well defined limit cycle and avoid quasi-periodic-like behavior the frequency of the limit cycle shall observe equation 2.16.

The real system is intrinsically discrete due to the controller and the sensors; it has been modeled as continuous. This approximation can be done if the bandwidth of the system is ten times smaller than the frequency of the slowest of the discrete blocks[1]. This requirement shall be checked at the end of the study of the limit cycle because the nonlinear block N depends on the specific input signal.

Table 3.2 summarizes requirements stated above.

Performance requirements		
Absolute pointing error	$APE \leq 10^{-1}$	$^\circ$
Frequency of the limit cycle	$f \leq \frac{1}{2\left(\tau_{on}+\tau_{off}\right)} = 2.5$	Hz
Bandwidth	$f_B \leq 10$	Hz

Table 3.2: Data and requirements of the reference scenario.

[1]As we stated in chapter 2 sensors are responsible of this bandwidth restriction.

Part II

Limit cycles detection

Chapter 4

Methods to predict limit cycles

Nonlinear systems can display oscillations of fixed amplitude and fixed period without external excitation and uncorrelated to initial conditions. These oscillations are called limit cycles or self-excited oscillations. Sustained oscillations can also be found in linear systems indeed, in the case of marginally stable linear systems or in the response to sinusoidal inputs. However, limit cycles in nonlinear systems are different from linear oscillations in a number of fundamental aspects.

- The amplitude of the self-sustained excitation is independent of the initial conditions.
- Marginally stable linear systems are very sensitive to changes in parameters[1], while limit cycles are not easily affected by parameters changes.

The system shown in figure 2.2 can present limit cycles and can not be well designed without considering this nonlinear behavior. The self-sustained oscillations shall be studied, understood and shaped in order to meet robust stability and performance requirements.

In literature there are many ways to study limit cycles. These methods emphasize some aspects of the system while neglecting others. In order to find the best way to describe our system these methods are studied, adapted to our specific case and compared with each other. The following sections will describe these methods in general underling pros and cons of each one.

[1] A slight change is capable of leading either to stable convergence or instability.

4.1 Simulation

The system is reproduced into a simulator[2]; a simulation is run and the output signal is studied using the Fourier analysis. Usually simulations are used only to verify what is found with other design methods due to its intrinsic high reliability.

It is the theoretically easiest way to deal with the system. The simulator can not simulate continuous systems thus a discretization shall be done by the program. The simulation time is divided into time-steps; the blocks behavior is checked every time a new time-step occurs. Increasing the frequency of time-steps decreases the difference between the simulation results and the reality. It is easy to demonstrate that:

$$\lim_{f \to +\infty} S_s = S_r \tag{4.1}$$

where:

- f is the frequency of the time-steps.
- S_s is the system simulated.
- S_r is the real system.

There can be also numerical issues due to the fact that also values of the signals can not be continuous. This is the most reliable way to simulate the behavior of the system due to the absence of important approximations.

Simulation analysis has its limitations as well. The main limitation of the use of this method is that simulations can not be easily incorporated in a design technique. The *trial and error*[3] method can be used via simulation but it does not guarantee convergence. Also the *bifurcation analysis*[4] uses simulations but with the increasing of the number of parameters the computational costs become prohibitive very quickly. Another limitation of this method is that it is very expensive in terms of computational costs and time due to the fact that the steady state is studied.

Pros	**Cons**
Highest reliability	Expensive in terms of computational costs and time
Largely used	Difficult to incorporate in a controller design method

[2]There are several programs capable of simulate linear and nonlinear systems. The program used in this thesis is MATLAB® SIMULINK®.

[3]This will be discussed further in section 7.1.

[4]This will be discussed further in section 7.2.

4.2 Phase plane analysis

The dynamics properties of the system can be described in terms of state differential equations, and an attempt made to solve for the trajectories of the system in the state space.

The method developed by MENDEL in [12] studies the system trajectory in the phase plane; it finds necessary conditions for existence of limit cycles and analytical cost functions in case of limit cycle behavior. These analytical functions can be easily used to derive a design method as is done by MENDEL in [13].

The main limitation of this method is that it is too specific. These analytical functions are valid only for the specific nonlinear problem. Any kind of adaptation to our system requires a reconsideration of all the analytical formulas. These analytical functions are:

- Fuel consumption.
- Average error.
- Limit cycle amplitude.
- Limit cycle period.

The system considers a disturbance incorporated in the plant block. This is not our case thus it shall be reconsidered. Delay is taken into account. Considering everything, we can say that the linear part of the system studied in [13] is very similar to our case and not much adaptation is needed. The nonlinear part, instead, is very different from our case. Limit cycles with more then two states could occur in our case and shall be considered. A phase plane approach could still be possible but the theory shall be heavily reconsidered and adapted. The adaptation is at least hard.

Pros	**Cons**
Analytical cost functions obtained	The system is fixed
The linear part is very similar to our case; not so much adaptation of it to our case is needed	The nonlinear part is very different to our case; the adaptation of it to our case is at least hard
A design method is already derived[5]	Not largely used

[5]For further informations see [13].

4.3 Describing function

It is a quasi-linearization method where only the first three terms of the FOURIER approximation of the input and the output of the nonlinear block are considered. The input signal of the nonlinear block is guessed in advance. The forms which may reasonably be expected to appear at the nonlinearity input are those resulting from the filtering of the linear part of the loop. This leads us to consider three basic signal forms in order to derive quasi-linear approximators for nonlinear operators:

- Bias.
- Sinusoid.
- Gaussian process.

The quasi-linear approximating functions, which describe approximately the transfer characteristics of the nonlinearity, are termed *describing functions*. Within the requirement that the linear part of the system filters the output of the nonlinearity sufficiently, *describing function* theory provides answers to a lot of general questions about nonlinear system operations. The response of systems to the whole class of inputs of linear combinations of these limiting signal forms can be calculated. Even more general system inputs can be handled; the only requirement is that the input to the nonlinearity be of appropriate form. This includes, of course, the special case of a bias plus sinusoid input.

The real advantage, which justifies the development of an approximate theory such as this, is that the *describing function* theory serves as a valuable aid to the design of nonlinear systems. The trends in system performance characteristics as functions of system parameters are clearly displayed using *describing function* theory.

The *describing function* technique has its limitations as well. The fundamental limitation is that the shape of the signal at the input of the nonlinearity must be guessed in advance. A less obvious limitation, is the fact that the analysis answers only the specific questions asked of it. If the designer does not ask about all important aspects of the behavior of a nonlinear system, *describing function* analysis will not disclose this behavior to him[6].

[6]For example, if one uses the 2-sinusoid-input *describing function* to study subharmonic resonance, he would conclude, as many writers have, that a system with an odd static single-valued nonlinearity can not support a subharmonic resonance of even order. Actually, the *describing function* is telling him that such a resonance can not exist with just the two assumed sinusoids at the input to the nonlinearity. An even resonance can indeed exist in such a system, but it will be a biased asymmetric mode.

Pros	Cons
All the theory about the frequency domain can be used	It is an approximation
Trends in system performance characteristics as functions of system parameters are clearly displayed	The input must be guessed in advance
There is a lot of literature about	It answers only the specific questions asked of it
It is the best quadratic-norm approximation[7]	

4.4 Tsypkin method

This method[8] is a further development of the *describing function* method that considers all the FOURIER series.

There are a lot of advantages with respect to the *describing function* method. First of all the whole FOURIER series is taken into account, thus no term is neglected. In second place the periodic input signal shall not be guessed in advance anymore. The only restriction is that it can cross 0 only one time during the period.

The main disadvantage is that the solution of the FOURIER series shall be known. An hybrid study between the Tsypkin method and the *describing function* method that considers a finite number of harmonics can be done without the knowledge of the solution of the FOURIER series but it is expensive in therms of computational costs.

Pros	Cons
It is not an approximation	The solution of the series shall be known
The input can be a general periodic general	The input can cross 0 only one time during the period
	There is not a lot of literature about

[7] As shown in [20].

[8] This has been developed by TSYPKIN in [19].

4.5 Remarks

The *describing function* method is chosen as limit cycle prediction because it is the fastest, easily implementable, most versatile and most studied method. A lot control design techniques are possible with this method.

The simulation is chosen as a validation method because it is the safest and the most accurate method for limit cycle detection, thus it is the best suitable method to check results.

Chapter 5

Describing functions

In this chapter we will first describe in detail the *classical describing function* method. After that we will adapt the *dual-input describing function* method which takes into account an input signal composed by a bias plus a sinusoid, presented in [20], to our system. In the end, everything will be tested using a simulator implemented in MATLAB® SIMULINK® on our reference scenario.

5.1 Classical describing function

Consider the very general system shown in 5.1 where there is a closed loop with a nonlinear block N and a linear one L.

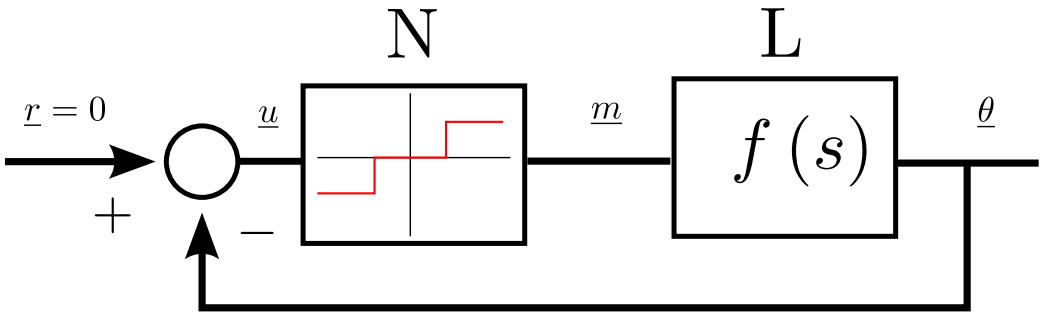

Figure 5.1: Block diagram of the general system.

We want to detect the possible limit cycles that can arise. A limit cycle is defined as a self-sustained oscillation, independent from initial conditions and small perturbations. Thus we set:

$$\underline{r} = 0, \tag{5.1}$$

$$\underline{\theta} = A \sin(\omega t). \tag{5.2}$$

where:

- A is the unknown amplitude of the limit cycle.
- ω is the unknown pulsation of the limit cycle.

In order to develop the *classic describing function* method, the system has to satisfy the following assumptions.

Assumptions

- There is only one single nonlinear component. It implies that if there are two or more nonlinear components in a system, one either has to lump them together into a single nonlinearity[1], or retain only the primary nonlinearity and neglect the others.
- The nonlinear component is time-invariant. It implies that we consider only autonomous nonlinear systems. It is satisfied by many nonlinearities in practice, such as saturation amplifiers, backlash in gears, Coulomb friction between surfaces and hysteresis in relays. The reason for this assumption is that for the Nyquist criterion, on which the *describing function* method is largely based, applies only to time-invariant systems.
- Corresponding to a sinusoidal input of the nonlinear block $\underline{u} = A\sin(\omega t)$, only the fundamental component $\underline{m}_1(t)$ in the output $\underline{m}(t)$ has to be considered. This is the fundamental assumption of the *describing function* method. It represents an approximation, because the output of the nonlinear element corresponding to a sinusoidal input usually contains higher order harmonics besides the fundamental. This assumption implies that high-frequency harmonics can all be neglected in the analysis, as compared with the fundamental component. For this assumption to be valid, it is important for the linear element following the nonlinearity to have low-pass properties, in formula:

$$|L(j\omega)| \gg |L(jn\omega)| \tag{5.3}$$

where:

$$n = 2, 3, \ldots \tag{5.4}$$

This implies that higher harmonics in the output will be filtered out significantly. Thus, this assumption is often referred to as the *filtering hypothesis*.

[1] As can be done with two nonlinearities in parallel.

- The nonlinearity is odd. This assumption means that the plot of the nonlinearity relation[2] between the input and output of the nonlinear element is symmetric about the origin[3].

Considering the assumptions stated before, we can substitute the nonlinear block N with its quasi-linearization. This quasi-linearized block is the so called *describing function.*

The quasi-linearization

Let us now discuss how to represent a nonlinear component by a *describing function.* Let us consider a sinusoidal input to the nonlinear element. The output of the nonlinear component $\underline{m}(t)$ is often a periodic, albeit generally non-sinusoidal, function. Note that this is always the case if the nonlinearity is single-valued[4], because the output is:

$$f\left[A\sin\left(\omega t+2\pi\right)\right]=f\left[A\sin\left(\omega t\right)\right]. \tag{5.5}$$

Using the Fourier series, the periodic function $\underline{m}(t)$ can be expanded as:

$$\underline{m}(t)=\frac{a_0}{2}+\sum_{n=1}^{\infty}\left[a_n\cos\left(n\omega t\right)+b_n\sin\left(n\omega t\right)\right] \tag{5.6}$$

where the Fourier coefficients a_i's and b_i's are generally functions of A and ω, determined by:

$$a_0\triangleq\frac{1}{\pi}\int_{-\pi}^{\pi}\underline{m}(t)\ \mathrm{d}\left(\omega t\right) \tag{5.7}$$

$$a_n\triangleq\frac{1}{\pi}\int_{-\pi}^{\pi}\underline{m}(t)\cos\left(n\omega t\right)\ \mathrm{d}\left(\omega t\right) \tag{5.8}$$

$$b_n\triangleq\frac{1}{\pi}\int_{-\pi}^{\pi}\underline{m}(t)\sin\left(n\omega t\right)\ \mathrm{d}\left(\omega t\right) \tag{5.9}$$

Due to the fourth assumption above:

$$a_0=0. \tag{5.10}$$

Furthermore, the third assumption implies that we only need to consider the fundamental component $\underline{m}_1(t)$, namely:

$$\underline{m}(t)\approx\underline{m}_1(t)=a_1\cos\left(\omega t\right)+b_1\sin\left(\omega t\right)=W\sin\left(\omega t+\phi\right) \tag{5.11}$$

[2] *E.g.* that one shown in figure 2.4.

[3] This assumption is introduced for simplicity, it will be relaxed in section 5.2.

[4] Single-valued means that there is no hysteresis.

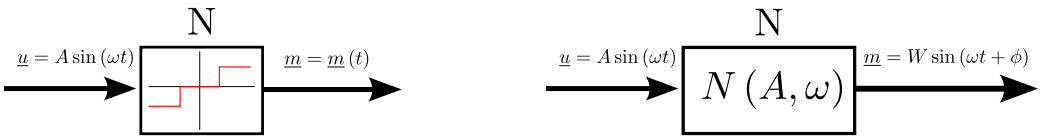

Figure 5.2: A nonlinear element and its describing function representation.

where:

$$W(A,\omega) = \sqrt{a_1^2 + b_1^2} \tag{5.12}$$

$$\phi(A,\omega) = \arctan\left(\frac{a_1}{b_1}\right). \tag{5.13}$$

Expression 5.11 indicates that the fundamental component corresponding to a sinusoidal input is a sinusoid at the same frequency. In complex representation, this sinusoid can be written as:

$$\underline{m}_1 = (b_1 + ja_1)\, e^{j\omega t}. \tag{5.14}$$

Similar to the concept of frequency response function, which is the frequency-domain ratio of the sinusoidal input and the sinusoidal output of the system, we define the *describing function* of the nonlinear element to be the complex ratio of the fundamental component of the nonlinear element by the input sinusoid:

$$N(A,\omega) = \frac{(b_1 + ja_1)\, e^{j\omega t}}{ae^{j\omega t}} = \frac{b_1 + ja_1}{a}. \tag{5.15}$$

With a *describing function* representing the nonlinear component. It, in presence of sinusoidal input, can be treated as if it were a linear element with a frequency response function $N(A,\omega)$, as is shown in figure 5.2. The concept of a describing function can thus be regarded as an extension of the notion of frequency response. For a linear dynamic system with frequency response function $H(j\omega)$, the describing function is independent of the input gain, as can be easily shown. However, the describing function of a nonlinear element differs from the frequency response function of a linear element in that it depends on the input amplitude A and on the frequency ω. Therefore, representing the nonlinear element as in figure 5.1 is also called quasi-linearization.

Generally, the *describing function* depends on the amplitude A and the frequency ω of the input signal. There are, however, a number of special cases. When the nonlinearity is single-valued, the *describing function* $N(A,\omega)$ is real and independent of the input frequency ω. The realness of N is due to the fact that:

$$a_1 = 0, \tag{5.16}$$

which is true because the integrand in the equation 5.8 for a_1, is an odd function of ωt, and the domain of integration is the symmetric interval $[-\pi, \pi]$. The frequency-independent nature is due to the fact that the integration of the integrand in the equation 5.8 is done in the variable ωt, which implies that ω does not explicitly appear in the integration.

Although we have implicitly assumed the nonlinear element to be a scalar nonlinear function, the definition of the *describing function* also applies to the case when the nonlinear element contains dynamics[5]. The derivation of *describing functions* for such nonlinear elements is usually more complicated and may require experimental evaluation.

5.1.1 Limit cycle detection

In order to find the variables ω and A that describe the limit cycle, let us study the closed loop equation of the system, focusing on the input of the nonlinear block:

$$\underline{u}\left[1 + N\left(A, \omega\right) L\right] = 0. \tag{5.17}$$

We are looking for self-sustained oscillations. This, coupled with the equation 5.17, brings us to:

$$1 + N\left(A, \omega\right) L = 0. \tag{5.18}$$

This is the *characteristic equation*. It is a complex equation, thus it provides two scalar equations. In order to obtain the frequency ω and the amplitude A of the limit cycle we have just to substitute the generic complex variable s with $j\omega$ and solve the set of simultaneous equations. In formulas:

$$\begin{cases} \Im\left\{\left|1 + N\left(A, \omega\right) L\right|_{s \to j\omega}\right\} = 0 \\ \Re\left\{\left|1 + N\left(A, \omega\right) L\right|_{s \to j\omega}\right\} = 0 \end{cases}. \tag{5.19}$$

Usually equation 5.18 is not solved in this way, a graphical approach is used instead. In order to describe it, the equation 5.18 shall be manipulated in order to separate linear and nonlinear components. The canonical form is:

$$L = -\frac{1}{N\left(A, \omega\right)}. \tag{5.20}$$

Now we can plot in the Nyquist diagram the linear L and the nonlinear parts $-\frac{1}{N(A,\omega)}$. The intersections are the solutions of the *characteristic*

[5] *i.e.*, is described by differential equations instead of a function.

equation. If the nonlinear block is single-valued, the corresponding *describing function* is real and, usually, it is also positive definite. Thus, varying the amplitude, the function $-\frac{1}{N(A,\omega)}$ is a line that comes from $-\infty$ when the amplitude approaches zero, runs always over the real axis, arrives at a certain negative point and after go back to $-\infty$ when A approaches ∞. If the nonlinear block is not single-valued[6] the real part remains the same while the imaginary part is a constant different from zero. Thus its shape in the Nyquist diagram is a line as before that does not pass over the real axis but it is moved from it by a quantity equal to the constant imaginary value of the function $-\frac{1}{N(A,\omega)}$. Considering how this line is made, the number of intersections are always even. Usually, half of them are unstable. The criterion needed to determine the stability of the limit cycles is[7]:

Criterion 1 (Limit cycle stability)**.** *Each intersection point of the curve $L(j\omega)$ and the curve $-\frac{1}{N(A,\omega)}$ corresponds to a limit cycle. If points near the intersection and along the increasing-A side of the curve $-\frac{1}{N(A,\omega)}$ are not encircled by the curve $L(j\omega)$, then the corresponding limit cycle is stable. Otherwise, the limit cycle is unstable.*

In order to clarify the graphical method, a common Nyquist diagram with a nonlinear block with hysteresis is presented in figure 5.3.

5.2 Dual-input describing function

In this section we will present the *dual-input describing function* method adapted to our system.

The system is depicted in chapter 2. First of all we need to guess the input of the nonlinear block N. Considering that there is a constant disturbance $\underline{d}$ as input of the entire system, the input of the nonlinear block is assumed:

$$\underline{u} = b + A\sin(\omega t)\,. \tag{5.21}$$

In this case the variables that shall be determined are three:

- b the bias.
- A the amplitude.
- ω the angular frequency.

[6] It means that it presents hysteresis

[7] For a detailed explanation of the determination of the stable limit cycles see [18] or [20].

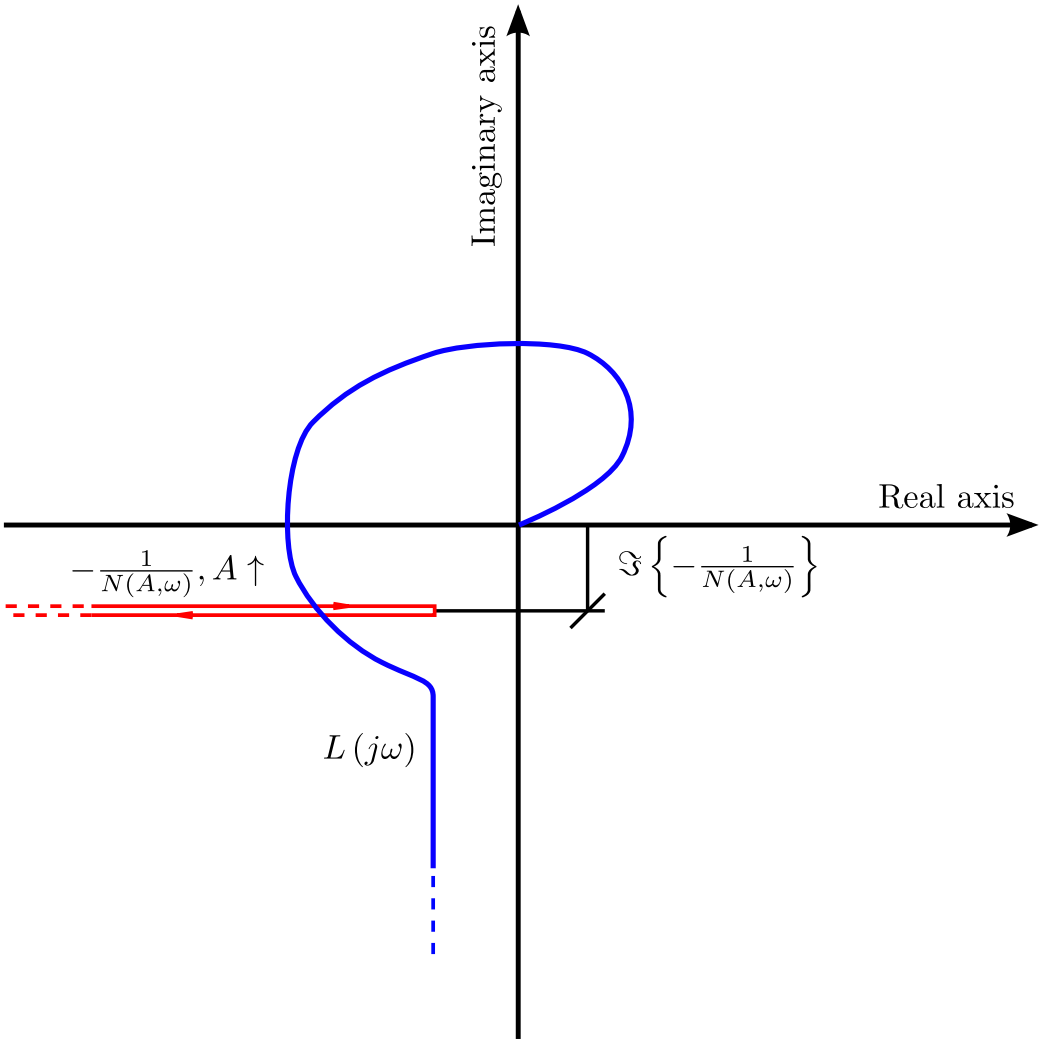

Figure 5.3: Nyquist diagram sample. Red lines does not overlap just for simplicity of exposition.

In comparison to the *classic describing function* theory, there is one more variable needed to determine the characteristics of the limit cycle; the bias b. Thus we need one more equation to determine the limit cycle. This equation is provided by the *bias subsystem* as will be explained in detail later. As we stated in section 5.1, the nonlinearity depicted in section 2.2 is single-valued, thus, it does not explicitly depend on the angular frequency ω of the input.

The system shown in figure 2.2 can be divided as described in figure 5.4 in the *bias subsystem* and the *sine wave subsystem*. In fact all the blocks, but the nonlinear one N, satisfy the principle of superposition. As is shown in figure 5.4, in every subsystem the nonlinear block N depends on the input of its block in its subsystem and on the input of the respective block in the other subsystem. We need to underline also that, due to the nonlinear nature of the block N, the quasi-linearization in the *bias subsystem* is different to that one in the *sine wave subsystem* indeed.

5.2.1 Bias subsystem

This subsystem focuses on the constant disturbance d. As we will see later, it provides the *auxiliary equation* needed to determine the bias b.

First of all we need to find the *describing function* $N_b(b, A)$ of the nonlinear block N in the *bias subsystem*. It is easy to prove[8] that:

$$N_b(b, A) = \frac{m}{b}\left[p\left(\frac{h+b}{A}\right) - p\left(\frac{h-b}{A}\right)\right] \tag{5.22}$$

where $p(x)$[9] is the following stepwise function:

$$p(x) = \begin{cases} -\frac{1}{2} & x < -1 \\ \frac{1}{\pi}\arcsin(x) & |x| \leq 1 \\ \frac{1}{2} & x > 1 \end{cases}. \tag{5.23}$$

As we did in section 5.1, the input of the nonlinear block is set:

$$\underline{u} = b. \tag{5.24}$$

Noticing that:

$$\underline{r} = 0, \tag{5.25}$$

$$\underline{d} = d, \tag{5.26}$$

[8]This result is stated in [20] and derived in appendix A.

[9]Obviously x is a generic variable that will be replaced in the specific case with the proper argument of the function: $\frac{h+b}{A}$ or $\frac{h-b}{A}$.

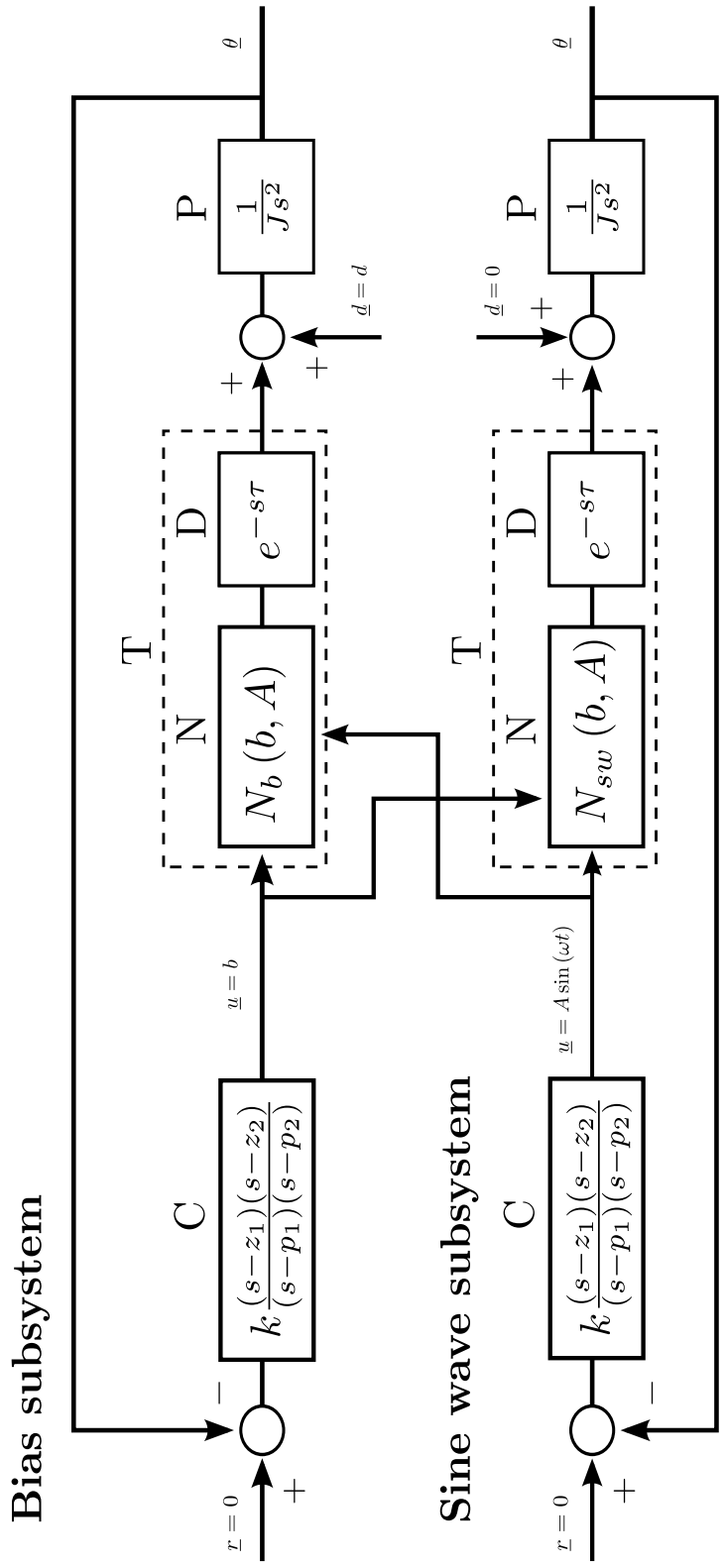

Figure 5.4: Bias and amplitude subsystems.

we can consider the disturbance signal $\underline{d}$ as the input of the subsystem, while, considering that we are interested on the input of the nonlinear block $\underline{u}$, we can assume it as the output of the subsystem. Thus, the transfer function H from $\underline{d}$ to $\underline{u}$ is:

$$H = -\frac{CP}{1 + CPDN_b(b, A)}. \tag{5.27}$$

In order to study this transfer function in more detail, we substitute the blocks with their expressions:

$$H = -\frac{k(s - z_1)(s - z_2)}{Js^2(s - p_1)(s - p_2) + k(s - z_1)(s - z_2)e^{-s\tau}N_b(b, A)}. \tag{5.28}$$

Considering that the Laplace transform of the input $\underline{d}$, due to what we explained in section 2.1, is:

$$\mathcal{L}\{\underline{d}\} = \frac{d}{s}, \tag{5.29}$$

the Laplace transform of the input of the nonlinear block $\underline{u}$ becomes:

$$\underline{u} = -\frac{k(s - z_1)(s - z_2)d}{[Js^2(s - p_1)(s - p_2) + k(s - z_1)(s - z_2)e^{-s\tau}N_b(b, A)]s}. \tag{5.30}$$

As in the *classical describing function*, the input, in the *bias subsystem*, is guessed as constant. Obviously, the Laplace transform is:

$$\mathcal{L}\{\underline{u}\} = \frac{b}{s}. \tag{5.31}$$

The following equation shall hold:

$$\underline{u} = -\frac{k(s - z_1)(s - z_2)d}{[Js^2(s - p_1)(s - p_2) + k(s - z_1)(s - z_2)e^{-s\tau}N_b(b, A)]s} = \frac{b}{s} + f(s). \tag{5.32}$$

In order to isolate the bias term b we can multiply both sides of this equation for s and successively take the limit to zero[10]:

[10]Practically this procedure resembles the *final value theorem*. The only difference is that we do not need to prove that the limit toward zero exists. In fact we are not interested in determining the complete signal $\underline{u}$ in steady-state motion but only its bias b. Thus we do not care about possible harmonic waves that negate the existence of the limit.

$$\lim_{s\to 0} \frac{-k\left(s-z_1\right)\left(s-z_2\right)d}{\left[Js^2\left(s-p_1\right)\left(s-p_2\right)+k\left(s-z_1\right)\left(s-z_2\right)e^{-s\tau}N_b\left(b,A\right)\right]} = \lim_{s\to 0}\left[b+f\left(s\right)s\right]. \tag{5.33}$$

By definition of $f\left(s\right)$ we have:

$$\lim_{s\to 0} f\left(s\right)s = 0. \tag{5.34}$$

We can develop the equation 5.33 obtaining:

$$bN_b\left(b,A\right)+d=0. \tag{5.35}$$

This is the *auxiliary equation* that links the bias b with the amplitude A:

$$b = f\left(A\right). \tag{5.36}$$

Unfortunately it can not be made explicit analytically but it can be evaluated numerically. Figure 5.5 shows the *auxiliary function* for three positive values of the disturbance d. The main purpose of the bias is the counteraction of the disturbance. Therefore, is obvious that, if the disturbance is positive, the bias must be negative. Conversely, if the disturbance is negative, the bias shall be positive. As you can see, when the amplitude A tends toward zero the bias $|b|$ tends toward $|h|$. After that, there is a linear zone where the bias increase or decrease depending on $\frac{d}{m}$. In the end there is a nonlinear decreasing zone. This behavior is clear, in fact, if the amplitude tends to zero, to obtain a limit cycle, which shall always occur, the bias shall approach $|h|$ to permit the switching of the thruster. If the disturbance is smaller than $\frac{m}{2}$ the absolute value of the bias shall be greater than $|h|$ because the thruster shall be switched on less than half of the time. The contrary happens when d is greater than $\frac{m}{2}$. When the amplitude A overtakes the point $h+b$, a limit cycle where the opposite set of thrusters counteract each other. This does not really happen because the limit cycle, usually, is not stable. Thus, when the thruster does not operate in counteracting mode, the following set of inequalities holds:

$$\begin{cases} \operatorname{sign} b = -\operatorname{sign} d & \\ |b| < \left|\frac{h}{2}\right| & |d| < \left|\frac{m}{2}\right| \\ |b| = \left|\frac{h}{2}\right| & |d| = \left|\frac{m}{2}\right| \\ |b| > \left|\frac{h}{2}\right| & |d| > \left|\frac{m}{2}\right| \end{cases}. \tag{5.37}$$

It is useful to see also the behavior of the function $N_b\left(b,A\right)$. Considering that the bias b is linked to the amplitude A by the *auxiliary function*, we

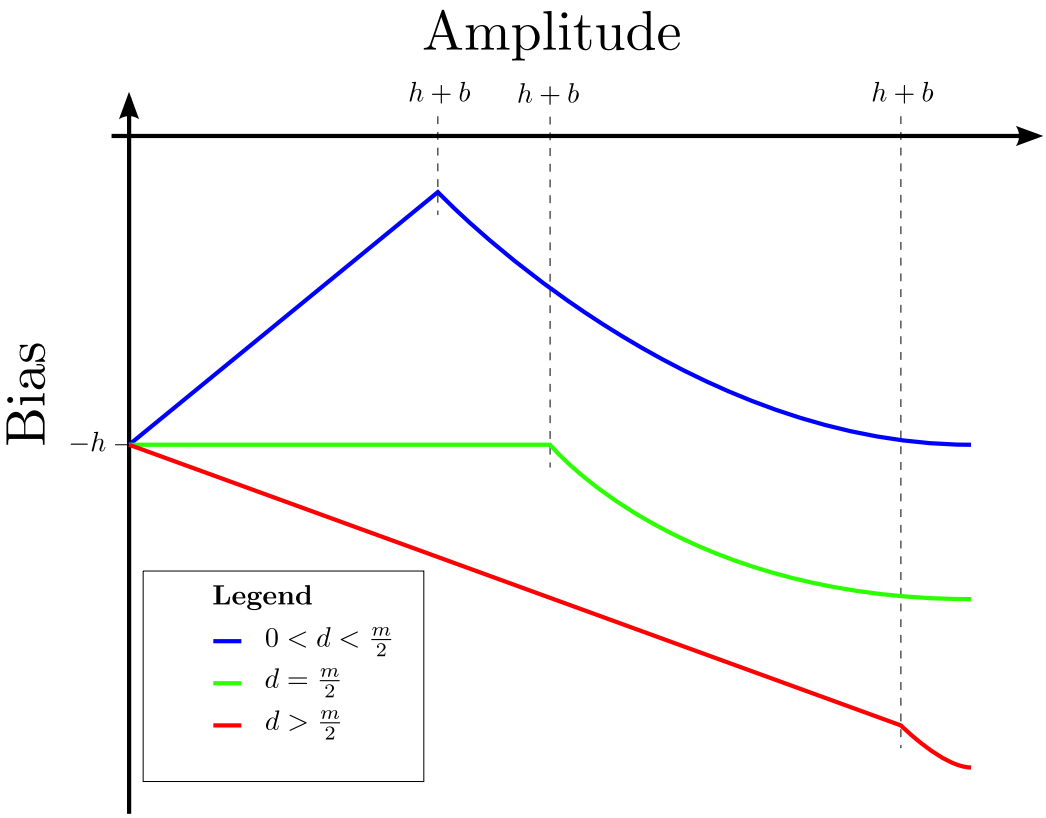

Figure 5.5: Samples of the *auxiliary function* for three values of the disturbance d_n.

can study it for different values of the disturbance d varying the amplitude A. Figure 5.6 shows three possible behavior of the function $N_b(A)$ for three different values of the disturbance d[11]. As you can see, the function begins, when A is near zero, at the value $\frac{d}{h}$; after that it increases or decreases depending on the value of the disturbance and, at the end, when A hits the value $h + d$, it decreases very quickly.

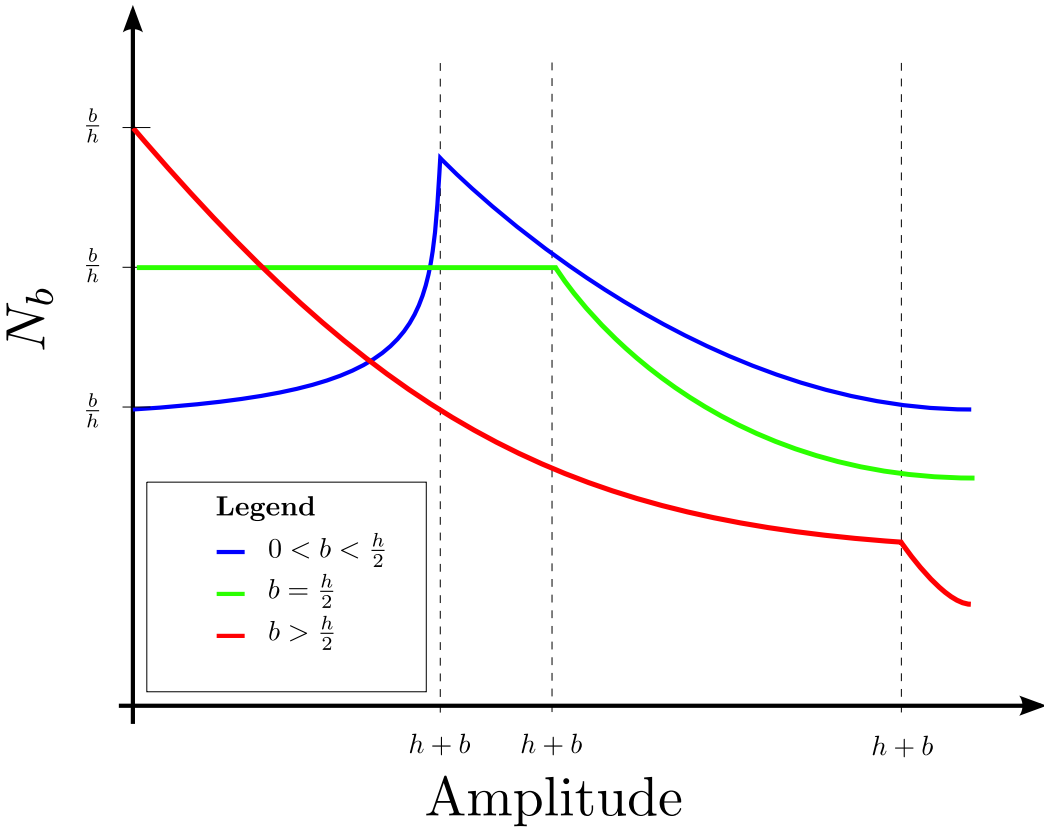

Figure 5.6: Samples of the *describing function* $|N_b(b, A)|_{b \to f(A)}$ for three values of the disturbance d_n.

5.2.2 Sine wave subsystem

First of all, in order to study this subsystem, we need the appropriate *describing function* $N_{sw}(b, A)$ that shall replace the nonlinear block N. It is easy to show that it is[12]:

[11] The dead zone h is fixed instead.

[12] It is derived in [20] and derived in appendix A.

$$N_{sw}(b, A) = \frac{m}{A}\left[q\left(\frac{h+b}{A}\right) + q\left(\frac{h-b}{A}\right)\right] \tag{5.38}$$

where $q(x)$[13] is the following stepwise function:

$$q(x) = \begin{cases} \frac{2}{\pi}\sqrt{1-x^2} & |x| \leq 1 \\ 0 & |x| > 1 \end{cases}. \tag{5.39}$$

The function $-\frac{1}{N_{sw}(b,A)}$ for different values of the bias is shown in figure 5.7. As you can see, if the bias is zero the function has one peak and limit cycle can be avoided. When the bias is not zero, the function presents another peak that approaches zero when the bias tends to $\frac{h}{2}$. The *auxiliary function* modifies the bias in order to let intersect this function and the linear part of the system CPD. This behavior will be studied in detail in subsection 5.2.3.

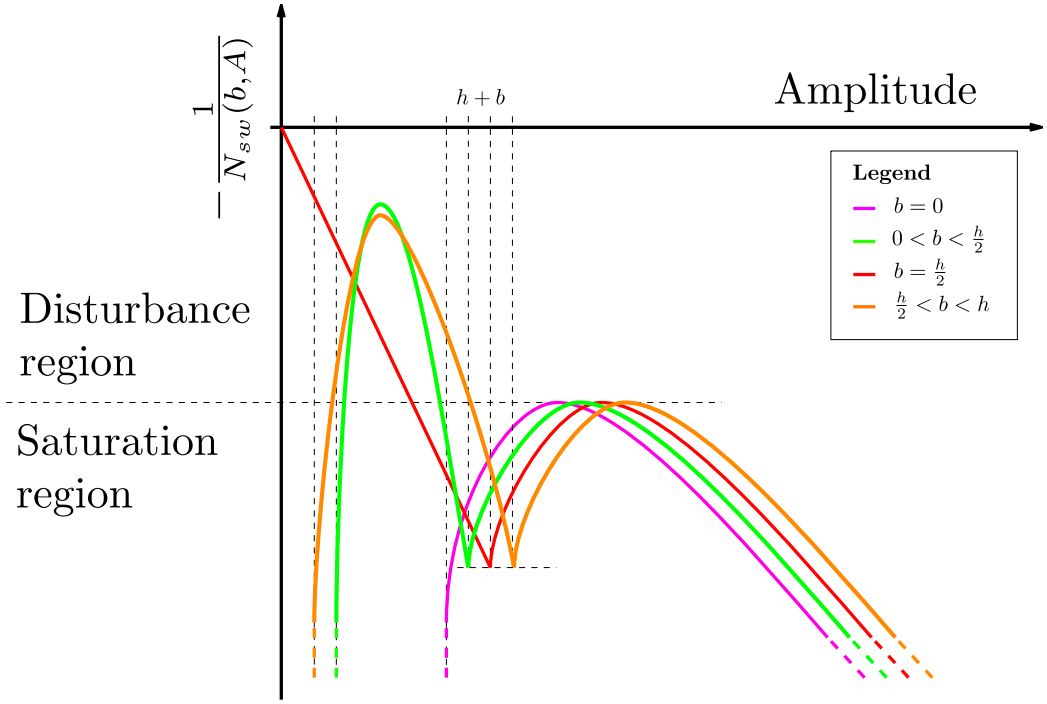

Figure 5.7: Sample of the function $-\frac{1}{N_{sw}(b,A)}$ for four different values of b.

Considering that in this subsystem the disturbance is:

$$\underline{d} = 0, \tag{5.40}$$

[13]Obviously x is a generic variable that will be replaced in the specific case with the proper argument of the function: $\frac{h+b}{A}$ or $\frac{h-b}{A}$.

the closed loop equation becomes:

$$\underline{u}\left[1 + CPDN_{sw}\left(b, A\right)\right] = 0. \tag{5.41}$$

As in the *classical describing function* theory, the *characteristic equation* is:

$$1 + CPDN_{sw}\left(b, A\right) = 0. \tag{5.42}$$

We have to underline that this complex equation have three unknowns related to the limit cycle signal:

- The bias b.
- The amplitude A.
- The frequency ω.

To the other hand the *characteristic equation* 5.42 can provide only two scalar equations. The *auxiliary equation* 5.35 is needed to solve the problem.

5.2.3 The final solution

In order to determine the three unknowns that characterize the limit cycle we need to solve the following set of simultaneous equations:

$$\begin{cases} bN_b\left(b, A\right) + d & = 0 \\ 1 + CPDN_{sw}\left(b, A\right) & = 0 \end{cases} \tag{5.43}$$

Where the first one is a scalar equation while the second one is complex. Considering that the nonlinear block is single-valued, its imaginary part is zero[14]. The system of equations 5.43 can be manipulated in the following way:

$$\begin{cases} \Im\left\{CPD\right\} = 0 & (5.44) \\ bN_b\left(b, A\right) + d = 0 & (5.45) \\ \Re\left\{CPD\right\} = -\dfrac{1}{N_{sw}\left(b, A\right)} & (5.46) \end{cases}$$

Note that in every equation the generic complex variable s has been replaced with $j\omega$. This is the final set of simultaneous equations needed to detect the limit cycles. The system of equations above can be solved in a

[14]This behavior is depicted in section 5.1.

numerical-graphical way which involve the Nyquist diagram. We can easily use the method explained in section 5.1 applied to the set of equations 5.44 and 5.46 with the difference that we have to substitute first the *auxiliary equation* 5.45 in the other two equations.

The typical Nyquist diagram of CPD and $-\frac{1}{N_{sw}(A)}$ is shown in figure 5.8. As we explained in section 5.1, the plot of $-\frac{1}{N_{sw}(A)}$ is a line that comes from $-\infty$, run over the real axis to a certain negative point and, after, returns back. The linear part of the system, $CPD\,(j\omega)$ has two poles at zero and a pure delay. Thus the Nyquist plot begin from $(-\infty, 0)$ when ω is zero, and approaches the origin encircling it an infinite number of times when ω approaches ∞.

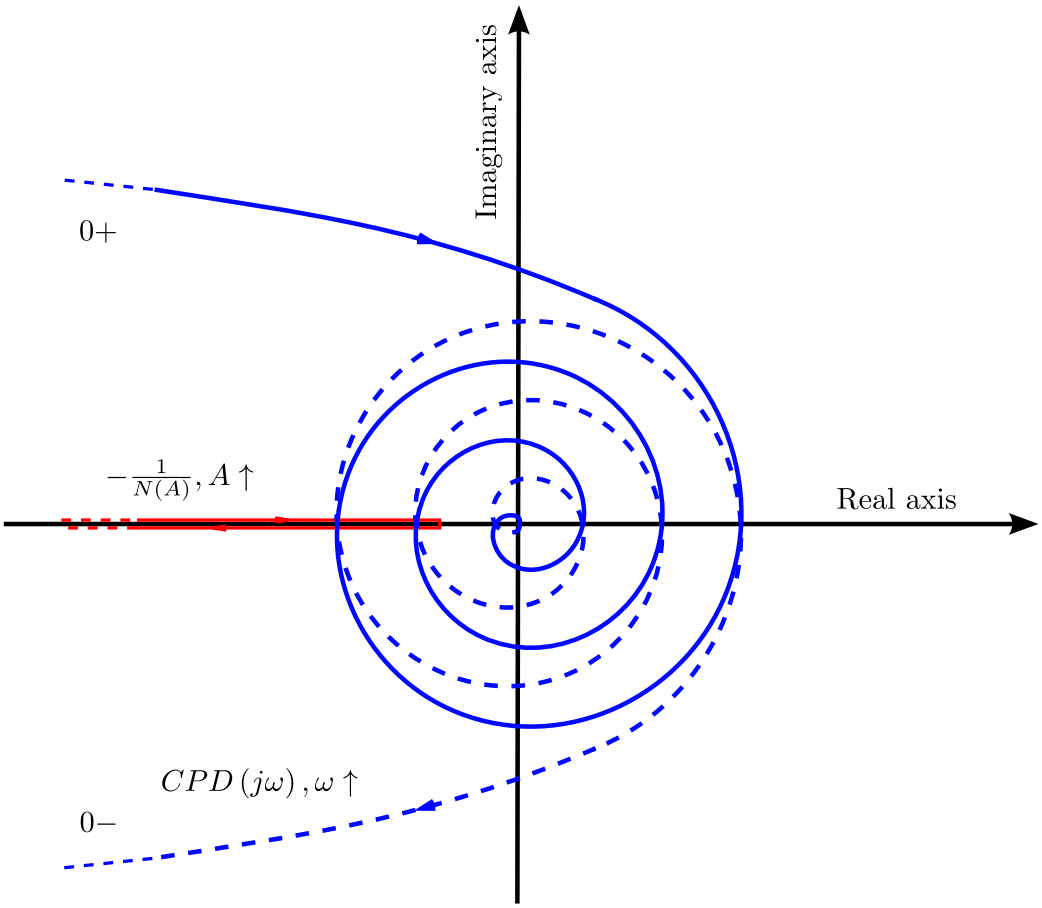

Figure 5.8: Sample of the Nyquist diagram needed to solve the limit cycle detection problem with the *dual-input describing function* method.

As we will see in detail in section 5.3, the intersection $(-\infty, 0)$ is trivial because the frequency ω is zero and the amplitude too, thus it shall not be

taken into account. Considering the other possible intersections, the farthest one from the origin that meets the *limit cycle stability* criterion 1 is the stable limit cycle that the system presents. The other intersections are neglected because of the *filtering hypothesis* of the linear part CPD or because are unstable.

Another useful way to graphically solve the set of equations 5.43 is presented in figure 5.9. The abscissa is the amplitude A while the ordinate is the real axis of the Nyquist diagram. The blue line is the intersection of CPD with the real axis. Obviously, it is horizontal because it does not vary with the amplitude A. The other lines are the function $-\frac{1}{N_{sw}(b,A)}$ evaluated for different values of the bias. Intersections between the blue line and the function $-\frac{1}{N_{sw}(b,A)}$ characterize the limit cycle. If there are two intersections the stable one is that one that which present the biggest amplitude. In order to distinguish different types of limit cycles we can define two regions:

- Saturation region. It is the zone beyond the second peak of the function $-\frac{1}{N_{sw}(b,A)}$ as shown in figure 5.9.
- Disturbance region. It is the zone below.

Intersections between $\Re\{CPD\}$ and $-\frac{1}{N_{sw}(b,A)}$ in the saturation region shall be avoided; these intersection are the usual limit cycles that are detected by the *classical describing function* theory. These limit cycles occur due to the saturation of the command and will be called *saturation limit cycles*.

Intersections in the disturbance region can not be avoided if the disturbance is not zero. These intersections occur due to the constant disturbance that tends to destabilize the system. These limit cycles will be called *disturbance limit cycles*.

This method can be improved by evaluating numerically the cumulative *describing function* $-\frac{1}{N_{sw}(f(A),A)}$. It is the usual *describing function* $-\frac{1}{N_{sw}(b,A)}$ where the bias has been substituted using the *auxiliary equation* 5.36 which can be evaluated numerically only. The resulting graphical method is shown in figure 5.10.

5.2.4 Remarks

In order to reduce computational costs, considering that possible high - frequency limit cycles are neglected in any case, the delay block D will be replaced with its first-order Padé approximant. Considering that the frequency of the limit cycle shall meet bandwidth requirements this approximation is always valid.

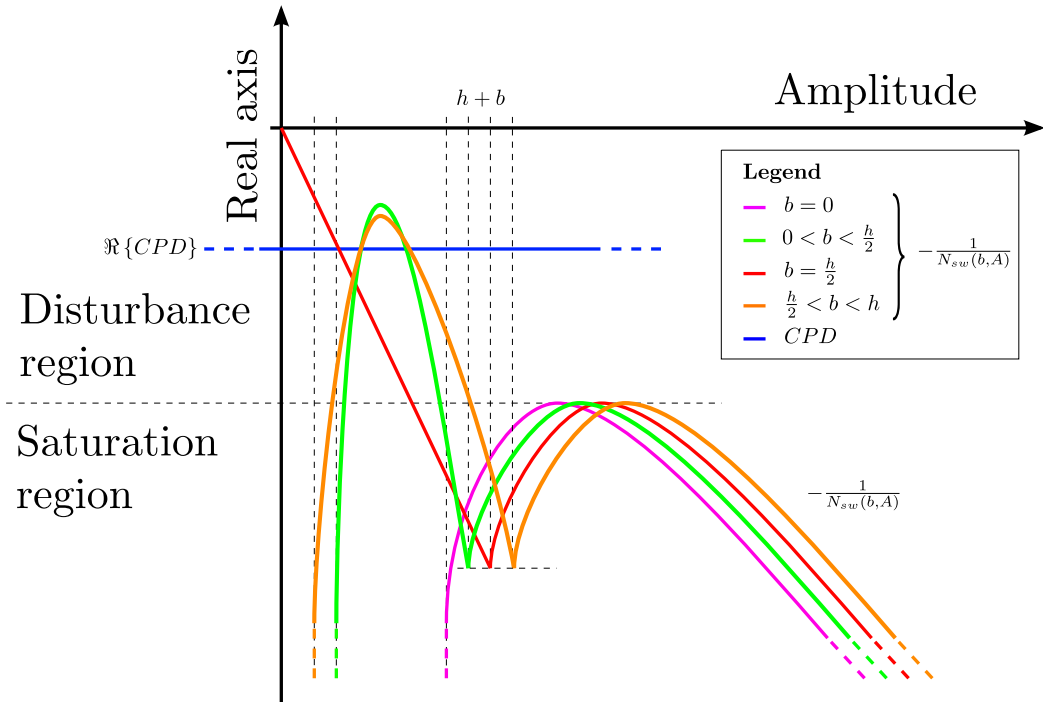

Figure 5.9: Sample of the function $-\frac{1}{N_{sw}(b,A)}$ for four different values of b. The blue line is the intersection of the linear part of the system CPD with the negative real axis.

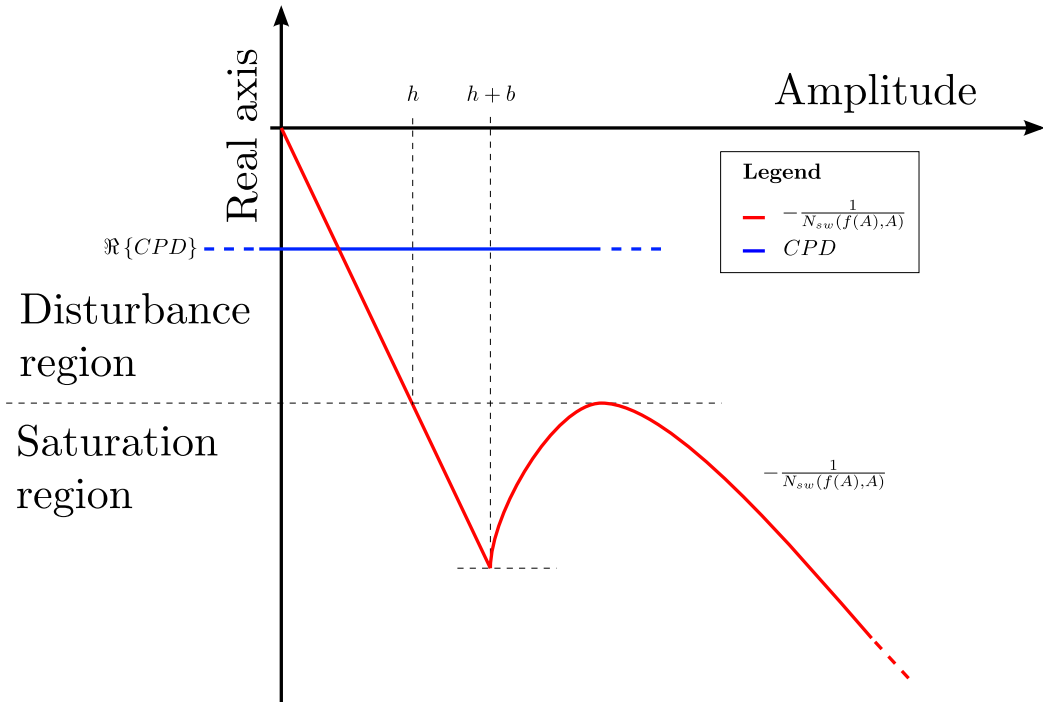

Figure 5.10: Sample of the cumulative function $-\frac{1}{N_{sw}(f(A),A)}$. The blue line is the intersection of the linear part of the system CPD with the negative real axis.

The transfer function of the controller, now that the system behavior has been studied, can be chosen wisely. Let us consider, from this point of view, what have been done. The equation 5.44 determines ω_{180} which is the angular frequency where the phase of the linear part of the open loop is 180°. This angular frequency does not rely on the gain of the controller k. In order to show it, we can manipulate the equation 5.44:

$$\begin{aligned} \Im\{CPD\} &= 0 \\ \Im\{kf(j\omega)\} &= 0 \\ k\Im\{f(j\omega)\} &= 0 \\ \Im\{f(j\omega)\} &= 0. \end{aligned} \tag{5.47}$$

Where $f(j\omega)$ is the transfer function CPD without the gain k where the variable s has been substituted by $j\omega$.

Let us now focus on the equation 5.46 in particular on the role of the *describing function* $N_{sw}(b, A)$. Practically it is a variable gain that is adjusted, changing properly b and A, to meet the equation 5.46. This is the same equation required to determine the angular crossover frequency ω_C of the system, thus, from a different point of view, the equation 5.46 adjusts $N_{sw}(b, A)$ to meet:

$$\omega_{180} = \omega_C. \tag{5.48}$$

Considering that the angular frequency is determined by the second equation of the system, the function $\Re\{f(j\omega)\}$ is a constant. Thus:

$$\begin{aligned} N_{sw}(b, A) &= -\frac{1}{\Re\{CPD\}} \\ N_{sw}(b, A) &= -\frac{1}{\Re\{kf(j\omega)\}} \\ N_{sw}(b, A) &= -\frac{1}{k}\frac{1}{\Re\{f(j\omega)\}} \\ N_{sw}(b, A) &\propto -\frac{1}{k}. \end{aligned} \tag{5.49}$$

This means that the angular crossover frequency ω_C, differently from the linear systems, does not rely on the gain of the controller k. In fact $N_{sw}(b, A)$ changes to exactly compensate the effect of k. On the other hand, considering that the equation 5.45 maintains the bias b around the saturation of the torque command m, we can assert that the amplitude of the limit cycle A

and, thus, the stability of the system are strictly related to the gain of the controller k.

In a second-order-like system, which is our case, the bandwidth is around the crossover frequency, thus:

$$f_B \approx f_C = f_{180} \tag{5.50}$$

where, obviously, f_C and f_{180} are the respective frequencies of the angular frequencies ω_C and ω_{180}. This means that the bandwidth f_B does not depend on the gain k, differently from linear systems. The real system is discrete and nonlinear, the nonlinearity completely inhibits the usual method that allows the approximation of continuous system by limiting the bandwidth by changing the gain of the controller. In order to correctly apply the *dual-input describing function* theory the system must be continuous thus an other way to limit the bandwidth shall be used. The easiest way to approximate the discrete system with its corresponding continuous version would be the addition to the continuous model of a delay equal to half of the sample time of the sensor. Unfortunately this way is not allowed because it is valid only if the system is stable and far enough from the neutral stability. This is not the case because the nonlinear block, as we saw before, brings the system to the neutral stability condition and produces, in this way, the limit cycle. The last alternative is the addition of a lag network to the controller. The lead part is needed to stabilize the system while the lag network, which slightly destabilize it, controls the bandwidth. We need to underline that this lag network added to the controller is harmful for what concern the stabilization of the system. It is needed only to limit the bandwidth and allow the application of the *dual-input describing function* theory. Better performance can be achieved by using only a lead network but the system can no more be studied in this way. The development of a *discrete dual-input describing function* theory that allows the study of that discrete system could be possible but it is beyond the scope of this thesis. The reasons of the choice of the lead-lag network are summarized below:

- The lead network $k\frac{s-z_1}{s-p_1}$ is necessary to stabilize the system.
- The lag network $\frac{s-z_2}{s-p_2}$ is needed to limit the bandwidth of the system. It slightly destabilize the system and degrades performance. It is needed only to permit the application of the *dual-input describing function* theory.

5.3 Simulations

In this section simulation results will be presented. First of all, the simulator is described. Secondly, data of the reference scenario, summarized in chapter 3, will be manipulated to fit the simulator. Successively, for the sake of clarity, we will present summarizing tables of the inputs. In the end the behavior of the system will be studied and discussed in detail.

The simulator is akin the block diagram shown in figure 2.2 with the addition of the sensor block. The sensor is modeled with a zero-order-hold that acts at the frequency of the sensor.

The simulation ends when steady state is achieved and a good amount of cycles have been performed. Only the steady state part of the signal $\underline{u}$ is considered by the analysis. The mean value of the signal b is calculated and subtracted from the signal itself. After that, a Fourier analysis is performed and the amplitude A and the frequency f of the limit cycle are evaluated.

5.3.1 Simulations data inputs

The maximum torque m that is provided by the set of thrusters is:

$$m = 2lT_{max}. \tag{5.51}$$

For the sake of simplicity the dead zone h is set:

$$h = m. \tag{5.52}$$

The fundamental sample time is set ten times smaller than the delay because continuous blocks shall appear as continuous. Thus:

$$dtsim = \frac{\min\{\tau_{on}, \tau_{off}\}}{10}. \tag{5.53}$$

Considering the orbit altitude of our reference scenario, the dominant disturbance is the aerodynamic drug. A disturbance range is determined accordingly to figure 2.3. Table 5.1 presents values of the simulator inputs of our reference scenario derived in this subsection. The transfer function of the controller is:

$$C = \frac{1}{4}\frac{(s+0.01)}{(s+0.1)}\frac{(s+1)}{(s+0.1)}. \tag{5.54}$$

Other inputs are summarized in tables 3.1 and 3.2.

Spacecraft data			
Maximum torque available	m	0.1	Nm
Dead zone	h	0.1	rad
Disturbance	d	$0.03 - 0.07$	Nm
Fundamental sample time of the simulator	$dtsim$	0.01	s
Total time of simulation	$tend$	10000	s

Table 5.1: Data inputs of the simulator derived in subsection 5.3.1.

5.3.2 Results

As we anticipated in chapter 3, simulations have been performed using MATLAB® SIMULINK® while the limit cycle have been predicted by MATHEMATICA®. The notebook evaluates the limit cycle with the *dual-input describing function* theory and creates two files: INPUTS.DAT and RESULTS.DAT. INPUTS.DAT is read by MATLAB® SIMULINK® and a simulation is run. Successively, MATLAB® SIMULINK® performs a Fourier analysis of $\underline{u}$. In the end, the routine presents the limit cycle evaluated by MATHEMATICA® and reported in RESULTS.DAT, the limit cycle of the simulator and the error in a table as shown, for instance, in figure 5.11 and in table 5.2. The errors are calculated as:

$$E_x = 100 \left| \frac{(x_{real} - x_{predicted})}{x_{real}} \right| \tag{5.55}$$

where x is the generic variable that will be replaced by b, A and f.

		Predicted	**Real**	**Error**[%]
Bias	b	-0.1000	-0.0999	0.05
Amplitude	A	0.0206	0.0224	7.92
Frequency	f	0.0157	0.0151	4.33

Table 5.2: Results of MATLAB® SIMULINK® and MATHEMATICA® when $d = 0.05$Nm using the *dual-input describing function* theory.

Studying simulations performed varying the disturbance over its range, some curious behaviors have been discovered.

As we can see in table 5.2 or in figure 5.11, when the disturbance is half of the maximum torque providable by the set of thrusters the errors are very

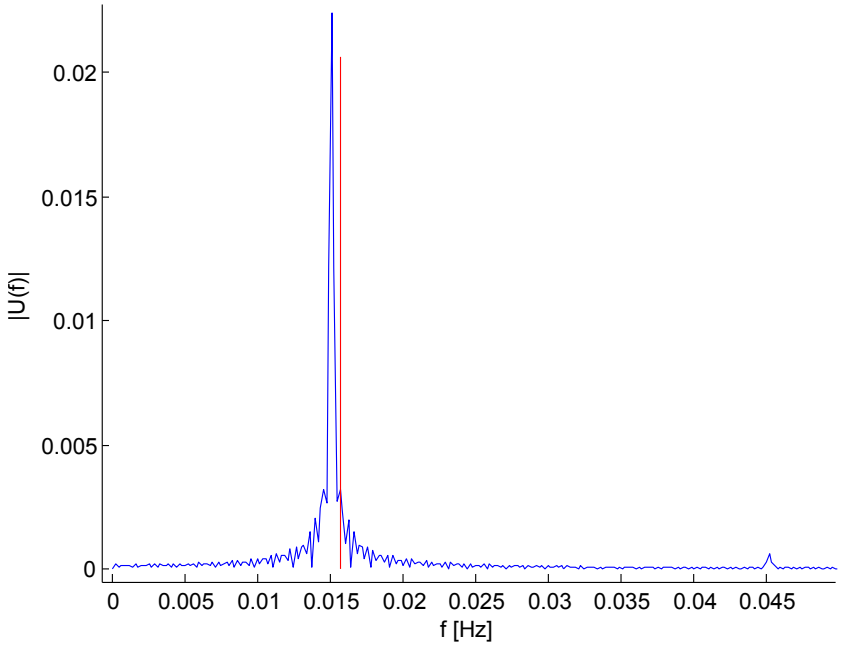

Figure 5.11: Single-sided amplitude spectrum simulated (blue) and predicted (red) of the signal $\underline{u}-b$ when $d = 0.05$Nm using the *dual-input describing function* theory.

small. The Fourier analysis of $\underline{u}$ presented in figure 5.11 confirms the *filtering hypothesis*. In fact the higher-frequency picks are very small compared to the first one.

When the disturbance moves away, errors increase and higher-order sine waves arise. In order to show this effect results with disturbance $d = 0.03$Nm are shown in figure 5.12 and in table 5.3.

		Predicted	**Real**	**Error**[%]
Bias	b	-0.0902	-0.0887	1.75
Amplitude	A	0.0167	0.0182	8.59
Frequency	f	0.0157	0.0139	12.9

Table 5.3: Results of MATLAB® SIMULINK® and MATHEMATICA® and MATHEMATICA® when $d = 0.03$Nm using the *dual-input describing function* theory.

In order to better characterize this behavior the MATHEMATICA® notebook has been modified to predict limit cycles using directly the frequency

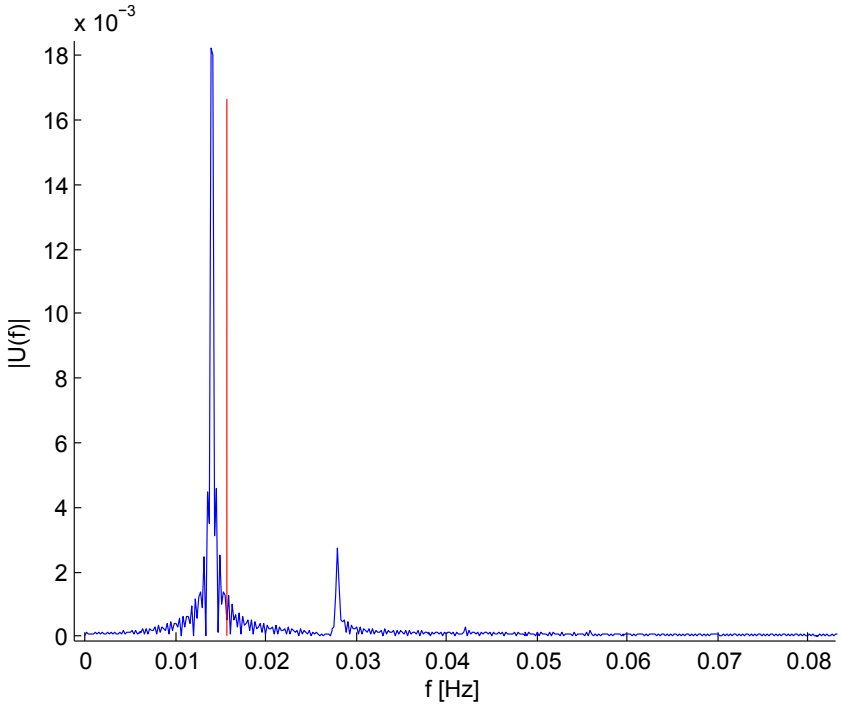

Figure 5.12: Single-sided amplitude spectrum simulated (blue) and predicted (red) of the signal $\underline{u}-b$ when $d = 0.03$Nm using the *dual-input describing function* theory.

obtained by the simulator replacing equation 5.44 and errors of bias and amplitude have been checked varying the disturbance. In this case the amplitude and the bias have been well predicted for every chosen disturbance. In other words, when the frequency is well predicted then the amplitude and the bias are well predicted too. This means that this odd behavior depends on the frequency of the limit cycle only. Thus the equation 5.44 and the part of the simulator concerning the determination of the frequency of the limit cycle shall be studied more closely. Therefore, simulations have been run varying the disturbance. The frequencies of the limit cycles predicted and simulated have been plotted in figure 5.13.

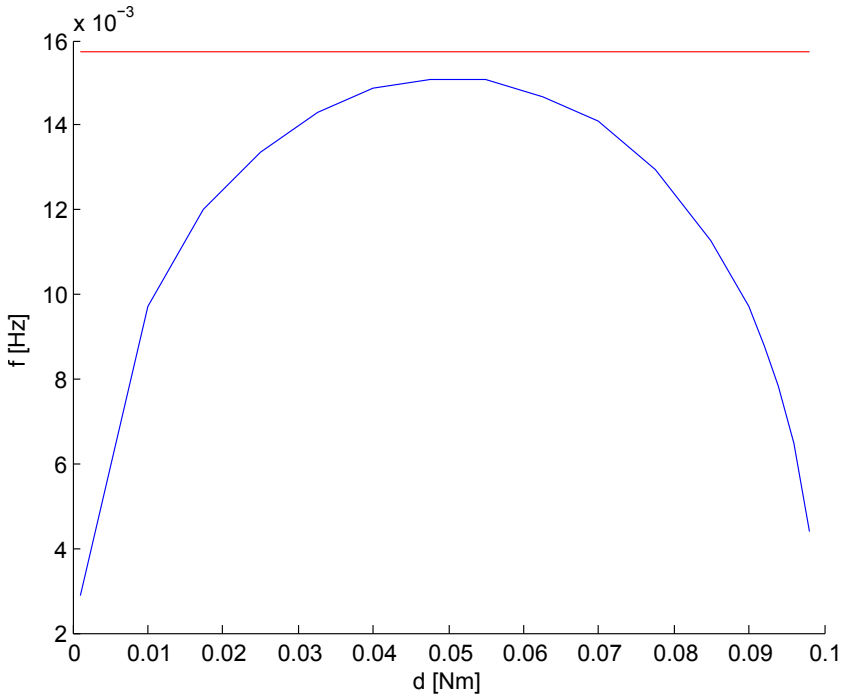

Figure 5.13: Frequency of the limit cycle simulated (blue) and predicted (red) using the *dual-input describing function* theory varying the disturbance.

Obviously, the frequency of the limit cycle predicted does not change because the disturbance does not modify the equation 5.44. The frequency of the limit cycle simulated instead has a parabolic behavior with the peak at $|d| = \frac{m}{2}$. Experimentally we can state that the error remain smaller than 15% if:

$$\left|\frac{d}{m}\right| \in \left[\frac{3}{10}, \frac{7}{10}\right]. \tag{5.56}$$

The Fourier analysis performed during this series of tests underlines that also high order sine waves arise when the absolute value of the disturbance moves away from the value $\frac{m}{2}$. An example is shown in figure 5.14.

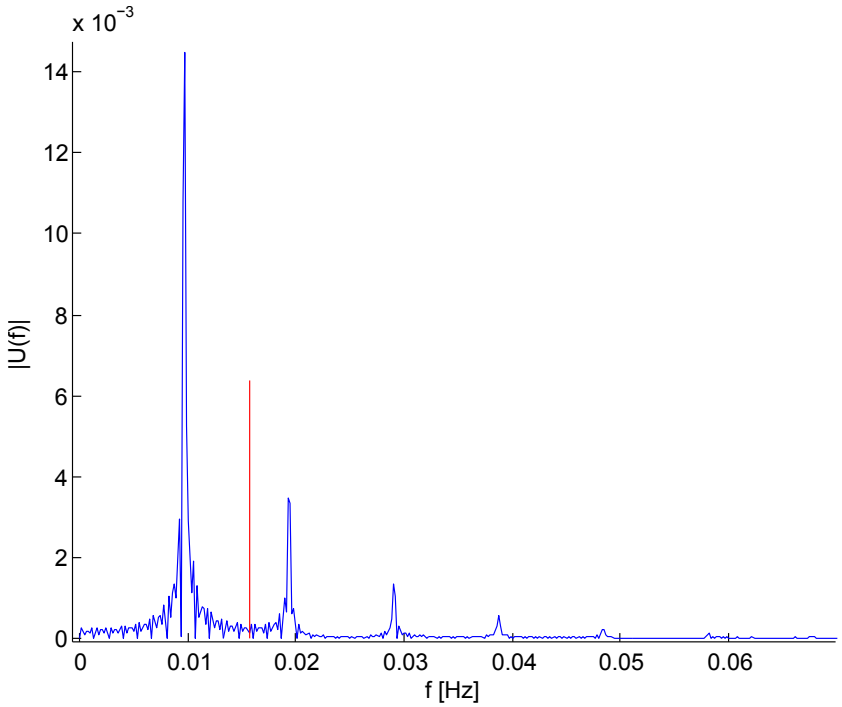

Figure 5.14: Single-sided amplitude spectrum simulated (blue) and predicted (red) of the signal $\underline{u}-b$ when $d = 0.01$Nm using the *dual-input describing function* theory.

Let us now consider input and output of the nonlinear block without replacing it with its *describing function* and assume that the linear part of the system does not filter enough higher-order harmonics. For the sake of clarity, the general situation is shown in figure 5.15. First of all, focus on the case:

$$d = \frac{m}{2}. \tag{5.57}$$

As we stated in subsection 5.2.1, the following equation holds:

$$b = d = \frac{m}{2}. \tag{5.58}$$

The switch occurs when:

$$\omega t = k\pi \tag{5.59}$$

At this point of the sine wave its derivative is maximum (or minimum). Other high order sine waves can not interfere significantly with the switching point due to the quick variation of the principal sine wave. When the disturbance moves away from $\frac{m}{2}$ the bias does qualitatively the same. This means that the switching point moves toward the peaks (or the valleys). Therefore, the system switches when the derivative of the sine wave is around zero. Other high order harmonics now can substantially modify the switch of the actuator. In fact, when the disturbance approaches zero, so does the bias and the switching point tends to the peak. In this case the signal remains around the switching point for a long time and other high order harmonics can pass trough the nonlinear block. This brings the system to chaotic motion. In order to establish if the high order harmonics are responsible of the decrease of the frequency of the limit cycle, the *hybrid Tsypkin-dual-input describing function* method will be developed and applied to our reference scenario in chapter 6.

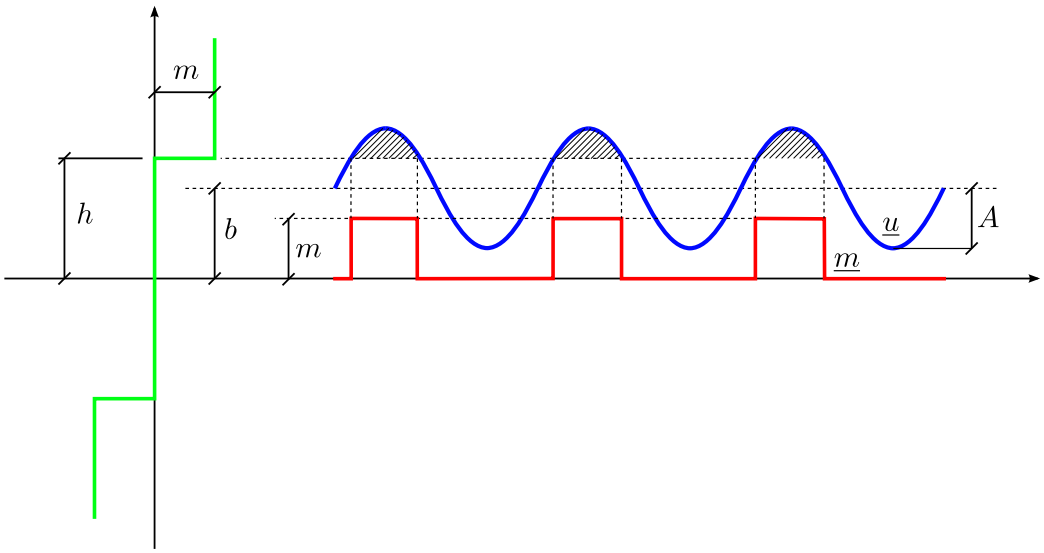

Figure 5.15: The nonlinear block and its input $\underline{u}$ and output $\underline{m}$.

Chapter 6

Tsypkin method

In this chapter we will present the *classic Tsypkin method* and its adaptation to our reference scenario. In order to expose this adjustment of the *classic Tsypkin method* we need to remind first some important results that have brought us to this study stated in section 5.3.2.

When the disturbance is around half of the maximum torque providable by the thrusters the limit cycle is well-predicted. The errors are very small. The Fourier analysis of the input signal $\underline{u}$ shows only one peak, thus, the *filtering hypothesis* is respected.

To the other side, when the disturbance is not around half of the maximum torque[1], the theory does not fit anymore with the simulation. In particular the error of the frequency increases parabolically while the disturbance moves away from $\frac{m}{2}$. We have demonstrated that the errors of the amplitude and the bias increase due to the error of the frequency. When the frequency is well-predicted the amplitude and the bias are well-predicted too, regardless of the disturbance. Finally, the Fourier analysis shows that a numerable number of higher-order harmonics arise.

In order to clarify this strange behavior we will adapt the *classical Tsypkin method* to our purposes. As you will see in section 6.1 the *classical Tsypkin method* is an exact technique that predicts just the frequency of the limit cycle. Fortunately we need only qualitative results because the *Tsypkin method* is not viable during the design study due to its high computational costs. An hybrid technique called *hybrid Tsypkin-dual-input describing function* that fuses the *classical Tsypkin method* and the *dual-input describing function* together will be developed.

In the end, simulations will be performed and general considerations about the system will be discussed.

[1] In other words when it is very small or very high with respect to the maximum torque.

6.1 Classical Tsypkin method

As we saw in chapter 5, the limit cycles can be studied with the *describing function* theory. The main limit of the *describing function* technique is that it is an approximation that requires the *filtering hypothesis*. In order to study systems that does not verify this hypothesis higher-order harmonics shall be taken into account.

The *classical Tsypkin method*[2] is the appropriate technique required to deal with these systems because it is not an approximation and, in particular, does not involve the *filtering hypothesis*. It was born to study limit cycles in systems where the nonlinear block was not single-valued albeit it can be easily extended to other nonlinearities.

Consider the general system that is described in section 5.1 and is shown in figure 5.1. For the sake of clarity let us fix the nonlinearity as a relay with passive hysteresis as is shown in figure 6.1.

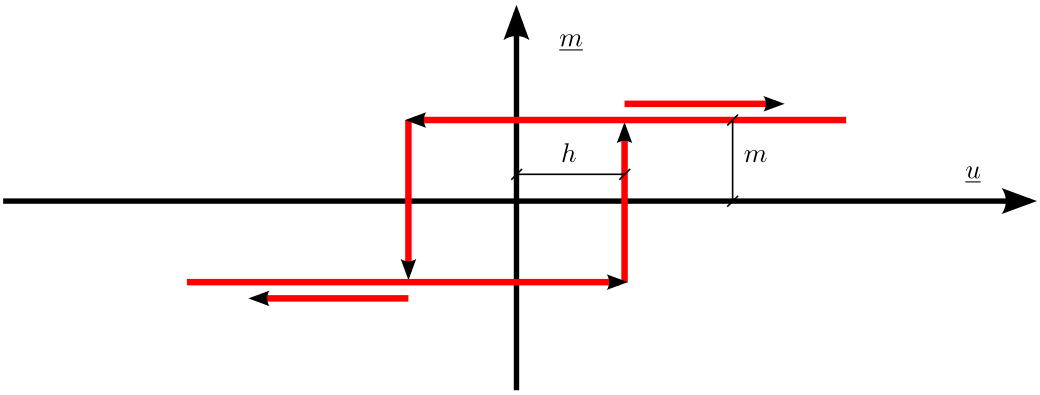

Figure 6.1: Relay with passive hysteresis.

Figure 6.2 shows a generic periodic signal (blue) not necessarily sinusoidal, with no mean value. When the input signal $\underline{u}$ rises above the dead zone h, the relay switches, changing the output from $-m$ to m. After, when the input decreases below the threshold $-h$, the relay reverts the output to $-m$. Therefore, the output $\underline{m}$ is a square wave with the same frequency of the input signal but with different phase.

Without loss of generality, we can set the initial time t_0 where the relay switches. This allow us to transform the output $\underline{m}$ with the Fourier series more easily. The period is $T = \frac{2\pi}{\omega}$ and its Fourier transform is:

[2]The *classical Tsypkin method* given here is akin to that in [10].

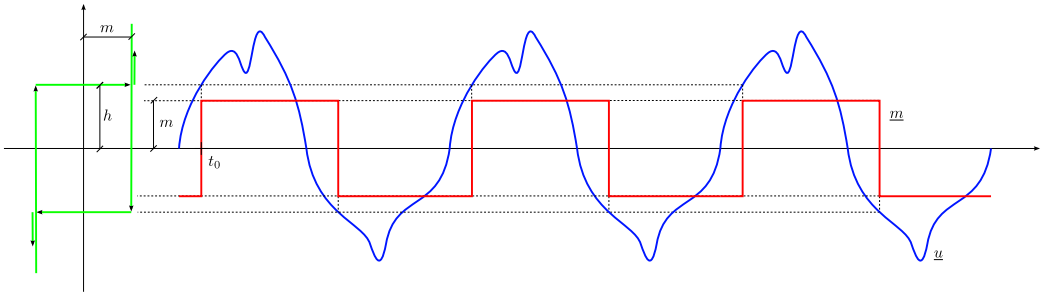

Figure 6.2: Input (blue) and output (red) of the relay with passive hysteresis.

$$\underline{m}(t) = \frac{4m}{\pi} \sum_{k=0}^{\infty} \frac{\sin\left[(2k+1)\,\omega t\right]}{2k+1}. \tag{6.1}$$

For the sake of simplicity we can manipulate the Fourier series in this way:

$$\underline{m}(t) = \frac{4m}{\pi} \sum_{n=odd}^{\infty} \frac{\sin(\omega_n t)}{n} = \frac{4m}{\pi} \sum_{n=odd}^{\infty} \frac{\Im\left\{e^{j\omega_n t}\right\}}{n}. \tag{6.2}$$

where we have defined:

$$n \triangleq 2k+1, \tag{6.3}$$

$$\omega_n \triangleq n\omega. \tag{6.4}$$

We need to underline that, in order to apply the *classical Tsypkin* theory, the signal $\underline{u}$ can be very complicated but, in a period, shall intersect just once the threshold h. This assumption is the only requirement on the input signal of the nonlinear block $\underline{u}$. Let us now remind assumptions required to apply the *classical Tsypkin* theory[3]:

- The relay has hysteresis but no dead zone.
- The transfer function $L(s)$ is rational in s, it is strictly proper and the real parts of its poles are negative.
- When the steady-state limit cycle begins the relay switches every half-period.

Let us now define the linear part as:

[3]As stated in [3].

$$L(j\omega) \triangleq R(\omega) + jI(\omega) = |L(j\omega)| e^{j\angle L(j\omega)} \tag{6.5}$$

The n-th sine wave of the output of the system $\underline{\theta}$ is:

$$\underline{\theta}_n(t) = \frac{4m}{\pi n} |L(j\omega_n)| \sin(\omega_n t + \angle L(j\omega_n)) \tag{6.6}$$

Considering the definition 6.5, equation 6.6 can be manipulated in this way:

$$\begin{aligned}
\underline{\theta}_n(t) &= \frac{4m}{\pi n} \Im \left\{ |L(j\omega)| e^{j[\omega_n t + \angle L(j\omega_n)]} \right\} = \\
&= \frac{4m}{\pi n} \Im \left\{ |L(j\omega)| e^{j\omega_n t} e^{j\angle L(j\omega_n)} \right\} = \\
&= \frac{4m}{\pi n} \Im \left\{ L(j\omega_n) e^{j\omega_n t} \right\} = \\
&= \frac{4m}{\pi n} \Im \left\{ L(j\omega_n) [\cos(\omega_n t) + j \sin(\omega_n t)] \right\} = \\
&= \frac{4m}{\pi n} \Im \left\{ [R(\omega_n) + jI(\omega_n)] [\cos(\omega_n t) + j \sin(\omega_n t)] \right\} = \\
&= \frac{4m}{\pi n} [R(\omega_n) \sin(\omega_n t) + I(\omega_n) \cos(\omega_n t)] .
\end{aligned} \tag{6.7}$$

Thus, the total input is:

$$\underline{\theta}(t) = \sum_{n=odd}^{\infty} \underline{\theta}_n(t) = \frac{4m}{\pi} \sum_{n=odd}^{\infty} \left[\frac{R(\omega_n)}{n} \sin(\omega_n t) + \frac{I(\omega_n)}{n} \cos(\omega_n t) \right]. \tag{6.8}$$

We need to remind now the hypothesis 5.1. The switching conditions, derivable from figure 6.2, are:

$$\begin{cases}
\underline{u}(0) = -\underline{\theta}(0) = h, & (6.9) \\
\dot{\underline{u}}(0) = -\dot{\underline{\theta}}(0) > 0. & (6.10)
\end{cases}$$

Or:

$$\begin{cases}
\underline{u}\left(\frac{T}{2}\right) = -\underline{\theta}\left(\frac{T}{2}\right) = -h, & (6.11) \\
\dot{\underline{u}}\left(\frac{T}{2}\right) = -\dot{\underline{\theta}}\left(\frac{T}{2}\right) < 0. & (6.12)
\end{cases}$$

Replacing these switching conditions in 6.8 we obtain:

$$\begin{cases} \underline{\theta}(0) = \dfrac{4m}{\pi} \displaystyle\sum_{n=odd}^{\infty} \dfrac{I(\omega_n)}{n} = -h, & (6.13) \\ \underline{\dot{\theta}}(0) = \dfrac{4m}{\pi} \displaystyle\sum_{n=odd}^{\infty} \dfrac{\omega_n R(\omega_n)}{n} < 0, & (6.14) \end{cases}$$

where equation 6.14 is equivalent to:

$$\underline{\dot{\theta}}(0) = \sum_{n=odd}^{\infty} R(\omega_n) < 0. \tag{6.15}$$

Let us now define the *hodograph* as:

$$T(j\omega) \triangleq \sum_{n=odd}^{\infty} \left[R(\omega_n) + j \frac{I(\omega_n)}{n} \right]. \tag{6.16}$$

The switching conditions becomes:

$$\begin{cases} \Re\{T(j\omega)\} < 0, & (6.17) \\ \Im\{T(j\omega)\} = \dfrac{h\pi}{4m}. & (6.18) \end{cases}$$

Now the limit cycle can be determined using the graphical solution in the Gauss plane of the problem using the *hodograph*. Consider the example that is shown in figure 6.3.

The blue line is the *hodograph* $T(j\omega)$ and varies with the angular frequency ω. The red line represents the switching condition. The intersections between these two lines determine the limit cycles that are exact results because the Tsypkin method takes into account also high-order harmonics.

From the graphical point of view we can build-up the *hodograph* $T(j\omega)$ starting from the function $L(j\omega)$ as shown in figure 6.4. For every angular frequency ω_i the *hodograph* is built-up adding the real parts of the linear part using the odd harmonics and the imaginary parts divided by the degree of the harmonic. For example, stopping at the fifth harmonic:

$$\begin{aligned} T_1(j\omega_1) &= R_1(\omega_1) + jI_1(\omega_1) \\ T_3(j\omega_1) &= R_1(\omega_1) + R_3(3\omega_1) + j\left[I_1(\omega_1) + \frac{I_3(3\omega_1)}{3} \right] \\ T_5(j\omega_1) &= R_1(\omega_1) + R_3(3\omega_1) + R_5(5\omega_1) + \\ &\quad + j\left[I_1(\omega_1) + \frac{I_3(3\omega_1)}{3} + \frac{I_5(5\omega_1)}{5} \right]. \end{aligned} \tag{6.19}$$

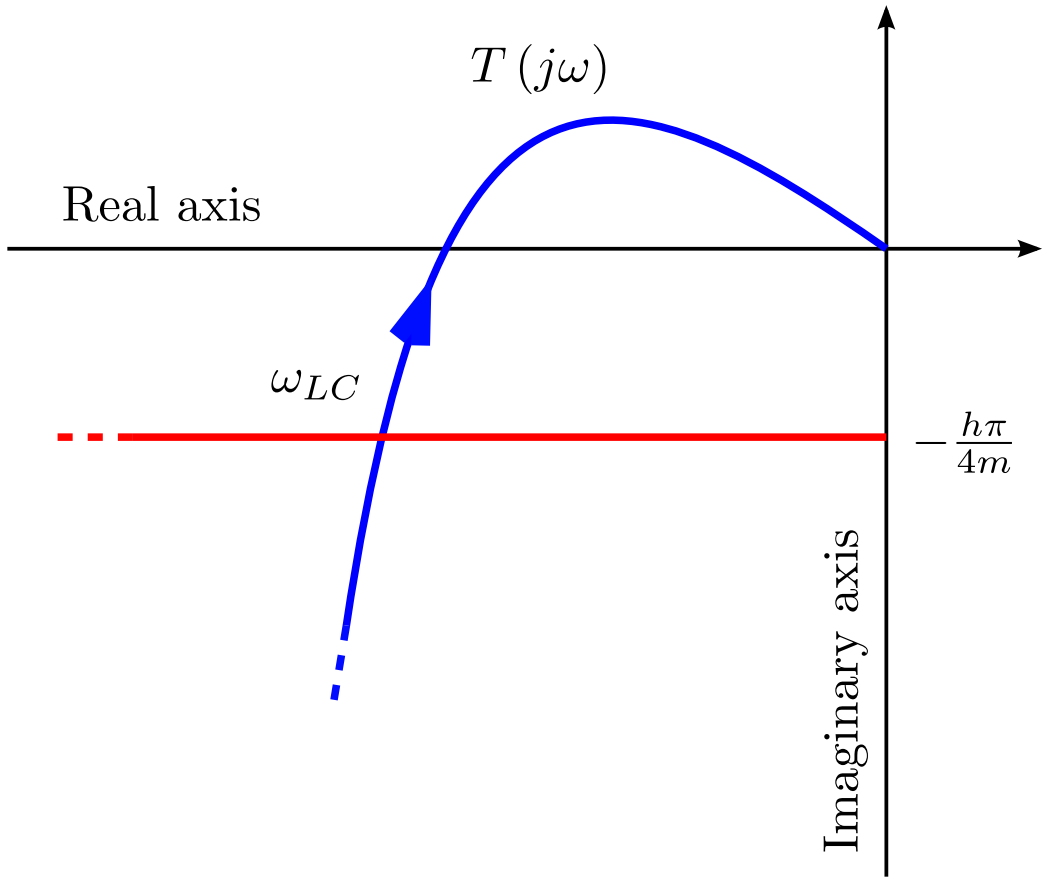

Figure 6.3: *hodograph* (blue) and switch condition (red). The intersections determine the angular frequency of the limit cycles.

The method is repeated until the real and imaginary components of the transfer function $L(j\omega)$ can be neglected.

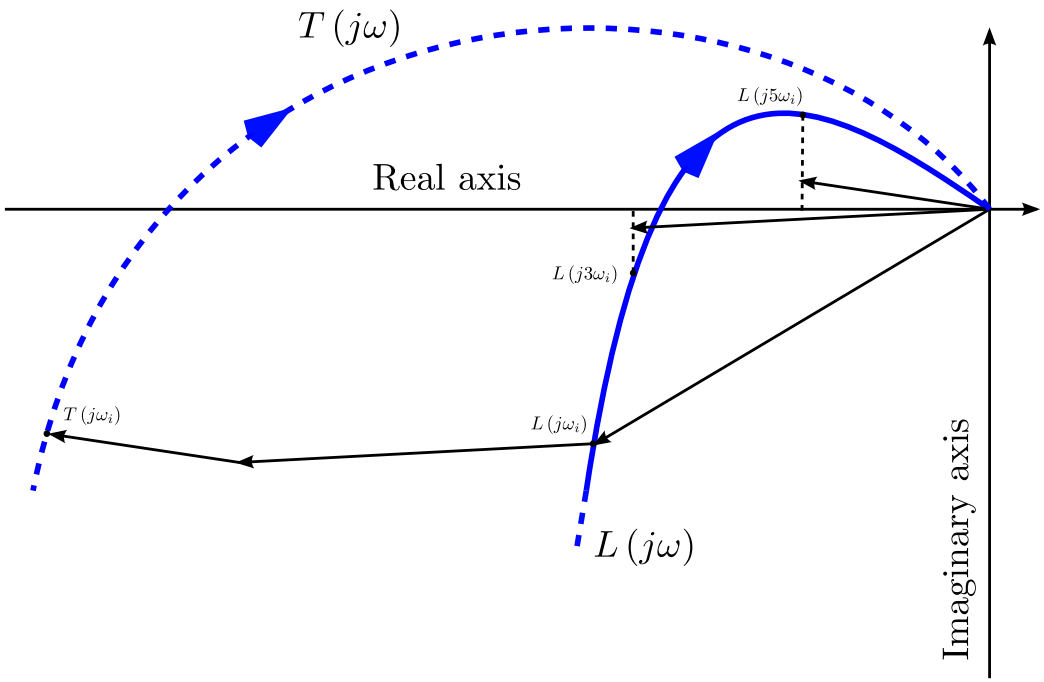

Figure 6.4: Graphical method used to determine the *hodograph* $T(j\omega)$ starting from $L(j\omega)$.

The stability of the limit cycle detected is investigated using the TSYPKIN version of the 1.

Criterion 2 (Limit cycle stability -TSYPKIN)**.** *The limit cycle previously determined by the Tsypkin method is stable if and only if the derivative of the imaginary part of the* hodograph *calculated for the angular frequency of the limit cycle with respect to* $j\omega$ *is positive. In other words the limit cycle at the angular frequency* ω_{LC} *is stable if and only if:*

$$\left.\frac{\mathrm{d}\left[\Im\left\{T(j\omega)\right\}\right]}{\mathrm{d}\omega}\right|_{\omega\to\omega_{LC}} > 0 \tag{6.20}$$

The closure of the series that most commonly appears in $T(j\omega)$ starting from $L(j\omega)$ are available in literature.

6.1.1 Remarks

The Tsypkin technique exactly determines the limit cycles that can appear in a nonlinear system that has a relay with hysteresis. This method can be

easily extended to other possible nonlinearities.

The main practical difference between the *classical describing function* method and the Tsypkin technique consists in the function that intersects the switching condition line or the function $-\frac{1}{N(A)}$. In the Tsypkin technique, the *hodograph* $T(j\omega)$ shall be considered while, in the *classical describing function*, the linear part of the system $L(j\omega)$ is used. Changing the method moves and usually decreases the angular frequency of the limit cycle predicted. This difference can be neglected if the linear part of the system satisfy the *filtering hypothesis*.

6.2 Hybrid Tsypkin-dual-input describing function

The *classical Tsypkin method* takes care just of the frequency of the limit cycle. On the other hand the bias and the amplitude of the limit cycle are already well-predicted by the *dual-input describing function* technique when the frequency is well-predicted. Thus, we will merge these two methods called into the *hybrid Tsypkin-dual-input describing function* technique.

The frequency is predicted by the *classical Tsypkin method*. In fact, as you can see in section 5.2, the frequency detection in the *dual-input describing function* technique does not rely on the disturbance or the amplitude or the bias of the limit cycle. Thus, this part can be directly replaced by the *classical Tsypkin method* without modifying the rest of the theory. Considering that the nonlinearity of our reference scenario has dead-zone and no hysteresis[4], the frequencies of the possible limit cycles are detected by the intersection of the *hodograph* of $L(j\omega)$ with the negative part of the real axis in the Gauss plane. Unfortunately the closure of the specific series of our case is not available in literature thus it is approximated using the equation 6.19 arrested at the third degree. Considering that we need just qualitative results to verify the considerations stated in section 5.3.2, this approximation is always acceptable. In order to determine the amplitude and the bias we use the *dual-input describing function* theory that already provides good results.

Finally we can state that the frequency is predicted by calculating the intersection of the approximated *hodograph* with the negative part of the real axis in the Gauss plane while the amplitude and the bias of the limit cycle are predicted using the usual *dual-input describing function* theory. In formulas, as we did in section 5.43, the set of equations and inequalities that allows the

[4] An extensive description of the *Tsypkin method* for this and other common nonlinearities is presented in [19].

determination of the limit cycle is:

$$\begin{cases} \Im\{T_3(j\omega)\} = 0, & (6.21) \\ \Re\{T_3(j\omega)\} < 0, & (6.22) \\ bN_b(b,A) + d = 0, & (6.23) \\ \Re\{T_3(j\omega)\} = -\dfrac{1}{N_{sw}(b,A)}, & (6.24) \end{cases}$$

where $T_3(j\omega)$ is the *hodograph* of the linear part of the system CPD arrested at the third degree. In formulas:

$$\begin{aligned} T_3(j\omega) = \Re\{CPD(\omega)\} + \Re\{CPD(3\omega)\} + \\ + j\left[\Im\{CPD(\omega)\} + \frac{\Im\{CPD(3\omega)\}}{3}\right]. \end{aligned} \tag{6.25}$$

As you can see, the equation 5.44 is replaced with the equations 6.21 and 6.22 derived from the *Tsypkin method*. Fortunately this modification is easily implementable in the routines already written during the development of the *dual-input describing function*. In the following section we will perform simulations to test this theory.

6.3 Simulations

The figures 6.5, 6.6, 6.7 and tables 6.1, 6.2, 6.3, respectively, show results of the simulations for three different values of the disturbance. Considering that this study has been performed to clarify the strange behavior of the system depicted in section 5.3.2, the disturbance varies out of the range defined in subsection 5.3.1.

		Predicted	**Real**	**Error**[%]
Bias	b	-0.1	-0.0999	0.0551
Amplitude	A	0.0225	0.0224	0.687
Frequency	f	0.0154	0.0151	2.430

Table 6.1: Results of MATLAB® SIMULINK® and MATHEMATICA® when $d = 0.05$Nm using the *hybrid Tsypkin-dual-input describing function* theory.

As you can see, the *hybrid Tsypkin-dual-input describing function* always produces more accurate results than the *dual-input describing function*.

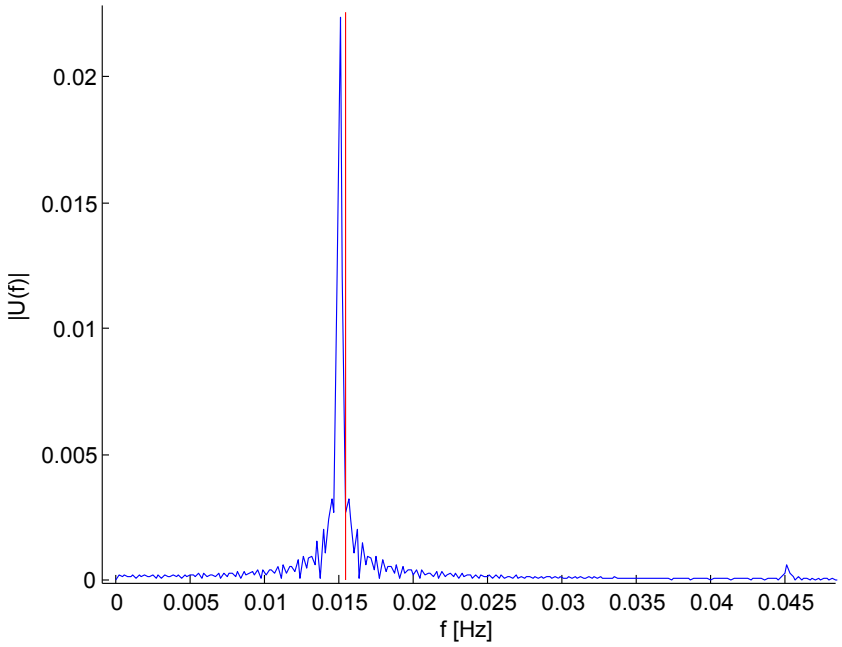

Figure 6.5: Single-sided amplitude spectrum simulated (blue) and predicted (red) using the *hybrid Tsypkin-dual-input describing function* theory of the signal $\underline{u}-b$ when $d = 0.05$Nm.

		Predicted	**Real**	**Error**[%]
Bias	b	-0.0893	-0.0887	0.715
Amplitude	A	0.0182	0.0182	0.0439
Frequency	f	0.0154	0.0139	10.8

Table 6.2: Results of MATLAB® SIMULINK® and MATHEMATICA® when $d = 0.03$Nm using the *hybrid Tsypkin-dual-input describing function* theory.

		Predicted	**Real**	**Error**[%]
Bias	b	-0.0934	-0.0828	12.8
Amplitude	A	0.007	0.0145	52
Frequency	f	0.0154	0.0097	58.7

Table 6.3: Results of MATLAB® SIMULINK® and MATHEMATICA® when $d = 0.01$Nm using the *hybrid Tsypkin-dual-input describing function* theory.

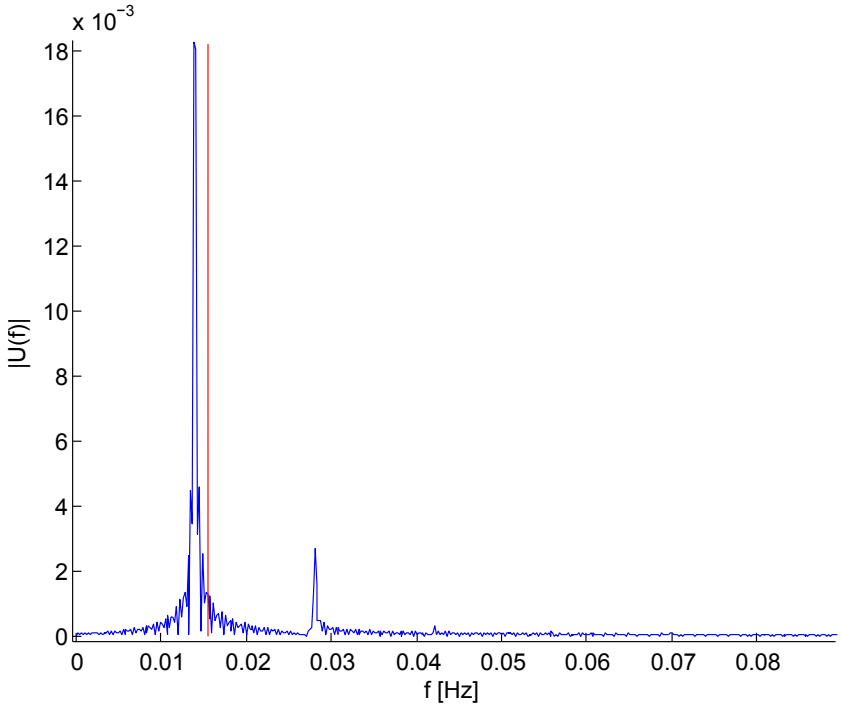

Figure 6.6: Single-sided amplitude spectrum simulated (blue) and predicted (red) using the *hybrid Tsypkin-dual-input describing function* theory of the signal $\underline{u}-b$ when $d = 0.03$Nm.

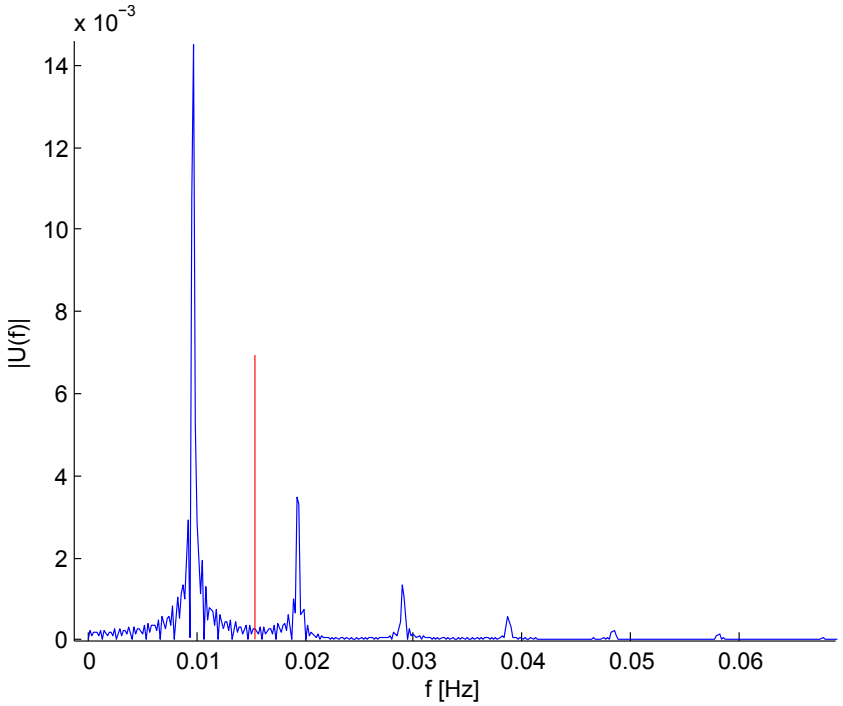

Figure 6.7: Single-sided amplitude spectrum simulated (blue) and predicted (red) using the *hybrid Tsypkin-dual-input describing function* theory of the signal $\underline{u}-b$ when $d = 0.01$Nm.

The determination of the frequency of the limit cycle in the *hybrid Tsypkin-dual-input describing function* does not rely on the disturbance. In fact, in equations 6.21 and 6.22, the disturbance does not appear. The analysis of the frequency error already performed in subsection 5.3.2 for the *dual-input describing function* method is shown in figure 6.8.

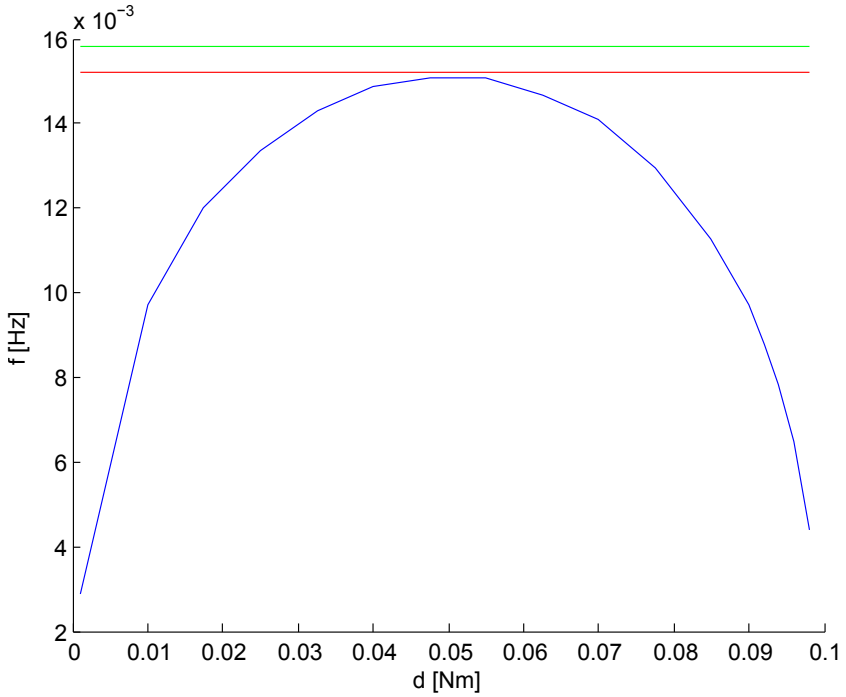

Figure 6.8: Frequency of the limit cycle simulated (blue), predicted (red) using the *hybrid Tsypkin-dual-input describing function* theory and predicted (green) using the *dual-input describing function* method varying the disturbance.

As you can see, the same strange behavior, described in subsection 5.3.2, occurs. The main difference with the analysis performed using the *dual-input describing function* is that the error decreases of a constant value independently on the disturbance. When the disturbance is around $\frac{m}{2}$ the frequency prediction is very close to the simulated. This behavior was expected due to the improved accuracy of the new method that takes into account also the second-order harmonic.

Considering the two analysis presented in figure 6.8 we can state that the consideration of the second-order harmonic has decreased the frequency of the limit cycle. Thus, it is reasonable that the addition of other high-order harmonics still decreases the frequency of the limit cycle.

As we said in subsection 5.3.2, when the disturbance moves away from the value $\frac{m}{2}$, other high-order harmonics can pass through the nonlinear block

more easily and can sensibly modify the output. Thus, we can state the following useful hypothesis verified by simulations:

Hypothesis 1 (Chaos zone)**.** *When the disturbance is not around* $\frac{m}{2}$*, a number* n *of high-order harmonics arise and pass trough the closed loop. This number* n *is strictly related to the disturbance value. In this case the system becomes very sensible to the disturbance signal. In other words, chaotic motion occurs.*

Thus, for a specific scenario, in order to avoid chaos motion, the thrusters shall be chosen so that the maximum torque provided is around twice the disturbance expected. From a different point of view we can state that, in order to apply the theory presented, the formula 5.56 shall be respected.

Part III

Limit cycles design

Chapter 7

Methods to design limit cycles

As we explained in chapter 5, a limit cycle occurs when the disturbance is not zero. It can be a *saturation limit cycle* or a *disturbance limit cycle*. In order to minimize fuel consumption *saturation limit cycles* shall be avoided. In fact, the counteracting behavior, characteristic of the *saturation limit cycle*, is very expensive in terms of fuel consumption. After this prerequisite, the *disturbance limit cycle* shall be well-shaped in order to meet bandwidth and *APE* requirements. All these aspects shall be considered during the design of the controller.

In the next sections we will present the *state of the art* concerning the design of the controller.

7.1 Trial and error

It is the first and simplest method possible. The parameters are guessed and a simulation trial is run. If the system does not meet the requirements the parameters are changed and a new simulation is run.

Many authors in [1], [16], [14] and [20] have presented searching algorithms of the parameters of the controller using the *trial and error* method. In particular, the *bifurcation analysis* presented in section 7.2 is a further development of the *trial and error* method.

The main disadvantage of this method is that the results of the previous simulation do not provide any aid for the next simulation. In other words the behavior trend of the system is uncorrelated with parameters. Therefore, the algorithm may not convergence. This means that computational costs may be prohibitive.

Pros	Cons
Theory is not required	Convergence is not guaranteed
It is very general	Computational costs may be prohibitive
	Computational costs can not be predicted
	The behavior trend of the system is uncorrelated with the parameters
	Every modification of the system requires a new fresh study

7.2 Bifurcation analysis

This method is the automatization of the *trial and error*. It determines an allowed region in the parameter space running simulations. Each parameter is varied over its span and the *Poincaré map*[1] is obtained. In the end, the requirements are checked and an allowed region in the parameter space is determined. This is the development of the *trial and error* method presented in section 7.1. The main difference is the goal; this method determines an allowed region, not only a possible solution. It has been studied in detail in [2], [15] and [17].

This technique is very general, it can be applied on every possible system. It can also study the chaos motion.

Considering that the whole parameter space shall be checked, computational costs rapidly increase with the increasing of the dimensions of the parameter space. Due to this problem, the number of parameters of the systems studied using this method is usually smaller than four.

Pros	Cons
Theory is not required	The behavior trend of the system is uncorrelated with the parameters
It is very general	Computational costs are high
	Computational costs become quickly unaffordable with the increasing of the number of parameters

[1]For further informations about the *Poincaré map* see [1].

7.3 Phase plane design

It is the natural development of the *phase plane analysis* depicted in section 4.2. It has been developed by MENDEL in [13]. As first the analytical functions that link the parameters and the limit cycle are derived by inverting the equations determined in the *phase plane analysis*. After that, these functions are used to determine an allowed region in the parameter space.

The hypothesis required by this technique are the same as those of the *phase plane analysis*. These functions are analytical, hence, they are related to the system. They are not general, every modification of the system requires the determination of new analytical functions.

Pros	**Cons**
Analytical cost functions	The system is fixed with some parameters that have to be settled
Graphical and analytical method	It is very specific
It is easy to see dynamics on the phase plane	The system may not be modified in order to include other possible parameters. Further study is needed

7.4 μ method

This is the natural extension of the μ method of the linear systems to the nonlinear ones. The *describing function* theory is applied and a more general version of the singular values is defined. Using this new definition, the nonlinear version of the usual theorems of the μ analysis are demonstrated. Obviously, the nonlinear version of the μ *method* is robust.

This technique requires some approximations and limitations. First of all, the usual hypothesis of the *describing function* theory shall be met. Moreover constant disturbances can not betaken into account explicitly. Anyway, the system can deal with them indirectly, if they are small enough, due to its robustness. The *classical describing function* theory is used. This means that the quasi-linearization of the nonlinear block does not explicitly rely on the bias. The bias is implicitly assumed small compared to the amplitude of the limit cycle. In particular, as stated in [20], the following inequality shall hold:

$$\frac{b}{A} \leq \frac{1}{3}. \tag{7.1}$$

The main goal of this technique is the determination of a robust controller which avoids *saturation limit cycles*. Constant disturbances are not considered,

hence, this method can not take into account *disturbance limit cycles*. In order to deal with these limit cycles, the *classical describing function* theory shall be replaced with the *dual-input describing function* technique. As a result a new, more general version of the singular values shall be defined and the usual theorems of the μ *method* proved.

Pros	**Cons**
Very general	Requires the usual *describing function* approximations
Allows the use of the μ analysis. A lot of literature about it is available	The bias is not taken into account explicitly
May be expanded with the *dual-input describing function* theory	The theory does not take into account *disturbance limit cycles*
The controller designed is robust	The usual theorems shall be reproved

7.5 Kharitonov approach

The *Kharitonov approach* is a systematic methodology that is developed to deal with nonlinear systems with parametric uncertainties. The selection of adjustable control parameters to predict and suppress the limit cycle is proposed. The *Kharitonov's theorem* is exploited. The characteristic equation of the considered system is decomposed into two related stability equations. By solving these two associated stability equations, a constant limit cycle locus can be plotted on the parameter plane. The locus divides the plane into stable and unstable regions to allow flexible choice of admissible parameter sets. The steady state limit cycle is then studied using a family of vertex characteristic polynomials. Thus we can confine the limit cycle to obtain a specified control system performance for the entire uncertain control system. The goal is to determine the feasible controller parameter sets in order to suppress *saturation limit cycles* persisting in an uncertain pitch orientation control system. The limit cycle behavior at the system output is also addressed.

This method provides an allowed region in the parameter space. It has been studied specifically to deal with uncertainties of the plant, thus, it is robust. In particular, each coefficient of the transfer function of the plant can range over its span. The number of ranging coefficients does not increase significantly the computational costs because the *Kharitonov's theorem* is used[2] in this method. The nonlinearity is approximated using the

[2]This property of the system will be discussed in detail in section 9.

classical describing function technique, hence, the usual approximations of the *describing functions* shall be valid. The disturbance is not taken into account explicitly, therefore, the approximation 7.1 shall be valid. The delay is replaced with its first-order PADÉ approximant. As we stated in subsection 5.2.4, the frequency of the limit cycle shall meet bandwidth requirements, therefore, this approximation is always valid. This method is very general and flexible. A solution remains valid also if the plant change slightly.

Disturbances are not taken into account, therefore, the theory shall be modified. The *dual-input describing function* shall replace the *classical describing function* theory.

Pros	**Cons**
Very general	The general assumptions of the *describing function* theory shall be valid
The delay can be always replaced with the PADÉ approximant	The delay can not be taken into account without approximation
May be expanded with the *dual-input describing function* theory getting rid of the approximation 7.1	*Disturbance limit cycles* can not be studied by the *classical describing function* theory. It must be replaced by the *dual-input describing function*
Very flexible	
It is robust	
Changing the parameters show the trend of the system	

7.6 Remarks

The *Kharitonov approach* is chosen because it is the most general and versatile method. Moreover it is robust and varying parameters show the trend of the system. In order to deal with *disturbance limit cycles*, the *classical describing function* will be replaced with the *dual-input describing function* theory. Thus, as we did in chapter 5, the *dual-input Kharitonov approach* will be developed.

As we saw in section 5.2.4 a lag network is needed just to approximate the system as continuous. This strange purpose requires to design it in an unconventional way. Moreover it is uncorrelated to the design of the rest of the system. At the contrary, the *dual-input Kharitonov approach* depends

on the lag network. Therefore, it will be studied as first and in a separate chapter.

Chapter 8

Lag network design

In order to approximate the discrete system with its continuous version, as is stated in section 5.2.4, a lag network is needed. Empirically, the delay needed is at least ten times greater than the sampling time of the slowest block. It shall be verified by simulations. In formulas:

$$\frac{10}{AOCS} \leq \tau_{C_2} \tag{8.1}$$

where τ_{C_2} is the equivalent delay of the lag network of the controller. When input signal does not contain high-order harmonics, as in our case, the lag network is equivalent to a pure delay. Using an inverse *Padé approximant*-like method:

$$\frac{s - z_2}{s - p_2} = \frac{z_2}{p_2} \frac{s\left(-\frac{1}{z_2}\right) + 1}{s\left(-\frac{1}{p_2}\right) + 1} \approx \frac{z_2}{p_2} \frac{e^{\left(-\frac{1}{z_2}\right)s}}{e^{\left(-\frac{1}{p_2}\right)s}} = \frac{z_2}{p_2} e^{-\left(\frac{1}{z_2} - \frac{1}{p_2}\right)s}. \tag{8.2}$$

Thus:

$$\tau_{C_2} \approx \frac{1}{z_2} - \frac{1}{p_2}. \tag{8.3}$$

Considering the equation 2.15, the equivalent delay τ_{C_2} is always positive as shall be.

Chapter 9

Kharitonov approach

The first section of this chapter will introduce the *classical Kharitonov approach*. After that, in order to fit our system, some adjustments will be performed. The lag network required to approximate the discrete sensor as continuous will be designed and the amplitude requirements of our scenario will be manipulated to fit the *Kharitonov approach*. Finally, the *dual-input Kharitonov approach* will be developed, simulations will be run and results will be discussed.

9.1 Classical Kharitonov approach

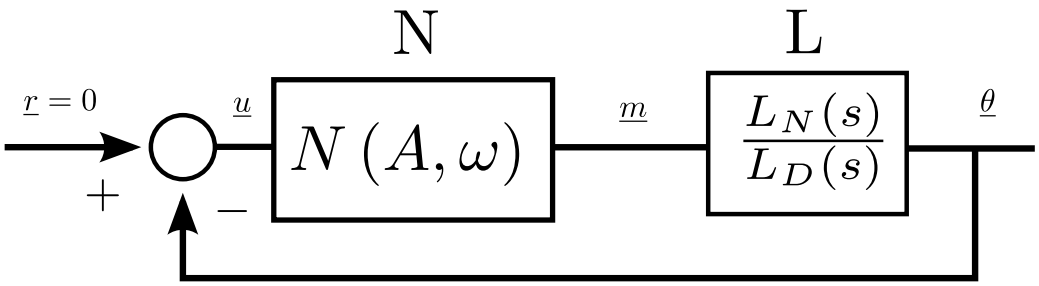

Figure 9.1: The control system with uncertain plant and nonlinearity.

Consider[1] a typical unity feedback control system with an inherent nonlinearity as shown in figure 9.1. Let the linear part of the entire system, $L(js)$, be the considered uncertain plant with bounded parametric uncertainties. Let us assume that the *philtering hypothesis* is verified, so that the high-order harmonics can be neglected. In this case the *classical describing function*

[1]The *classical Kharitonov approach* given here is akin to that in [10].

theory can be applied and the nonlinearity can be replaced with its *describing function*. In general, the nonlinearity may involve saturation, hysteresis, dead-zone or relay, that are usually found in practical control systems. Without loss of generality, a hysteresis component is considered here.

The general expression of the frequency response of the uncertain linear plant $L(js)$ can be given as:

$$L(j\omega) = \left| \frac{a_0 + a_1 s + a_2 s^2 + \cdots + a_m s^m}{b_0 + b_1 s + b_2 s^2 + \cdots + b_n s^n} \right|_{s \to j\omega} = \frac{L_N(j\omega)}{L_D(j\omega)} \tag{9.1}$$

where:

$$a_i \in \left[a_i^-, a_i^+\right], \tag{9.2}$$
$$b_j \in \left[b_j^-, b_j^+\right], \tag{9.3}$$
$$a_m \neq 0, \tag{9.4}$$
$$b_n \neq 0, \tag{9.5}$$
$$n \geq m. \tag{9.6}$$

The *describing function* of the nonlinear component is:

$$N(A, \omega) = R(A, \omega) + jI(A, \omega) \tag{9.7}$$

where:

$$R(A, \omega) = \Re\{N(A, \omega)\}, \tag{9.8}$$
$$I(A, \omega) = \Im\{N(A, \omega)\}. \tag{9.9}$$

As is stated in [20], all the most common nonlinearities does not explicitly rely on the frequency ω. In formulas:

$$N = N(A). \tag{9.10}$$

As usual the *characteristic equation* is:

$$1 + L(j\omega) N(A) = 0. \tag{9.11}$$

The nonlinearity induces limit cycles when a solution of:

$$L(j\omega) = -\frac{1}{N(A)} \tag{9.12}$$

can be found.

Since the plant considered is subject to parametric uncertainties, a family of polynomials can be arranged from the left hand side of equation 9.12 and expressed as:

$$F\left(s,\vec{r},\vec{q}\right)=\sum_{i=0}^{n}\left(r_i+jq_i\right)s^i \tag{9.13}$$

where:

$$[\vec{q},\vec{r}]\in\Re. \tag{9.14}$$

These vectors of coefficients $\vec{r}$ and $\vec{q}$ denote the real and the imaginary part of the coefficients of s^i respectively. For the sake of clarity they are 0-indexed. It is assumed that:

$$r_i^-\leq r_i\leq r_i^+ \tag{9.15}$$
$$q_i^-\leq q_i\leq q_i^+ \tag{9.16}$$

where the variables r_i^- and q_i^- are the lower parameter bounds, and r_i^+ and q_i^+ are the higher parameter bounds. A set of transfer functions can be generated by picking up the boundary values of the perturbed coefficients. Given R and Q as the uncertain bounding sets for r and q, respectively, we call:

$$\Gamma=\left\{F\left(s,\vec{r},\vec{q}\right)|r\in R,q\in Q\right\} \tag{9.17}$$

as a complex coefficient interval polynomial family. Henceforth, the polynomial 9.13 can be further written as:

$$F\left(s,\vec{r},\vec{q}\right)=\sum_{i=0}^{n}\left(\left[r_i^-,r_i^+\right]+j\left[q_i^-,q_i^+\right]\right)s^i. \tag{9.18}$$

It turns out that investigating the stability of the closed-loop uncertain control system is equivalent to testing the stability of the entire family of interval polynomials 9.18. The *Kharitonov's theorem* can be exploited to analyze the stability characteristics of an interval polynomial as shown below.

Theorem 1 (Kharitonov's theorem)**.** *A complex coefficient interval polynomial family* Γ *with invariant degree is robustly stable if and only if the following eight* vertex polynomials *are stable. The first four polynomials,*

$$
\begin{aligned}
K_1^+(s) &= \left(r_0^- + jq_0^-\right) + \left(r_1^- + jq_1^+\right)s + \left(r_2^+ + jq_2^+\right)s^2 + \left(r_3^+ + jq_3^-\right)s^3 + \cdots, \\
K_2^+(s) &= \left(r_0^+ + jq_0^+\right) + \left(r_1^+ + jq_1^-\right)s + \left(r_2^- + jq_2^-\right)s^2 + \left(r_3^- + jq_3^+\right)s^3 + \cdots, \\
K_3^+(s) &= \left(r_0^+ + jq_0^-\right) + \left(r_1^- + jq_1^-\right)s + \left(r_2^- + jq_2^+\right)s^2 + \left(r_3^+ + jq_3^+\right)s^3 + \cdots, \\
K_4^+(s) &= \left(r_0^- + jq_0^+\right) + \left(r_1^+ + jq_1^+\right)s + \left(r_2^+ + jq_2^-\right)s^2 + \left(r_3^- + jq_3^-\right)s^3 + \cdots,
\end{aligned}
\tag{9.19}
$$

are associated with positive ω^+, and the second four polynomials,

$$
\begin{aligned}
K_1^-(s) &= \left(r_0^- + jq_0^-\right) + \left(r_1^+ + jq_1^-\right)s + \left(r_2^+ + jq_2^+\right)s^2 + \left(r_3^- + jq_3^+\right)s^3 + \cdots, \\
K_2^-(s) &= \left(r_0^+ + jq_0^+\right) + \left(r_1^- + jq_1^+\right)s + \left(r_2^- + jq_2^-\right)s^2 + \left(r_3^+ + jq_3^-\right)s^3 + \cdots, \\
K_3^-(s) &= \left(r_0^+ + jq_0^-\right) + \left(r_1^+ + jq_1^+\right)s + \left(r_2^- + jq_2^+\right)s^2 + \left(r_3^- + jq_3^-\right)s^3 + \cdots, \\
K_4^-(s) &= \left(r_0^- + jq_0^+\right) + \left(r_1^- + jq_1^-\right)s + \left(r_2^+ + jq_2^-\right)s^2 + \left(r_3^+ + jq_3^+\right)s^3 + \cdots,
\end{aligned}
\tag{9.20}
$$

are associated with negative ω^-.

for the sake of completion the theorem 1 will be demonstrate in appendix B.

We need to underline that, if the vector coefficients $\vec{r}$ and $\vec{q}$ are real, then, the sets of equations 9.19 and 9.20 are equal.

The complex nonlinearities result in complex coefficients in the characteristic polynomial, as shown in equation 9.18. According to the *Kharitonov's theorem*, the entire family of interval polynomials 9.18 is asymptotically stable if and only if the eight fixed Kharitonov polynomials 9.19 and 9.20 are asymptotically stable.

In order to determine an allowed region in the parameter space, its boundary is searched. Therefore, the amplitude is set equal to the requirement. This means that the right hand of the equation 9.12 is a number. At this point the complex equation 9.12 can be divided in a set of two scalar equations:

$$
\begin{cases}
\Re\left\{L(j\omega)\right\} &= -\Re\left\{\frac{1}{N(A)}\right\}, \\
\Im\left\{L(j\omega)\right\} &= -\Im\left\{\frac{1}{N(A)}\right\}.
\end{cases}
\tag{9.21}
$$

For every *vertex polynomial*, this set of equations is a function of the frequency and of the unknown parameters of the controller. These parameters are extrapolated as functions of the frequency and eight parametric curves are plotted in the parameter space. Each curve divide the space in two zones. Which of them is the allowed zone depends on the Jacobian of the

set of equations 9.21 as stated in [9]. The intersection of the allowed zones is the allowed region of the parameter space that respects the amplitude requirements. The typical allowed zone for a system with two unknown parameters is shown in figure 9.2.

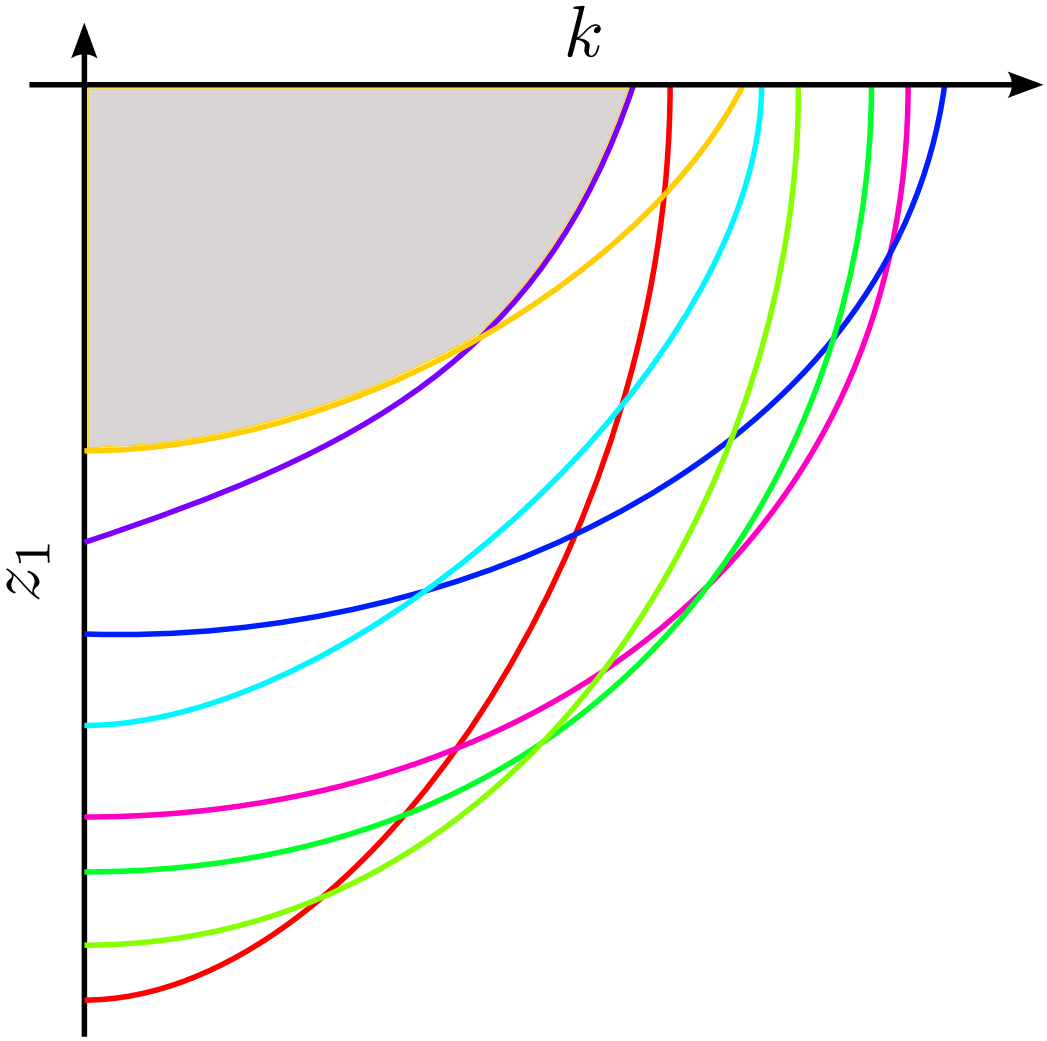

Figure 9.2: Robust allowed region for $A \leq \overline{A}$.

9.2 The amplitude requirement

Before presenting the *dual-input Kharitonov approach* the amplitude requirement shall be manipulated. In fact, in the *classical Kharitonov approach*, the

amplitude constraint refers to the input of the nonlinearity $\underline{u}$ while the APE, our amplitude requirement, refers to the amplitude of $\underline{\theta}$.

For the sake of convenience let us define A_θ as the amplitude of the limit cycle of $\underline{\theta}$. Moreover let us recall that A is the amplitude of the limit cycle of $\underline{u}$.

Consider the main loop of our generic system reproposed in figure 9.3. We want to translate the APE requirement in an amplitude constraint for $\underline{u}$. In order to do so, we have to study the transfer function between $\underline{\theta}$ and $\underline{u}$. There are two possible paths:

- The feed-forward pathway.
- The feedback pathway.

The feed-forward pathway

It passes trough the nonlinearity, the delay and the plant. Considering that we are interested on the amplitude, the nonlinearity can be replaced with the *describing function* of the sine wave subsystem[2] $N_{sw}(b, A)$. The pure delay, instead, can be replaced with its usual *Padé approximant*.

The *Kharitonov approach* is intrinsically robust because the coefficients of the plant are defined by their ranges. Therefore the transfer function from $\underline{u}$ to $\underline{\theta}$ is:

$$NDP = N_{sw}(b, A)\, D(\tau, s)\, P(MoI, s) \tag{9.22}$$

where we have specified the unknown variables $\{b, A\}$ and the varying coefficients $\{\tau, MoI\}$. As we will show in section 9.3, the bias will be:

$$b = f(d, A) \tag{9.23}$$

where f is the stepwise, *auxiliary function*.

This means that the transfer function, following the feed-forward path, is:

$$\begin{aligned} NDP &= N_{sw}(b, A)\, D(\tau, s)\, P(MoI, s) = \\ &= N_{sw}[f(d, A), A]\, D(\tau, s)\, P(MoI, s). \end{aligned} \tag{9.24}$$

Due to the properties of the LTI blocks and considering that $N_{sw}(b, A)$ is a variable gain, the link between A and A_θ is:

[2]We are adapting the *Kharitonov approach* to take care of the disturbances, hence, the *dual-input describing function* shall be used.

$$A \left\| |NDP|_{s\to j\omega} \right\| = A \left\| N_{sw}\left[f\left(d,A\right),A\right] D\left(\tau,j\omega\right) P\left(MoI,j\omega\right) \right\| = A_\theta \quad (9.25)$$

where ω is the angular frequency of the limit cycle[3].

We need to stress that $N_{sw}\left(b,A\right)$ is a stepwise function. This means that NDP is a stepwise function nested in a stepwise function that can not be easily simplified. Thus, the use of the feed-forward pathway is very complicate.

The feedback pathway

It passes just through the controller. The lag part has been already designed in chapter 8. The lead network, instead, has not been already determined because the *dual-input Kharitonov approach* needs the translation of the amplitude requirement. Therefore, letting the lead network unknown, the transfer function between $\underline{\theta}$ and $\underline{u}$ is:

$$A_\theta \left\| |C|_{s\to j\omega} \right\| = \left\| C\left(z_1,p_1,k,j\omega\right) \right\| = A \quad (9.26)$$

where, as before, ω is the angular frequency of the limit cycle.

This pathway is much easier than the feed-forward pathway. In particular there are no stepwise functions. The only issue is the presence of the unknown lead network.

Considering the issues presented by the two paths, the feedback pathway will be used.

Let us now recall the APE requirement:

$$A_\theta \leq APE \quad (9.27)$$

Substituting equation 9.26 into the APE constraint we have:

$$\frac{A}{\left\| C\left(z_1,p_1,k,j\omega\right) \right\|} \leq APE. \quad (9.28)$$

In order to obtain an amplitude constraint, we can manipulate the inequality:

$$A \leq \left\| C\left(z_1,p_1,k,j\omega\right) \right\| APE. \quad (9.29)$$

As we stated before, the lead network can not be determined at this stage. This also means that the angular frequency ω of the limit cycle can not be

[3]We need to underline that the limit cycle of $\underline{u}$ has the same frequency of the limit cycle of $\underline{\theta}$ because neither the nonlinearity nor the plant nor the pure delay modify it.

determined. Therefore, the constraint 9.29 shall be replaced with a stricter but computable one. It is obvious that the largest stricter constraint which is computable is:

$$A \leq \min_{z_1,p_1,k,j\omega} \{\|C(z_1,p_1,k,j\omega)\|\} APE. \tag{9.30}$$

Let us now focus on this minimization of C. In particular let us recall the transfer function of the controller:

$$C = k\frac{(s-z_1)}{(s-p_1)}\frac{(s-z_2)}{(s-p_2)}. \tag{9.31}$$

For definition, the magnitude of C for a generic angular frequency ω is:

$$\|C(z_1,p_1,k,j\omega)\| \triangleq |k| \sqrt{\frac{(\omega^2+z_1^2)(\omega^2+z_2^2)}{(\omega^2+p_1^2)(\omega^2+p_2^2)}}. \tag{9.32}$$

We need to recall that the lag network has been already designed in chapter 8. In particular z_2 and p_2 are known parameters.

In order to avoid the null solution, let us fix some bounds for $\{z_1, p_1, k\}$. In particular these unknowns shall fulfill the following inequalities:

$$\begin{cases} z_1 & \leq z_1^+, \\ p_1 & \geq p_1^-, \\ k & \geq k^-. \end{cases} \tag{9.33}$$

We have to add to this set of constraints the following inequalities which come from the definition of lead network:

$$p_1 < z_1 < 0. \tag{9.34}$$

In the end, considering that ω is the angular frequency of the limit cycle, from section 5.2.3, the following equation shall hold:

$$\Im\{CPD(\tau, MoI, \omega)\} = 0 \tag{9.35}$$

where we have specified the varying parameters $\{\tau, MoI\}$ and the unknown variable ω. In fact, in the *Kharitonov approach*, the coefficients of the plant are not specified. They can vary over specific ranges. As we did in section 9.1, let us define their spans:

$$\tau \in \left[\tau^-, \tau^+\right], \tag{9.36}$$

$$MoI \in \left[MoI^-, MoI^+\right]. \tag{9.37}$$

Let us focus on the angular frequency of the limit cycle ω, due to a corollary of the *fundamental theorem of algebra*, if ω is a solution of 9.35, then, also $-\omega$ is a solution. Moreover, due to the fact that ω appears always to the square, the function 9.32 assumes the same value for ω and for $-\omega$. Therefore, we can limit our study to the positive ω without loss of generality.

9.2.1 Summary

Let us now summarize the results of this section.

The amplitude constraint required by the *dual-input Kharitonov approach* is:

$$A \leq \min_{z_1,p_1,k,j\omega} \{\|C(z_1,p_1,k,j\omega)\|\} APE. \tag{9.38}$$

For the sake of convenience we can define:

$$\overline{A} \triangleq \min_{z_1,p_1,k,j\omega} \{\|C(z_1,p_1,k,j\omega)\|\} APE. \tag{9.39}$$

Therefore, the constraint 9.38 becomes:

$$A \leq \overline{A}. \tag{9.40}$$

The minimization $\min_{z_1,p_1,k,j\omega} \{\|C(z_1,p_1,k,j\omega)\|\}$ shall be performed considering the following additional constraints:

$$\begin{cases} z_1 \leq z_1^+, & (9.41)\\ p_1 \geq p_1^-, & (9.42)\\ k \geq k^-, & (9.43)\\ p_1 < z_1 < 0 & (9.44)\\ \Im\{CPD(\tau, MoI, j\omega)\} = 0 & (9.45)\\ \omega > 0, & (9.46)\\ \tau \in \left[\tau^-, \tau^+\right], & (9.47)\\ MoI \in \left[MoI^-, MoI^+\right]. & (9.48) \end{cases}$$

This minimization, albeit very expensive in terms of computational costs, can be carried out by MATHEMATICA®.

In the end we need to stress that, in order to avoid *saturation limit cycles*, the following inequality shall hold:

$$A < h. \tag{9.49}$$

It can be easily extrapolated from figure 5.10. This is another amplitude requirement. Obviously only the stricter constraint between inequalities 9.38 and 9.49 shall be taken into account in the *dual-input Kharitonov approach.*

Typically the translation of the APE requirement is stricter. Usually:

$$\overline{A} \ll h. \tag{9.50}$$

9.3 Dual-input Kharitonov approach

The *classical Kharitonov approach* can not be applied directly to our system. In fact the method uses the *classical describing function* theory which is not suitable for systems with slowly varying disturbances. In this case, as we saw in chapter 5, the *dual-input describing function* technique shall be used instead. Thus, in this section we will develop the *dual-input Kharitonov approach* which, using the *dual-input describing function* theory, takes into account slowly varying disturbances without the approximation 7.1. This new approach let us shape *disturbance limit cycles* to meet requirements while avoiding *saturation limit cycles.*

First of all, let us fix, as has been done in the *classical Kharitonov approach*, the amplitude A equal to its upper bound:

$$A = \overline{A}. \tag{9.51}$$

which have been determined in section 9.2. For the sake of simplicity, without loss of generality, we can set also:

$$d > 0. \tag{9.52}$$

Now focus on the main loop reproposed in figure 9.3.

The lag part of the controller has already been designed in chapter 8. Thus, the main purpose of the *dual-input Kharitonov approach* is the design of the lead network of the controller. In particular we have to chose the zero z_1, the pole p_1 and the gain k keeping in mind that, for definition of lead network, the inequalities 2.14 hold. Moreover, in order to allow the translation of the APE requirement, these parameters shall fulfill the set of inequalities 9.33.

Let us now divide the main loop, as we did in section 5.2, in the *bias* and the *sine wave subsystems* shown in figure 5.4 and reproposed in 9.4 for the sake of convenience. Following the theory presented chapter 5, let us consider the *auxiliary equation* 5.35. This time, conversely to subsection 5.2.1, the amplitude is known and the disturbance can vary over its span. Therefore, the *auxiliary equation* links the bias b with the disturbance d:

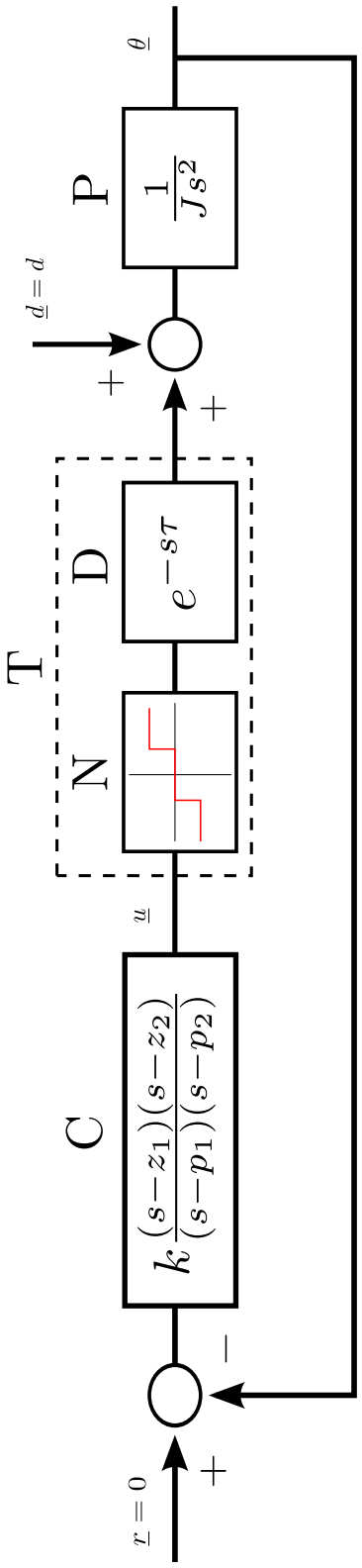

Figure 9.3: Block diagram of the controlled system.

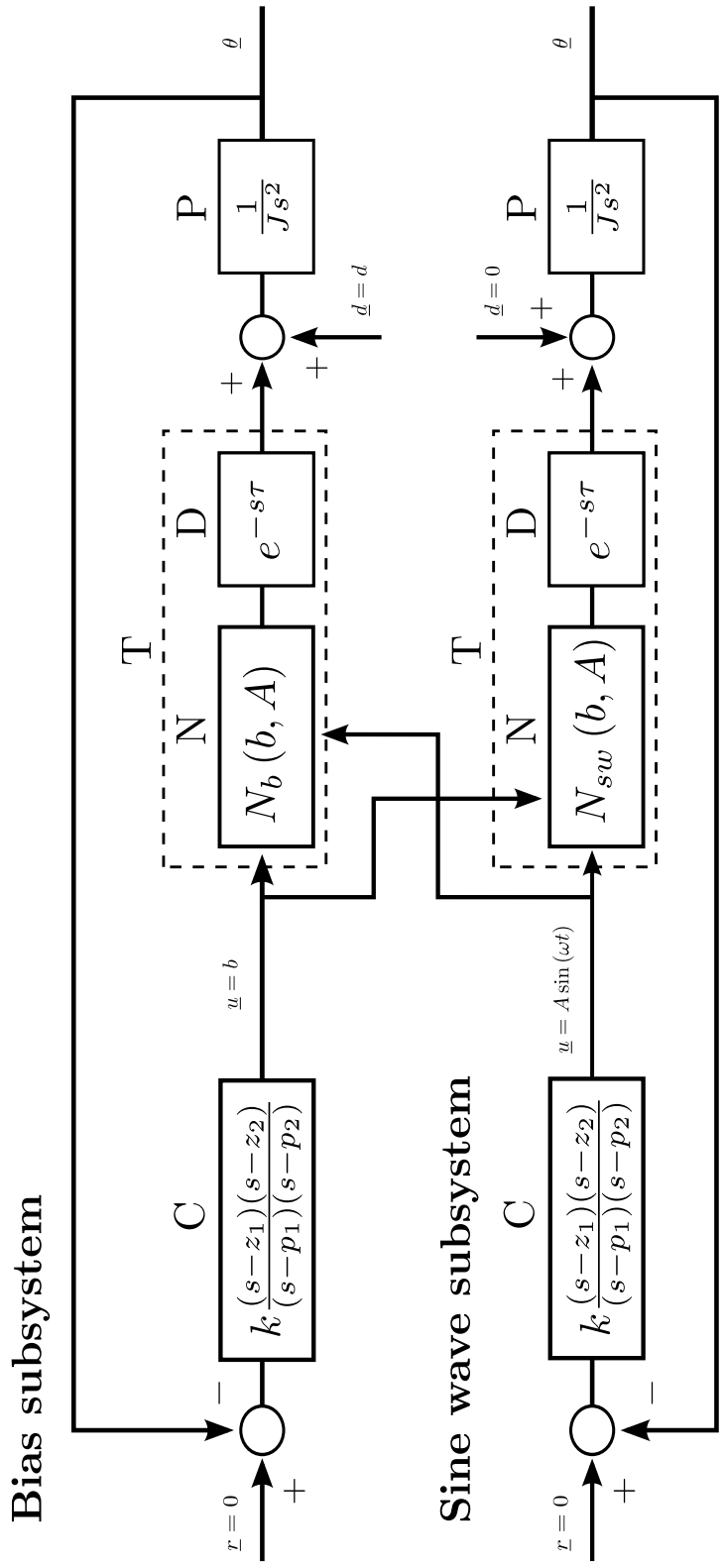

Figure 9.4: Bias and amplitude subsystems.

$$b = f(d) \tag{9.53}$$

where:

$$d \in \left[d^-, d^+\right]. \tag{9.54}$$

In order to apply the theory, as stated in chapter 6, the set 9.54 shall be:

$$\left[d^-, d^+\right] \subseteq \left[\frac{3m}{10}, \frac{7m}{10}\right]. \tag{9.55}$$

Let us now recall, for the sake of convenience, the implicit version of the *auxiliary equation*:

$$bN_b\left(b, \overline{A}\right) + d = 0. \tag{9.56}$$

where:

$$N_b\left(b, \overline{A}\right) = \frac{m}{b}\left[p\left(\frac{h+b}{\overline{A}}\right) - p\left(\frac{h-b}{\overline{A}}\right)\right] \tag{9.57}$$

and:

$$p(x) = \begin{cases} -\frac{1}{2} & x < -1 \\ \frac{1}{\pi}\arcsin(x) & |x| \leq 1 \\ \frac{1}{2} & x > 1 \end{cases}. \tag{9.58}$$

Replacing equation 9.57 in 9.56 and manipulating the result we get:

$$p\left(\frac{h-b}{\overline{A}}\right) - p\left(\frac{h+b}{\overline{A}}\right) = \frac{d}{m}. \tag{9.59}$$

For the sake of clarity, the stepwise function $p(x)$ is shown in figure 9.5.

Let us now study the behavior of the stepwise function $p\left(\frac{h-b}{\overline{A}}\right) - p\left(\frac{h+b}{\overline{A}}\right)$. Considering that the inequality 9.50 holds, the zone where:

$$p\left(\frac{h-b}{\overline{A}}\right) = \frac{1}{\pi}\arcsin\left(\frac{h-b}{\overline{A}}\right) \tag{9.60}$$

does not overlap the region where:

$$p\left(\frac{h+b}{\overline{A}}\right) = \frac{1}{\pi}\arcsin\left(\frac{h+b}{\overline{A}}\right). \tag{9.61}$$

Therefore, the stepwise function $p\left(\frac{h-b}{\overline{A}}\right) - p\left(\frac{h+b}{\overline{A}}\right)$ is:

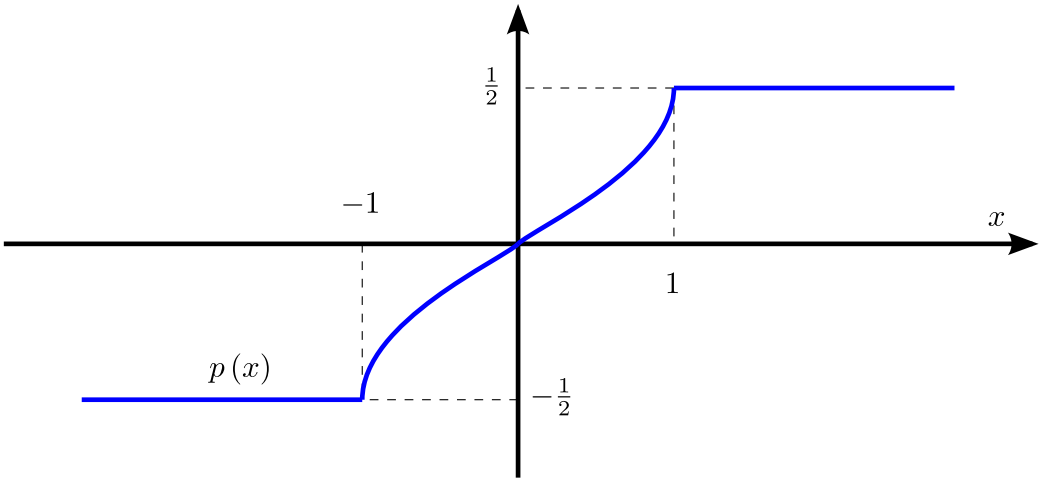

Figure 9.5: The function $p(x)$.

$$p\left(\frac{h-b}{\overline{A}}\right)-p\left(\frac{h+b}{\overline{A}}\right)=\begin{cases}1 & b\leq -h-\overline{A}\\ \frac{1}{2}-\frac{1}{\pi}\arcsin\left(\frac{h+b}{\overline{A}}\right) & -h-\overline{A}<b\leq -h+\overline{A}\\ 0 & -h+\overline{A}<b\leq h-\overline{A}\\ -\left[\frac{1}{2}-\frac{1}{\pi}\arcsin\left(\frac{h-b}{\overline{A}}\right)\right] & -h-\overline{A}<b\leq -h+\overline{A}\\ -1 & h+\overline{A}<b\end{cases} \tag{9.62}$$

Its shape is shown in figure 9.6.

The blue line is the function $p\left(\frac{h-b}{\overline{A}}\right)-p\left(\frac{h+b}{\overline{A}}\right)$. As you can see, considering that the disturbance is positive and bounded by 9.55, we can restrict our study to the zone:

$$b\in\left[-h-\overline{A},-h+\overline{A}\right]. \tag{9.63}$$

Therefore, we can explicit analytically the bias in the *auxiliary function*. Keeping in mind that the bias is bounded, as stated in 9.63, it becomes:

$$\begin{aligned} b&=\overline{A}\sin\left[\pi\left(\frac{1}{2}-\frac{d}{m}\right)\right]-h=\\ &=\overline{A}\cos\left(\frac{\pi d}{m}\right)-h. \end{aligned} \tag{9.64}$$

Obviously, if the disturbance is negative and bounded in:

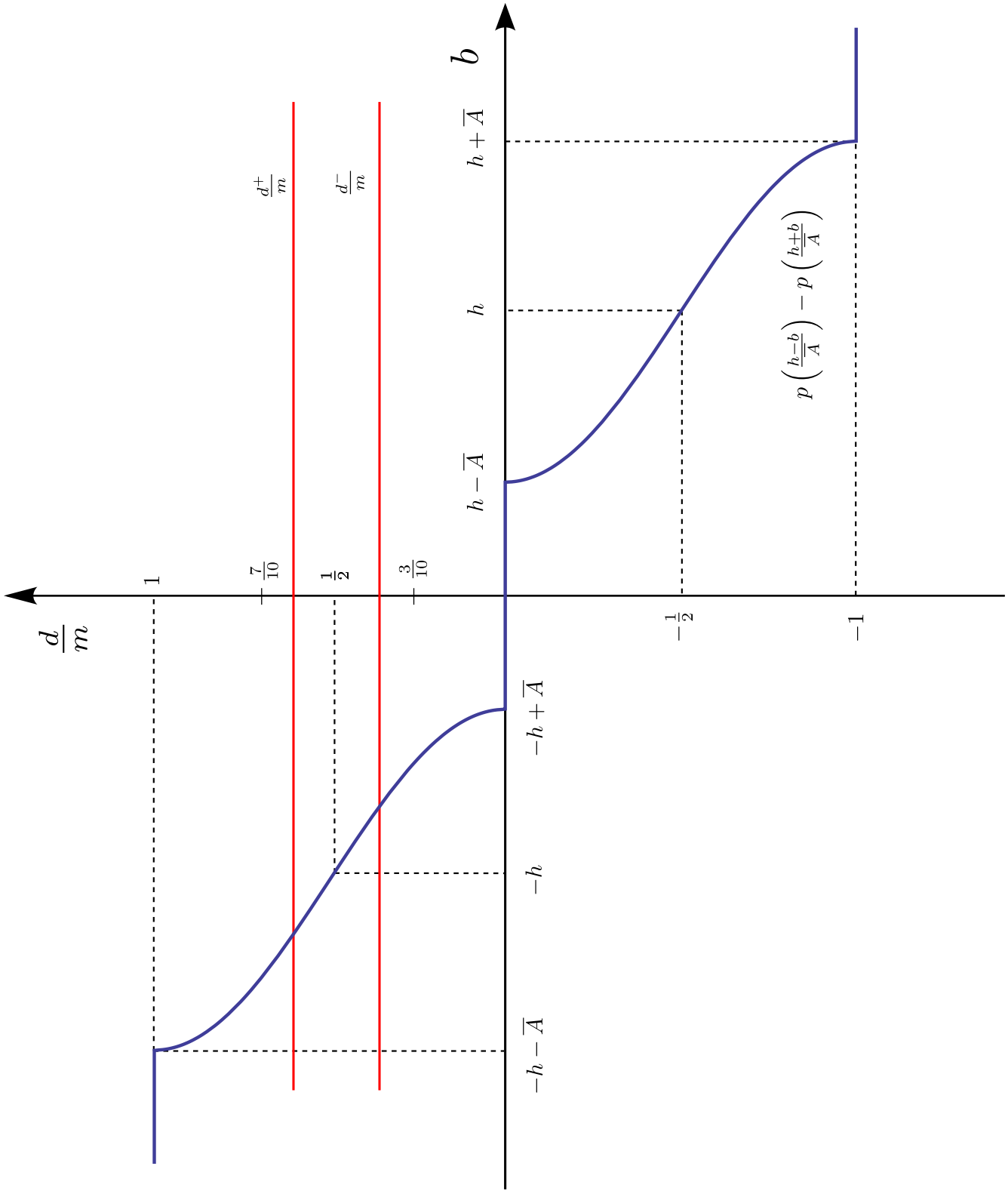

Figure 9.6: $p\left(\frac{h-b}{A}\right)-p\left(\frac{h+b}{A}\right)$ as function of b (blue) and dimensionless bounds of the disturbance (red).

$$\left[d^-, d^+\right] \subseteq \left[-\frac{7m}{10}, -\frac{3m}{10}\right]. \tag{9.65}$$

the bias is:

$$b \in \left[h - \overline{A}, h + \overline{A}\right] \tag{9.66}$$

and the *auxiliary function* becomes:

$$b = h - \overline{A}\cos\left(\frac{\pi d}{m}\right) \tag{9.67}$$

Let us now focus on the *sine wave subsystem*. In particular, let us study the *dual-input describing function* $N_{sw}(b, A)$. For the sake of convenience we will repropose it:

$$N_{sw}(b, A) = \frac{m}{A}\left[q\left(\frac{h+b}{A}\right) + q\left(\frac{h-b}{A}\right)\right], \tag{9.68}$$

where:

$$q(x) = \begin{cases} \frac{2}{\pi}\sqrt{1-x^2} & |x| \leq 1 \\ 0 & |x| > 1 \end{cases}. \tag{9.69}$$

Differently from subsection 5.2.2, this time the amplitude is known and the bias is linked by the *auxiliary function* to the disturbance. Therefore, keeping in mind that the bias and the disturbance are bounded, we can explicit the value of N_{sw}:

$$N_{sw} = N_{sw}(d) \tag{9.70}$$

Substituting 9.64 in 9.68 we obtain:

$$\begin{aligned} N_{sw}(d) &= \frac{m}{A}\left[q\left(\frac{h+b}{A}\right) + q\left(\frac{h-b}{A}\right)\right] = \\ &= \frac{2m}{\pi A}\sqrt{1 - \left(\frac{h+b}{A}\right)^2} = \\ &= \frac{2m}{\pi A}\sqrt{1 - \cos^2\left(\frac{\pi d}{m}\right)} = \\ &= \frac{2m}{\pi A}\sin\left(\frac{\pi d}{m}\right). \end{aligned} \tag{9.71}$$

It is easy to show that, if the disturbance is negative, the equation 9.71 does not change.

We can now identify the bounds of the variable gain $N_{sw}(d)$. In fact its obvious that,keeping in mind that the disturbance is bounded:

$$\min_d \{N_{sw}(d)\} \leq N_{sw}(d) \leq \max_d \{N_{sw}(d)\}. \tag{9.72}$$

For the sake of convenience, let us define:

$$N_{sw}^- = \min_d \{N_{sw}(d)\}, \tag{9.73}$$

$$N_{sw}^+ = \max_d \{N_{sw}(d)\}. \tag{9.74}$$

Thus:

$$N_{sw}(d) \in \left[N_{sw}^-, N_{sw}^+\right]. \tag{9.75}$$

Finally, we are ready to apply the *Kharitonov theorem*. Let us consider the *characteristic equation* which will be reproposed here for convenience:

$$1 + CPDN_{sw}(d) = 0. \tag{9.76}$$

Since the coefficients $\{\tau, MoI, N_{sw}\}$ are uncertain and the lead network is unknown, a family of polynomials Γ can be arranged. These coefficients are bounded and the unknowns shall satisfy some inequalities. These constraints are:

$$\begin{cases} \tau \in \left[\tau^-, \tau^+\right], & (9.77) \\ MoI \in \left[MoI^-, MoI^+\right], & (9.78) \\ N_{sw} \in \left[N_{sw}^-, N_{sw}^+\right], & (9.79) \\ z_1 \leq z_1^+, & (9.80) \\ p_1 \geq p_1^-, & (9.81) \\ k \geq k^-, & (9.82) \\ p_1 < z_1 < 0. & (9.83) \end{cases}$$

Exactly as we did in section 9.1, we can now find the four *Kharitonov polynomials*[4] and define in the parameter space an allowed region W:

$$W \in \mathbb{R}^3. \tag{9.84}$$

The typical allowed zone for a system with two unknown parameters is shown in figure 9.7.

[4]They are only four because the coefficients are all real.

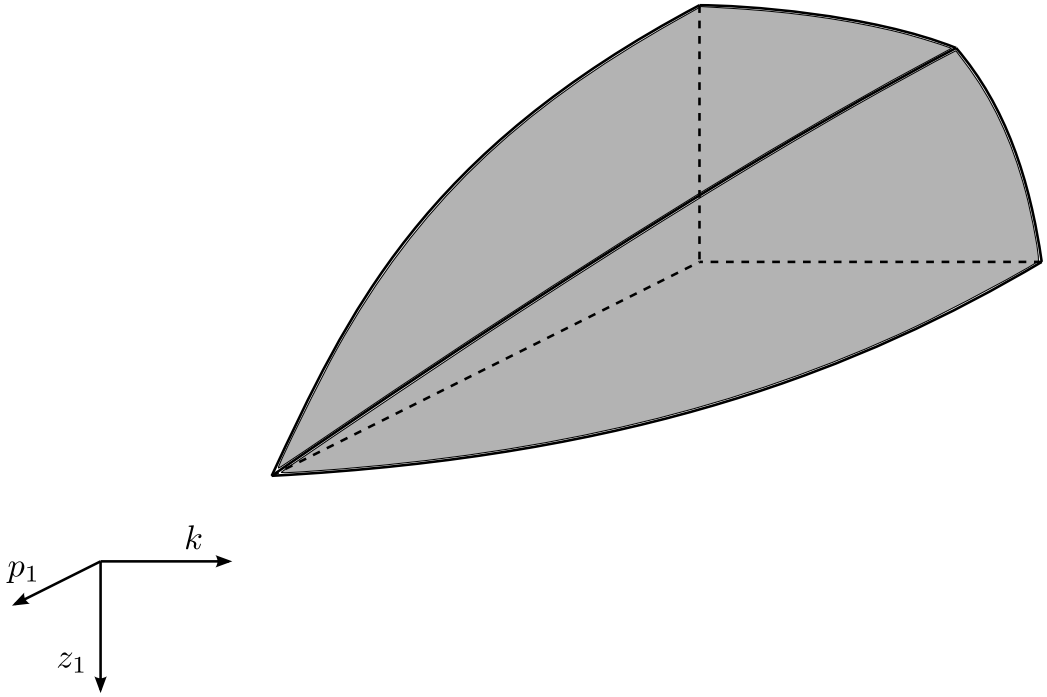

Figure 9.7: Robust allowed region for $A \leq \overline{A}$.

9.3.1 Remarks

In order to apply the *Kharitonov approach*, a constraint on the amplitude of the signal $\underline{u}$ is needed. There are two requirement that involve it:

- The avoiding of the *saturation limit cycles*. They shall be prevented because, due to the the typical counteracting behavior, they are very expensive in terms of fuel consumption.
- The APE requirement. It is a constraint on A_θ which obviously affects A.

Usually the APE requirement is the more compelling one. The translation from the APE requirement to a constraint on A is possible albeit very expensive in terms of computational costs. In particular it becomes prohibitive when the number of unknowns grows up.

The *dual-input Kharitonov approach*, improving the *classical Kharitonov approach*, takes into account the disturbance. Due to the fact that the disturbance is difficult to find precisely, it is a new uncertain parameter which varies over its range. This means that the bias is uncertain too because the *auxiliary function* links them analytically. Consequently N_{sw}, which

depends also on the bias, is an uncertain parameter that ranges over a span. Therefore, the *dual-input Kharitonov approach* uses the *dual-input describing function* theory to find a link between the disturbance and N_{sw}. After that, the problem is solved with the *classical Kharitonov approach* where shall be kept in mind that, this time, N_{sw} is an additional uncertain gain.

The parameters of the controller define the parameter space. Therefore, if the number of parameters is n and they are real, the parameter space $\mho$ is:

$$\mho \subseteq \mathbb{R}^n. \tag{9.85}$$

Obviously, if the parameters are complex:

$$\mho \subseteq \mathbb{C}^n. \tag{9.86}$$

Let us define the region defined by each *Kharitonov polynomial* as $\wp$. Each *vertex polynomial* provides two scalar equations. These equations depend on the parameters of the controller and on the unknown ω. Thus:

$$\wp \subseteq \mathbb{R}^{n+1-2} = \mathbb{R}^{n-1}. \tag{9.87}$$

If the parameters are complex:

$$\wp \subseteq \mathbb{C}^{n-1}. \tag{9.88}$$

The allowed region is bounded by the *vertex polynomials*, which have $n-1$ dimensions, and by the direct constraints on the parameters used to translate the APE requirement.

The major issue of this method is the computational cost needed to determine the amplitude constraint. In fact they become almost prohibitive when the parameters of the lead network are three or more. In the following section we will present the *sectioning variant* of the *dual-input Kharitonov approach* which greatly mitigates this problem.

9.3.2 Sectioning variant

In this variant the allowed region is created by an interpolation of *2-D* allowed zones. For the sake of clarity and convenience, let us focus on the general system shown in figure 9.3 where the unknown part of the controller is a lead network. First of all we shall preventively set an array of poles $\underline{p}$ linearly or logarithmically spaced over the range of the allowed poles. For each pole we can find the *2-D* allowed region in the *restricted parameter space*. Obviously, it is the plane of the zero and the gain of the lead network. In the general parameter space, it corresponds to the section defined by the fixed pole.

At the end, the allowed region in the general parameter space is built up interpolating the *2-D* zones. Figure 9.8 graphically explains this method.

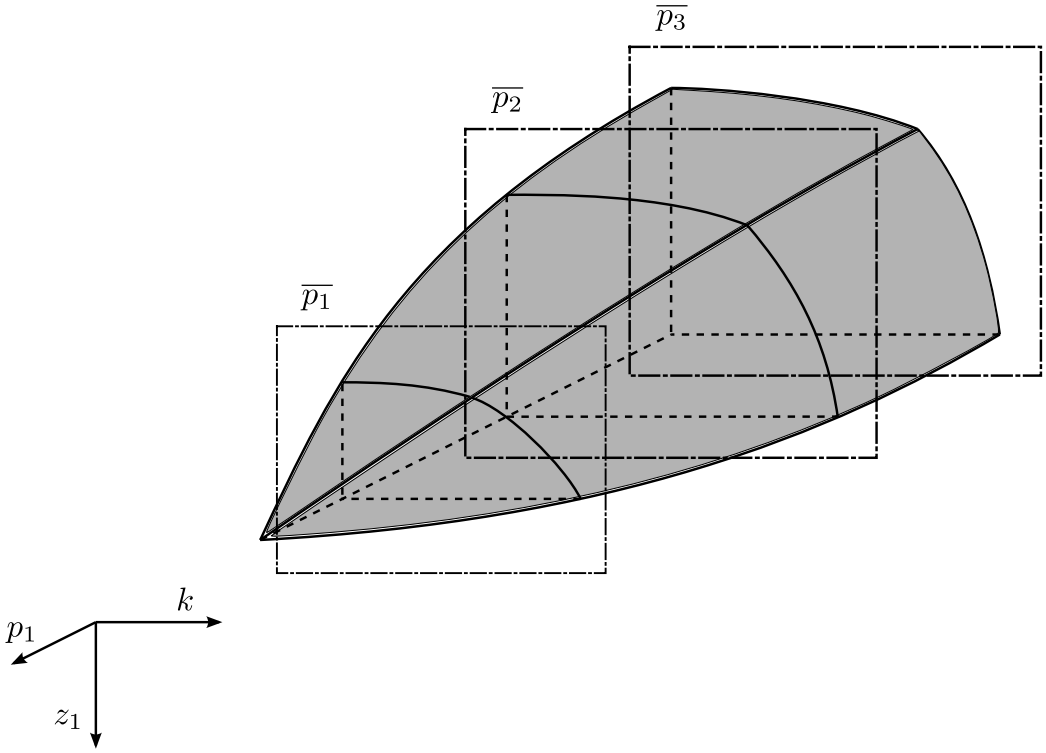

Figure 9.8: Robust allowed region for $A \leq \overline{A}$ built up interpolating the allowed sections.

With this method, the amplitude constraint is calculated separately for each section. It is obvious that:

$$\overline{A} \leq \overline{A}_i \tag{9.89}$$

where $\overline{A}_i$ is the amplitude constraint for the section i. This means that:

$$|\wp|_{p_1=\overline{p_i}} \subseteq \wp_i \tag{9.90}$$

where $|\wp|_{p_1=\overline{p_i}}$ is the section i of the allowed zone calculated in the general way and $\wp_i$ is the same section calculated by the *sectioning variant*. Therefore, the interpolated allowed zone in the total parameter space $\wp_s$ is:

$$\wp \subseteq \wp_s. \tag{9.91}$$

Let us recall now that, in order to ensure the APE requirement, the amplitude constraint is greatly underestimated. Moreover, it is even more

underestimated with the increasing number of the parameters. This means that the computed allowed zone is much more smaller then the effective one. Consequently, another major advantage of the *sectioning variant* method is that it underestimates less the allowed region.

9.4 Testing of the theory

In this section we will present the application of the *dual-input Kharitonov approach* to our reference scenario. The purpose is the determination of the parameters of the controller to fit the requirements. After that, simulations will be performed to test the new approach. In the end, considerations will be stated.

9.4.1 Application of the theory

First of all, let us summarize the principal steps of the theory that shall be executed:

1. Determination of the lag network.
2. Determination of the amplitude constraint.
3. Application of the *dual-input Kharitonov approach.*

Determination of the lag network

As we stated in section 7.6, the lag network shall be determined first. Equations 8.1 and 8.3 provide a constraint between z_2 and p_2. In our reference scenario it is:

$$1 \leq \frac{1}{z_2} - \frac{1}{p_2} \tag{9.92}$$

Considering that z_2 and p_2 shall be strictly negative, we can derive the following inequalities:

$$-1 \leq p_2 \leq 0, \tag{9.93}$$

$$z_2 \leq \frac{p_2}{p_2 + 1}. \tag{9.94}$$

Thus, in order to satisfy these constraints, we set:

$$p_2 = -10^{-1} \text{ Hz} \tag{9.95}$$
$$z_2 = -1 \text{ Hz} \tag{9.96}$$

The constraint 8.1 becomes:

$$1 \text{ Hz} = \frac{10}{AOCS} \leq \frac{1}{z_2} - \frac{1}{p_2} = 9 \text{ Hz}. \tag{9.97}$$

Determination of the amplitude constraint

First of all let us recall the two requirements that involve amplitude constraints:

- *Saturation limit cycles* avoiding.
- The APE requirement.

Saturation limit cycles avoiding As is stated in section 9.2, the inequality 9.49 ensures that the *saturation limit cycles* do not occur. In our reference scenario it is:

$$A < 10^{-1} \text{ rad}. \tag{9.98}$$

The APE requirement The determination of the APE requirement is almost always the strictest one. As we stated in subsection 9.3.1, the direct computation of the allowed zone in the *3-D* parameter space is prohibitive. Moreover, as is stated in 9.3.2, the allowed region computed with the general method is heavily underestimated. In order to solve these issues we will use the *sectioning variant* of the *dual-input Kharitonov approach.*

First of all, let us set the array of the allowed poles $\vec{p_1}$:

$$\vec{p_1} = -\{2, 3, 4, 5, 6, 7, 8, 9, 10\} \text{ Hz}, \tag{9.99}$$

which is an array of nine elements $p_{1,i}$ linearly spaced.

In order to derive the corresponding array of amplitude constraints, we need to translate the APE requirement. It is expressed in degrees while it is needed in radiants.

$$APE = 10^{-1} \, ^\circ = 10^{-1} \frac{\pi}{180} \text{ rad} \tag{9.100}$$

Now we are ready to evaluate the array of amplitude constraints[5]. As is stated in section 9.2, each A_i shall be evaluated by the following minimization:

$$A_i = \left(10^{-1}\frac{\pi}{180}\right) \min_{z_1,k,j\omega} \left\{ k\sqrt{\left(\frac{z_1^2+\omega^2}{p_{1,i}^2+\omega^2}\right)\left(\frac{1+\omega^2}{10^{-2}+\omega^2}\right)} \right\} \tag{9.101}$$

where:

$$\begin{cases} z_1 \leq -\dfrac{1}{1000} \text{ Hz}, & (9.102) \\ k \geq \dfrac{1}{10}\dfrac{\text{V}}{\text{rad}}, & (9.103) \\ p_{1,i} < z_1 < 0 & (9.104) \\ \Im\left\{\dfrac{10k\,(j\omega - z_1)\,(j\omega+1)\,(\tau j\omega - 2)}{(j\omega - p_{1,i})\,(10j\omega+1)\,(\tau j\omega+2)}\right\} = 0 & (9.105) \\ \omega > 0, & (9.106) \\ \tau \in \left[\dfrac{1}{10}, \dfrac{3}{10}\right] \text{ s}, & (9.107) \\ MoI \in [350, 450] \text{ kgm}^2. & (9.108) \end{cases}$$

It can be carried out by MATHEMATICA®. The resulting $\vec{A}$ is:

$$\begin{aligned} \vec{A} = \Big\{ &\frac{\pi}{18540}, \frac{\pi}{35280}, \frac{\pi}{52020}, \frac{\pi}{68760}, \frac{\pi}{85500}, \\ &\frac{\pi}{102240}, \frac{\pi}{118980}, \frac{\pi}{135720}, \frac{\pi}{152460}, \frac{\pi}{169200} \Big\}. \end{aligned} \tag{9.109}$$

Application of the dual-input Kharitonov approach

First of all, for the sake of clarity, we need to recall that we decided to apply the *sectioning variant* of the *dual-input Kharitonov approach*. Thus, the following generic operations shall be performed for every section associated to p_i and A_i.

Let us now set the range of the disturbance. Keeping in mind the equation 9.55, we have:

$$d \in \left[\frac{3}{100}, \frac{7}{100}\right] \text{ Nm} \tag{9.110}$$

[5]For the sake of simplicity, it will be called $\vec{A}$ instead of $\overrightarrow{A}$.

Now we are ready to apply the *dual-input Kharitonov approach* to the reference scenario.

The *auxiliary function* 9.64 is:

$$b = A_i \cos(10\pi d) - \frac{1}{10}. \tag{9.111}$$

Thus, $N_{sw}(d)$ of 9.71 is:

$$N_{sw,i}(d) = \frac{1}{5\pi A_i} \sin(10\pi d). \tag{9.112}$$

Now, keeping in mind equation 9.110, we can compute the range of 9.112:

$$N_{sw,i}(d) \in \left[\frac{1}{20\pi A_i}\left(1+\sqrt{5}\right), \frac{1}{5\pi A_i}\right]. \tag{9.113}$$

The coefficients $\vec{r}$ of the *characteristic equation*[6] 9.13 depends on $\{\tau, MoI, N_{sw,i}, z_1, p_i, k\}$. In the canonical form the *characteristic equation* 9.76 is:

$$\begin{aligned} &-(20kN_{sw,i}z_1) + (20kN_{sw,i} - 20kN_{sw,i}z_1 + 10kN_{sw,i}z_1\tau)\, s + \\ &+ (20kN_{sw,i} - 2MoIp_i - 10kN_{sw,i}\tau + 10kN_{sw,i}z_1\tau)\, s^2 + \\ &+ (2MoI - 20MoIp_i - 10kN_{sw,i}\tau - MoIp_i\tau)\, s^3 + \\ &+ (20MoI + MoI\tau - 10MoIp_i\tau)\, s^4 + (10MoI\tau)\, s^5 = 0 \end{aligned} \tag{9.114}$$

The elements of $\vec{r}$ are, for definition:

$$r_0 \triangleq 20kN_{sw,i}z_1, \tag{9.115}$$
$$r_1 \triangleq 20kN_{sw,i} - 20kN_{sw,i}z_1 + 10kN_{sw,i}z_1, \tau \tag{9.116}$$
$$r_2 \triangleq 20kN_{sw,i} - 2MoIp_i - 10kN_{sw,i}\tau + 10kN_{sw,i}z_1\tau, \tag{9.117}$$
$$r_3 \triangleq 2MoI - 20MoIp_i - 10kN_{sw,i}\tau - MoIp_i\tau, \tag{9.118}$$
$$r_4 \triangleq 20MoI + MoI\tau - 10MoIp_i\tau, \tag{9.119}$$
$$r_5 \triangleq 10MoI\tau. \tag{9.120}$$

Their ranges are:

[6]The coefficients of the reference scenario are strictly real. Thus, $\vec{q}$ is not needed and the *vertex polynomials* are only four.

$$r_0 \in \left[\min_{N_{sw,i}} \{r_0\}, \max_{N_{sw,i}} \{r_0\} \right], \tag{9.121}$$

$$r_1 \in \left[\min_{N_{sw,i,\tau}} \{r_1\}, \max_{N_{sw,i,\tau}} \{r_1\} \right], \tag{9.122}$$

$$r_2 \in \left[\min_{N_{sw,i,\tau,MoI}} \{r_2\}, \max_{N_{sw,i,\tau,MoI}} \{r_2\} \right], \tag{9.123}$$

$$r_3 \in \left[\min_{N_{sw,i,\tau,MoI}} \{r_3\}, \max_{N_{sw,i,\tau,MoI}} \{r_3\} \right], \tag{9.124}$$

$$r_4 \in \left[\min_{\tau,MoI} \{r_4\}, \max_{\tau,MoI} \{r_4\} \right], \tag{9.125}$$

$$r_5 \in \left[\min_{\tau,MoI} \{r_5\}, \max_{\tau,MoI} \{r_5\} \right]. \tag{9.126}$$

They are computed by MATHEMATICA®. Now the four *Kharitonov polynomials* K_i can be determined. Each one produces the following pair of equations:

$$\Re \{ \mid K_i(z_1, k, s) \mid_{s \to j\omega} \} = 0, \tag{9.127}$$

$$\Im \{ \mid K_i(z_1, k, s) \mid_{s \to j\omega} \} = 0, \tag{9.128}$$

that define a parametric curve in the z_1-k plane where the parameter is ω. All these four curves plus the constraints on z_1 and k determine the section of the allowed region in the section related to the pole p_i.

In the end, the interpolation of these sections in the general parameter space defines the total allowed region.

9.4.2 Results

The *restricted allowed zones*, for different values of the pole p_1, are shown in figures 9.9, 9.10, 9.11, 9.12, 9.13, 9.14, 9.15, 9.16 and , 9.17. As you can see, the behavior is similar to that one depicted in 9.3.2.

In figure 9.18 is presented the general allowed region. For the sake of clarity, it is rotated with respect to the qualitative graphic presented in figure 9.7.

9.4.3 Simulations

Let us now test results.

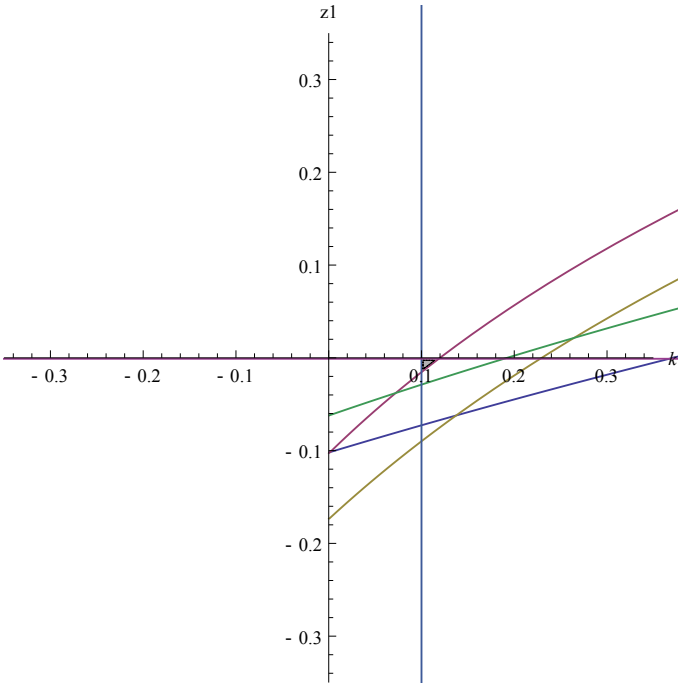

Figure 9.9: The *restricted allowed zone* (grey) for $p_1 = -2$ Hz.

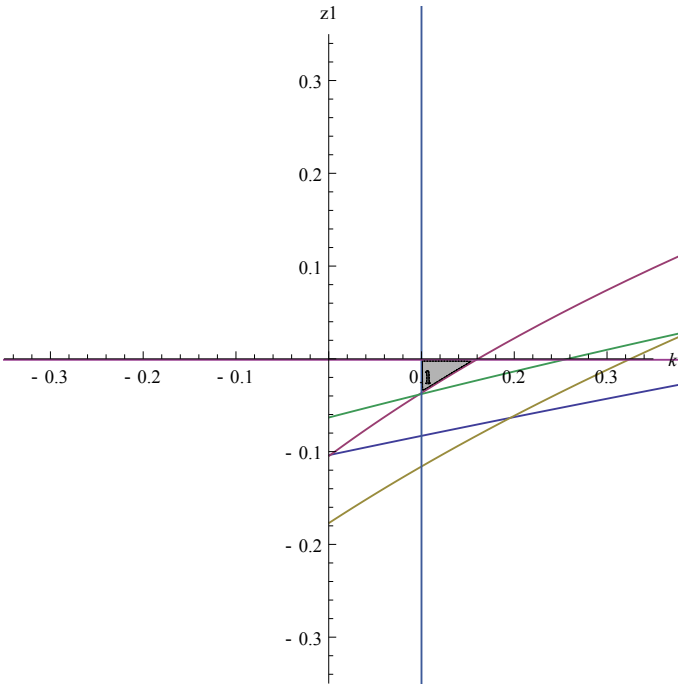

Figure 9.10: The *restricted allowed zone* (grey) for $p_1 = -3$ Hz.

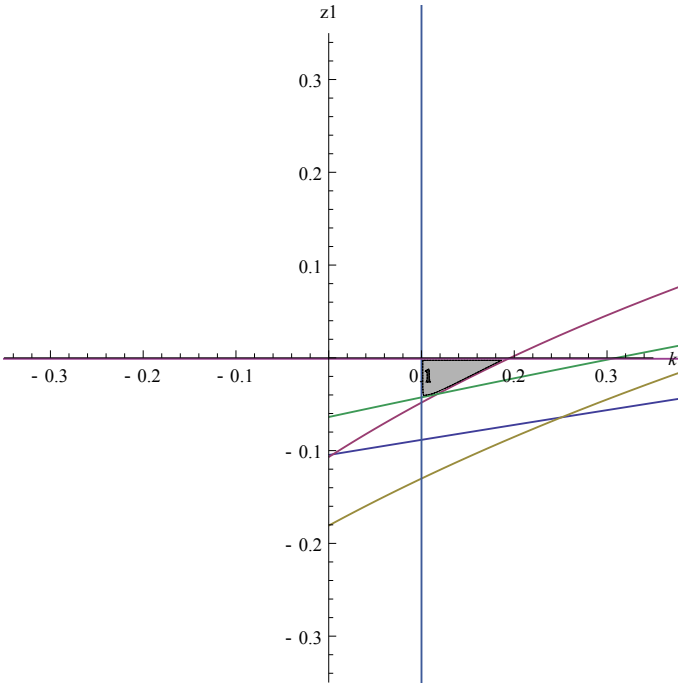

Figure 9.11: The *restricted allowed zone* (grey) for $p_1 = -4$ Hz.

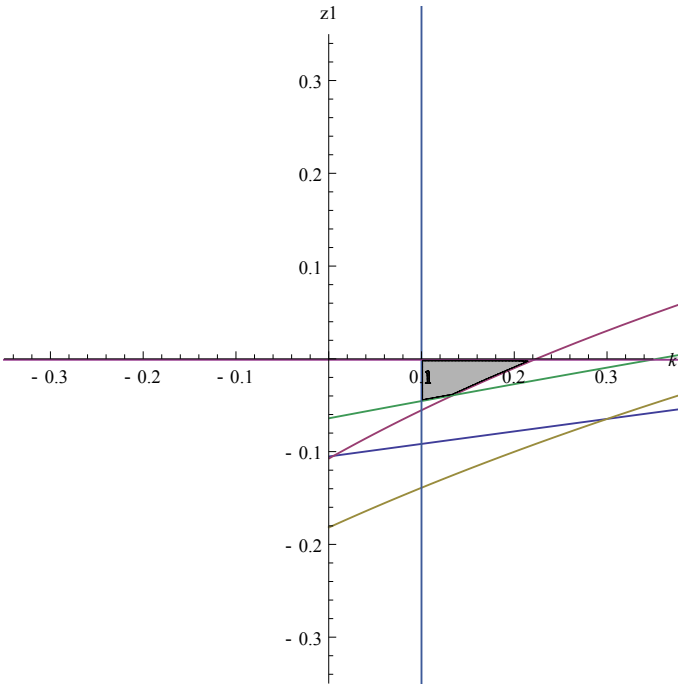

Figure 9.12: The *restricted allowed zone* (grey) for $p_1 = -5$ Hz.

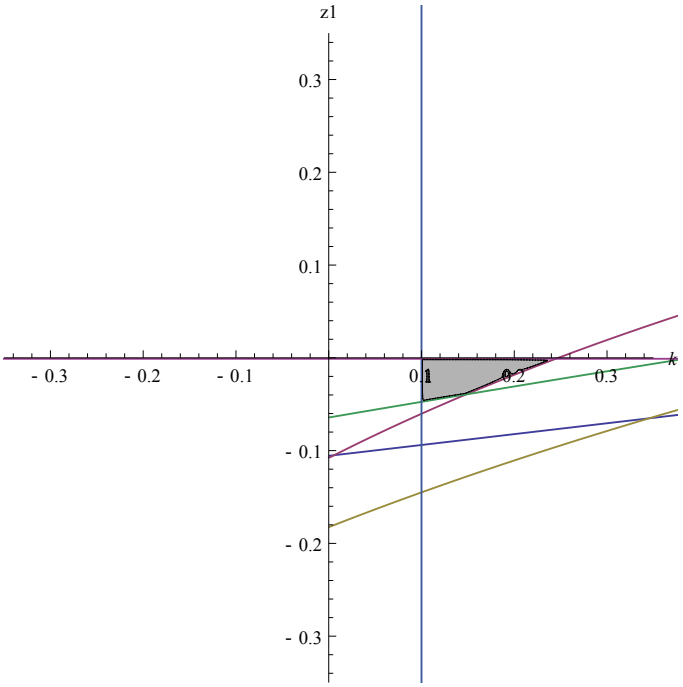

Figure 9.13: The *restricted allowed zone* (grey) for $p_1 = -6$ Hz.

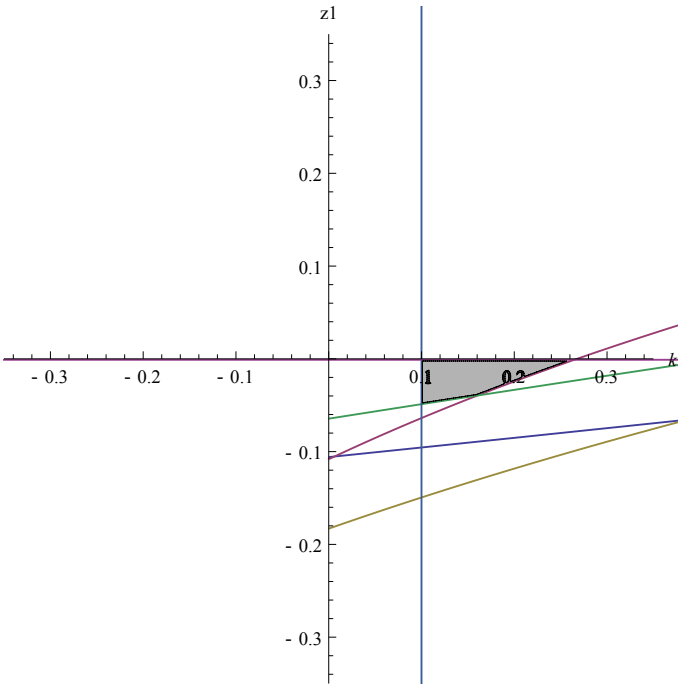

Figure 9.14: The *restricted allowed zone* (grey) for $p_1 = -7$ Hz.

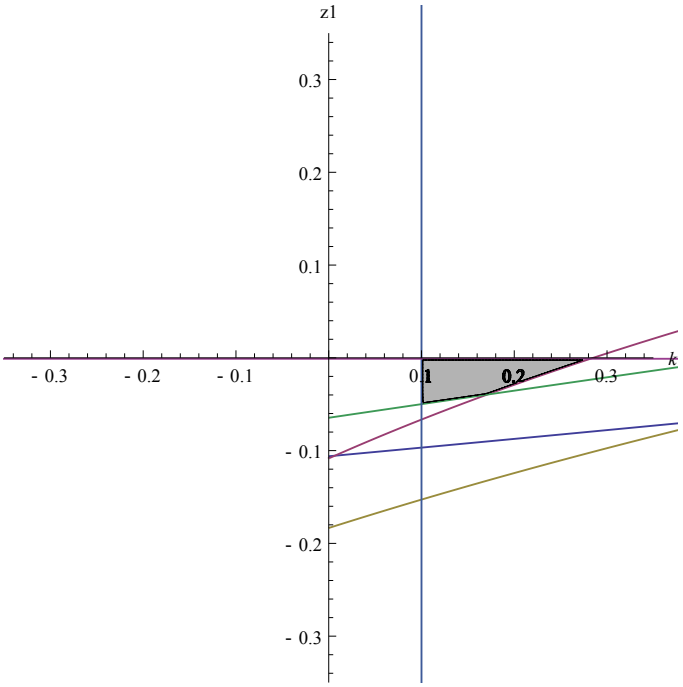

Figure 9.15: The *restricted allowed zone* (grey) for $p_1 = -8$ Hz.

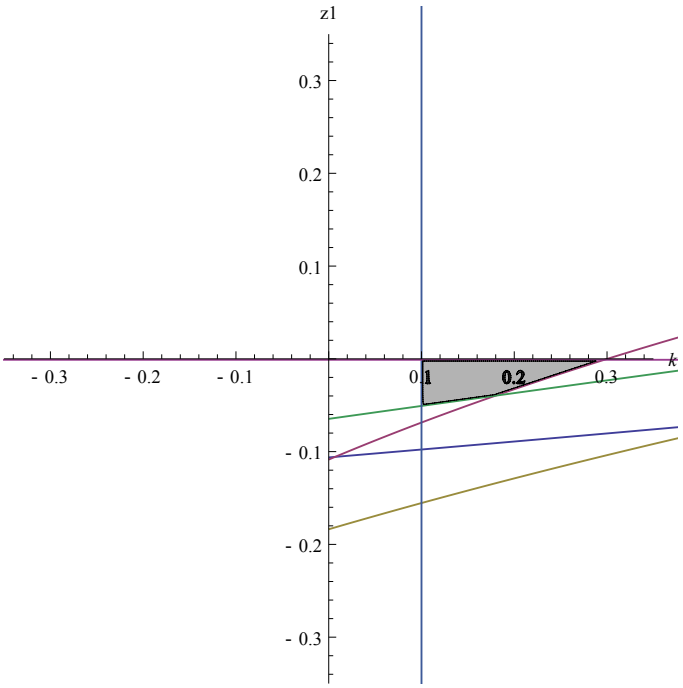

Figure 9.16: The *restricted allowed zone* (grey) for $p_1 = -9$ Hz.

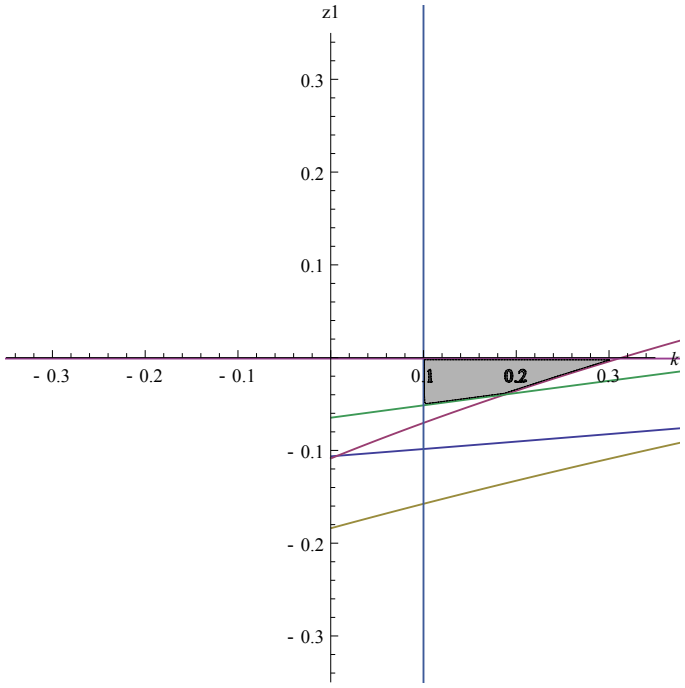

Figure 9.17: The *restricted allowed zone* (grey) for $p_1 = -10$ Hz.

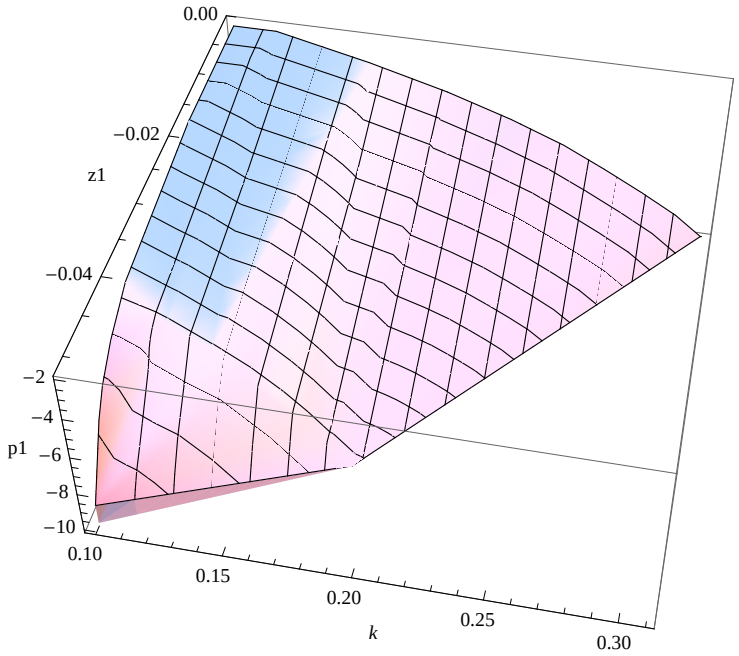

Figure 9.18: The allowed region

First of all, we need to define the order of the triplet that determines a point in the parameter space:

$$\{z_1, p_1, k\}\,. \tag{9.129}$$

Let us recall the APE requirement:

$$APE \leq 0.1\ ^\circ. \tag{9.130}$$

For the sake of brevity we will present only seven characteristics points. The results of the simulations are summarized in table 9.1. The parameters are, if not specified:

$$MoI = 400\ \text{kgm}^2 \tag{9.131}$$

$$\tau = \frac{3}{10}\ \text{s} \tag{9.132}$$

$$d = \frac{5}{100}\ \text{Nm} \tag{9.133}$$

As you can see, varying the uncertain parameters, the APE requirement is always largely satisfied. When the point is chosen on the boundary of the allowed region the requirement is still satisfied.

9.4.4 Remarks

Results fit perfectly with the theory. In fact, considering that we have heavily overestimated the amplitude constraint, the allowed region is smaller than the real one. Therefore, the amplitude constraint is largely satisfied also on the boundary.

These results demonstrate also that the approach is robust.

Point	**Description of the point**	A_θ [rad]	A_θ [°]
$\{-0.015, -7, 0.12\}$	In the middle of the allowed region	$1.24 \cdot 10^{-5}$	$7.10 \cdot 10^{-4}$
$\{-0.015, -7, 0.12\}$	In the middle of the allowed region, $MoI = 350$ km^2	$1.42 \cdot 10^{-5}$	$8.14 \cdot 10^{-4}$
$\{-0.015, -7, 0.12\}$	In the middle of the allowed region, $\tau = \frac{3}{10}$ s	$4.84 \cdot 10^{-5}$	$2.80 \cdot 10^{-3}$
$\{-0.015, -7, 0.12\}$	In the middle of the allowed region, $d = \frac{3}{100}$ Nm	$1.16 \cdot 10^{-5}$	$6.65 \cdot 10^{-4}$
$\{-0.037, -10, 0.18\}$	On the boundary of the allowed zone	$6.42 \cdot 10^{-5}$	$3.7 \cdot 10^{-3}$
$\{-0.25, -7, 0.12\}$	Out of the allowed zone because of z_1	unstable	unstable
$\{-0.015, -0.1, 0.12\}$	Out of the allowed zone because of p_1	$1.99 \cdot 10^{-2}$	1.14

Table 9.1: Results of the simulations on the five characteristic points.

Chapter 10

Conclusions

Satellites, especially in the lower atmosphere, are subjected to slowly varying attitude disturbances. Throughout the last decades, the use of switching actuators to control spacecrafts attitude has increased. These actuators are typically sets of on-off thrusters with switching constraints, such as hydrazine, cold-gas and pulse plasma thrusters.

The first part of this thesis studies the attitude behavior of a spacecraft with on-off actuators subjected to slowly varying disturbances controlled by a lead network. This system is intrinsically nonlinear and discrete. It always operates in limit cycle conditions. A general, useful and easy way to study these systems is the *describing function* theory. This technique takes into account the nonlinearity neglecting the discrete nature of the system. This approximation can be done if the bandwidth of the system is ten times smaller than the frequency of the slowest of the discrete blocks. In the ordinary linear systems this is not a problem because the bandwidth can be manipulated by changing the gain of the controller. In our system the gain controls the amplitude of the limit cycle instead of the bandwidth because of the nonlinearity. Therefore, in order manipulate the bandwidth, a lag network shall be added to the controller. The *classical describing function* theory can not take care of disturbances. Therefore the *dual-input describing function* has been adapted to our system. The results of this study has shown that two kinds of limit cycles can occur:

- *Saturation limit cycles.* They are very expensive due to the typical counteracting behavior of the sets of thrusters. Fortunately they can be avoided.
- *Disturbance limit cycles.* They are intrinsic of the on-off actuators therefore they can not be avoided. Luckily the fuel consumption is strictly related to the disturbance and there is no counteracting behavior.

In order to validate the theory, simulations on a reference scenario have been performed. These tests have underlined that, if the disturbance is not around half of the saturation of the command, high order harmonics arise. In this case the characteristics of the signal become dependent on the initial conditions, the motion becomes quasi-periodic or completely chaotic. The *filtering hypothesis* and *dual-input describing function* theory are no more valid.

The second part of the thesis provides a design method of the controller that shall meet some requirements:

- Robustness.
- APE, the Absolute Pointing Error.
- Bandwidth constraints.

The *Kharitonov approach* has been studied in detail. The robustness of the controller is ensured by the *Kharitonov's theorem* which is widely used by this technique. Unfortunately its classical version does not take into account disturbances or the discrete nature of the system. Thus, its generalization, the *dual-input Kharitonov approach*, have been developed. First of all the lag network is chosen to approximate the system as continuous and to satisfy bandwidth constraints. After that, using the APE requirement, the *Kharitonov's theorem* and the *dual-input describing function* theory, is created an allowed region in the parameter space. This is the zone where the parameters of the lead network shall be chosen to satisfy requirements. Tests have been performed to validate this method. These simulations have underlined that the requirements are largely satisfied and that the allowed region is heavily underestimated. This happens because of the robustness of the controller.

In the end some considerations about these systems shall be stressed.

The actuators are intrinsically nonlinear. If the controller is well designed, the system can be constrained in a *disturbance limit cycle* where the actuators counter just the slowly varying disturbance. This kind of limit cycles have no counteracting behavior, therefore, the fuel consumption is already minimized.

If the disturbance is not around half of the saturation of the command the behavior of the system becomes quasi-periodic-like or chaotic. In these cases tests have shown that the fuel consumption remains strictly related to the disturbance, instead, the frequency and the amplitude of the limit cycles vary. In particular the amplitude can be greater than the APE requirement. Therefore, the saturation of the actuators shall be around twice the disturbance expected.

Typically, these systems use sun sensors to evaluate attitude. These sensors are slower than the actuators. This means that the system is intrinsically discrete and can not be approximated as continuous. In order to apply the *describing function* a lag network shall be added albeit it is noxious for the control of the system. In fact it degrades performances introducing an harmful delay.

A next step in this research is to develop a *discrete describing function* theory for discrete systems. It would make useless the lag network and increase system performances.

Appendix A

Determination of the describing functions N_b and N_{sw}

In this appendix we will derive the $N_b(b, A)$ and $N_{sw}(b, A)$ *dual-input describing functions* stated respectively in equations 5.22 and 5.38.

Let us consider the system shown in figure 2.2. The *filtering hypothesis* allow the approximation of the output of the nonlinear block with the FOURIER transform arrested to the third term as described in 5.1. By definition:

$$N_b(b, A) \triangleq \frac{\mathcal{L}\left\{\frac{a_0}{2}\right\}}{\mathcal{L}\{b\}} = \frac{a_0}{2b}, \tag{A.1}$$

$$N_{sw}(b, A) \triangleq \frac{\mathcal{L}\{b_1 \sin(\omega t)\}}{\mathcal{L}\{A \sin(\omega t)\}} = \frac{b_1}{A}. \tag{A.2}$$

Obviously the FOURIER coefficient a_1 is null because the nonlinear block is single-valued. Now the determination of the *describing functions* rely only on the disclosure of the FOURIER coefficients a_0 and b_1.

Let us consider the shape of the nonlinear block as a series of two simpler nonlinear blocks as shown in figure A.1.

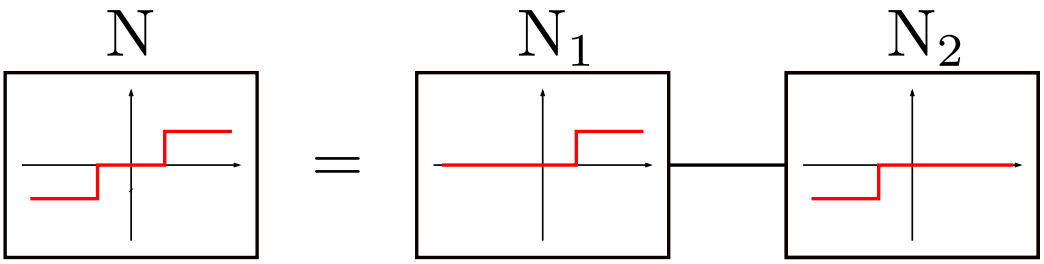

Figure A.1: Decomposition of the nonlinear block.

Considering that the FOURIER coefficients are integral results, the *describing functions* maintain the property of *linearity*[1] characteristic of the integrals. Thus the following equations hold:

$$N_b = N_{1b} + N_{2b}, \tag{A.3}$$
$$N_{sw} = N_{1sw} + N_{2sw}. \tag{A.4}$$

Let us, now, focus on the nonlinear block N_1. Consider the generic case shown in figure A.2.

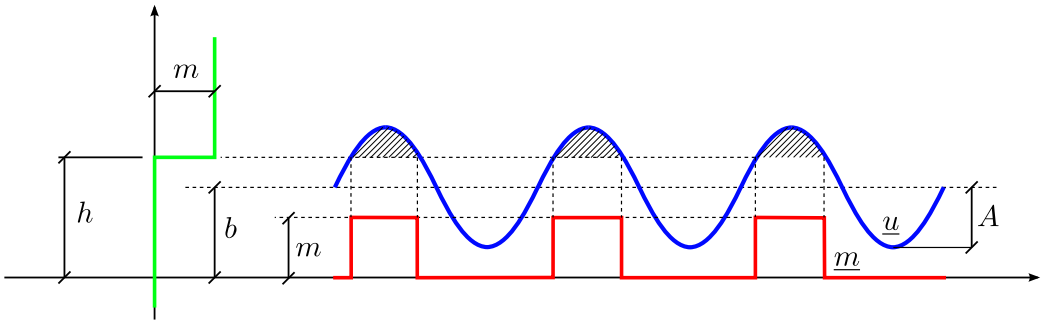

Figure A.2: Generic input and output of the nonlinear block N_1.

The output $\underline{m}$ is:

$$\underline{m} = \begin{cases} m & b - A > h \\ 0 & b + A < h \\ \begin{cases} m & \arcsin\left(\frac{h-b}{A}\right) < \omega t < \pi - \arcsin\left(\frac{h-b}{A}\right) \\ 0 & \text{otherwise} \end{cases} & \text{otherwise} \end{cases}. \tag{A.5}$$

By definition, the FOURIER coefficient a_0 is:

$$a_0 \triangleq \frac{1}{\pi} \int_{-\pi}^{\pi} \underline{m}\,(t)\ \mathrm{d}\,(\omega t) =$$
$$= \frac{1}{\pi} \begin{cases} 2\pi m & b - A > h \\ 0 & b + A < h \\ \int_{\arcsin\left(\frac{h-b}{A}\right)}^{\pi - \arcsin\left(\frac{h-b}{A}\right)} m\,\mathrm{d}\,(\omega t) = \left(\pi - 2\arcsin\left(\frac{h-b}{A}\right)\right) m & \text{otherwise} \end{cases}. \tag{A.6}$$

[1] This consideration is also stated in [10] and [20].

Thus:

$$N_{1b} = \frac{a_0}{2b} = \frac{m}{b} \begin{cases} 1 & b - A > h \\ 0 & b + A < h \\ \frac{1}{2} - \frac{1}{\pi} \arcsin\left(\frac{h-b}{A}\right) & \text{otherwise} \end{cases} . \tag{A.7}$$

Similarly, the *describing function* N_{2b} is:

$$N_{2b} = -\frac{m}{b} \begin{cases} 1 & b + A < -h \\ 0 & b - A < -h \\ \frac{1}{2} - \frac{1}{\pi} \arcsin\left(\frac{h+b}{A}\right) & \text{otherwise} \end{cases} . \tag{A.8}$$

Finally, by evaluating A.3 and manipulating the result, N_b becomes:

$$N_b = N_{1b} + N_{2b} = \frac{m}{b} \left[p\left(\frac{h+b}{A}\right) - p\left(\frac{h-b}{A}\right) \right] \tag{A.9}$$

where:

$$p(x) = \begin{cases} -\frac{1}{2} & x < -1 \\ \frac{1}{\pi} \arcsin(x) & |x| \leq 1 \\ \frac{1}{2} & x > 1 \end{cases} . \tag{A.10}$$

Let us now focus on the *describing function* N_{sw}. Following the same method used to derive N_b, the FOURIER coefficient b_1 for the nonlinear block N_{1sw} is:

$$\begin{aligned} b_1 &\triangleq \frac{1}{\pi} \int_{-\pi}^{\pi} \underline{m}(t) \sin(\omega t) \, \mathrm{d}(\omega t) = \\ &= \frac{m}{\pi} \begin{cases} 0 & b - A > h \\ 0 & b + A < h \\ \int_{\arcsin\left(\frac{h-b}{A}\right)}^{\pi - \arcsin\left(\frac{h-b}{A}\right)} m \sin(\omega t) \, \mathrm{d}(\omega t) = 2\sqrt{1 - \left(\frac{h-b}{A}\right)^2} & \text{otherwise} \end{cases} . \end{aligned} \tag{A.11}$$

Thus:

$$N_{1sw} = \frac{b_1}{A} = \frac{m}{A} \begin{cases} 0 & b - A > h \\ 0 & b + A < h \\ \frac{2}{\pi} \sqrt{1 - \left(\frac{h-b}{A}\right)^2} & \text{otherwise} \end{cases} . \tag{A.12}$$

Similarly to what has been done in A.8:

$$N_{2sw} = \frac{m}{A} \begin{cases} 0 & b + A < -h \\ 0 & b - A > -h \\ \frac{2}{\pi}\sqrt{1 - \left(\frac{h+b}{A}\right)^2} & \text{otherwise} \end{cases}. \tag{A.13}$$

In the end the *describing function* N_{sw}, by adding these two blocks and manipulating the result, becomes:

$$N_{sw}(b, A) = N_{1sw} + N_{2sw} = \frac{m}{A}\left[q\left(\frac{h+b}{A}\right) + q\left(\frac{h-b}{A}\right)\right] \tag{A.14}$$

where:

$$q(x) = \begin{cases} \frac{2}{\pi}\sqrt{1 - x^2} & |x| \leq 1 \\ 0 & |x| > 1 \end{cases}. \tag{A.15}$$

□

Appendix B

Kharitonov's theorem

The demonstration of the *Kharitonov's theorem* is akin to that in [8]. It is restricted to polynomials with real coefficients and positive frequency. Therefore, as we stated before, the eight *vertex polynomials* of the general case are reduced to the first four B.1. We have chosen this restricted demonstration because the proof of the general theorem is substantially the same of the restricted one, just more laborious, and because, for our specific case, we need only the restricted version of the theorem. The general demonstration of the theorem can be found in [7] and in [8].

Theorem 2 (Kharitonov's theorem)**.** *A complex coefficient interval polynomial family* Γ *with invariant degree is robustly stable if and only if the following eight* vertex polynomials *or* Kharitonov's polynomials *are stable. The first four polynomials,*

$$\begin{aligned}
K_1^+(s) &= \left(r_0^- + jq_0^-\right) + \left(r_1^- + jq_1^+\right)s + \left(r_2^+ + jq_2^+\right)s^2 + \left(r_3^+ + jq_3^-\right)s^3 + \cdots, \\
K_2^+(s) &= \left(r_0^+ + jq_0^+\right) + \left(r_1^+ + jq_1^-\right)s + \left(r_2^- + jq_2^-\right)s^2 + \left(r_3^- + jq_3^+\right)s^3 + \cdots, \\
K_3^+(s) &= \left(r_0^+ + jq_0^-\right) + \left(r_1^- + jq_1^-\right)s + \left(r_2^- + jq_2^+\right)s^2 + \left(r_3^+ + jq_3^+\right)s^3 + \cdots, \\
K_4^+(s) &= \left(r_0^- + jq_0^+\right) + \left(r_1^+ + jq_1^+\right)s + \left(r_2^+ + jq_2^-\right)s^2 + \left(r_3^- + jq_3^-\right)s^3 + \cdots,
\end{aligned} \tag{B.1}$$

are associated with positive ω^+*, and the second four polynomials,*

$$\begin{aligned}
K_1^-(s) &= \left(r_0^- + jq_0^-\right) + \left(r_1^+ + jq_1^-\right)s + \left(r_2^+ + jq_2^+\right)s^2 + \left(r_3^- + jq_3^+\right)s^3 + \cdots, \\
K_2^-(s) &= \left(r_0^+ + jq_0^+\right) + \left(r_1^- + jq_1^+\right)s + \left(r_2^- + jq_2^-\right)s^2 + \left(r_3^+ + jq_3^-\right)s^3 + \cdots, \\
K_3^-(s) &= \left(r_0^+ + jq_0^-\right) + \left(r_1^+ + jq_1^+\right)s + \left(r_2^- + jq_2^+\right)s^2 + \left(r_3^- + jq_3^-\right)s^3 + \cdots, \\
K_4^-(s) &= \left(r_0^- + jq_0^+\right) + \left(r_1^- + jq_1^-\right)s + \left(r_2^+ + jq_2^-\right)s^2 + \left(r_3^+ + jq_3^+\right)s^3 + \cdots,
\end{aligned} \tag{B.2}$$

are associated with negative ω^-.

Proof. In order to proof the *Kharitonov's theorem* we shall first enunciate the *Introductory lemma* and propose and discuss the *Kharitonov's plane*. Before giving it we need to define some useful notations.

Let $r(\cdot)$ be a generic polynomial:

$$r(s) \triangleq r_0 + r_1 s^1 + r_2 s^2 + r_3 s^3 + r_4 s^4 + r_5 s^5 \cdots . \tag{B.3}$$

We will denote by $r_{even}(\cdot)$ the even part of $r(\cdot)$, and by $r_{odd}(\cdot)$ its odd part, that are:

$$r_{even}(s) \triangleq r_0 + r_2 s^2 + r_4 s^4 + \cdots , \tag{B.4}$$

$$r_{odd}(s) \triangleq r_1 s + r_3 s^3 + r_5 s^5 + \cdots . \tag{B.5}$$

We will also denote:

$$r^e(\omega) \triangleq r_{even}(j\omega) = r_0 - r_2\omega^2 + r_4\omega^4 + \cdots , \tag{B.6}$$

$$r^o(\omega) \triangleq \frac{r_{odd}(j\omega)}{j\omega} = r_1 - r_3 w^2 + r_5 w^4 + \cdots . \tag{B.7}$$

Now, we can state the *introductory lemma.*

Lemma 1 (Introductory lemma)**.** *Let $r_1(\cdot)$ and $r_2(\cdot)$ be two arbitrary polynomials (not necessarily stable). Then λ such that:*

$$\exists \lambda \in [0,1], \overline{\omega} > 0 \,|\, (1-\lambda) r_1(j\overline{\omega}) + \lambda r_2(j\overline{\omega}) = 0 \Leftrightarrow \begin{cases} r_1^e(\overline{\omega}) r_2^o(\overline{\omega}) = r_2^e(\overline{\omega}) r_1^o(\overline{\omega}) \\ r_1^e(\overline{\omega}) r_2^e(\overline{\omega}) \leq 0 \\ r_1^o(\overline{\omega}) r_2^o(\overline{\omega}) \leq 0 \end{cases} . \tag{B.8}$$

Proof. Suppose first that:

$$\exists \lambda \in (0,1), \overline{\omega} > 0 \,|\, (1-\lambda) r_1(j\overline{\omega}) + \lambda r_2(j\overline{\omega}) = 0. \tag{B.9}$$

We can write:

$$r_i(j\overline{\omega}) = r_{i,even}(j\overline{\omega}) + r_{i,odd}(j\overline{\omega}) = r_i^e(\overline{\omega}) + j\overline{\omega} r_i^o(\overline{\omega}) \tag{B.10}$$

Thus, taking equation B.10 and the fact that $\overline{\omega}$ shall be positive into account, B.9 is equivalent to the set of equations:

$$\begin{cases} (1-\lambda)\, r_1^e(\overline{\omega}) + \lambda r_2^e(\overline{\omega}) & = 0 \\ (1-\lambda)\, r_1^o(\overline{\omega}) + \lambda r_2^o(\overline{\omega}) & = 0 \end{cases}. \tag{B.11}$$

But, if the system B.11 holds, then necessarily:

$$r_1^e(\overline{\omega})\, r_2^o(\overline{\omega}) = r_2^e(\overline{\omega})\, r_1^o(\overline{\omega}). \tag{B.12}$$

Since λ and $1-\lambda$ are both nonnegative, the set of equations B.11 also implies that:

$$r_1^e(\overline{\omega})\, r_2^e(\overline{\omega}) \leq 0, \tag{B.13}$$
$$r_1^o(\overline{\omega})\, r_2^o(\overline{\omega}) \leq 0 \tag{B.14}$$

and therefore equation B.12 and inequalities B.13 and B.14 prove that our condition is necessary.

For the converse, there are the following two cases:

- Suppose that:

$$r_1^e(\overline{\omega})\, r_2^o(\overline{\omega}) = r_2^e(\overline{\omega})\, r_1^o(\overline{\omega}), \tag{B.15}$$
$$r_1^e(\overline{\omega})\, r_2^e(\overline{\omega}) \leq 0, \tag{B.16}$$
$$r_1^o(\overline{\omega})\, r_2^o(\overline{\omega}) \leq 0, \tag{B.17}$$

  but that we do not have:

$$r_1^e(\overline{\omega}) = r_2^e(\overline{\omega}) = 0, \tag{B.18}$$

  then:

$$\lambda = \frac{r_1^e(\overline{\omega})}{r_1^e(\overline{\omega}) - r_2^e(\overline{\omega})} \tag{B.19}$$

  satisfies the system B.11 and can be easily checked that:

$$\lambda \in [0,1]. \tag{B.20}$$

- Suppose now that:

$$r_1^e(\overline{\omega})\, r_2^o(\overline{\omega}) = r_2^e(\overline{\omega})\, r_1^o(\overline{\omega}), \tag{B.21}$$
$$r_1^e(\overline{\omega}) = r_2^e(\overline{\omega}) = 0. \tag{B.22}$$

  Then we are left with:

$$r_1^o(\overline{\omega})\, r_2^o(\overline{\omega}) \leq 0. \tag{B.23}$$

  Here again, there are two cases.

– If we do not have:

$$r_1^o(\overline{\omega}) = r_2^o(\overline{\omega}) = 0, \tag{B.24}$$

then the following value of λ satisfies the system B.11:

$$\lambda = \frac{r_1^o(\overline{\omega})}{r_1^o(\overline{\omega}) - r_2^o(\overline{\omega})}. \tag{B.25}$$

– If:

$$r_1^o(\overline{\omega}) = r_2^o(\overline{\omega}) = 0, \tag{B.26}$$

then from B.21 and B.22 we conclude that:

$$\lambda = 0 \text{ or } 1 \tag{B.27}$$

satisfy the set of equations B.11.

□

Let us now consider the family $\mathcal{K}$ of polynomials:

$$r(s) = r_0 + r_1 s + \cdots + r_n s^n \tag{B.28}$$

Let us denote:

$$\underline{r} = \{r_0, r_1, \cdots, r_n\}. \tag{B.29}$$

Obviously, it is 0-based. Thus it is:

$$\underline{r} \in \mathbb{R}^{n+1} \tag{B.30}$$

where every term belongs to:

$$\begin{aligned} r_0 &\in \left[r_0^-, r_0^+\right], \\ r_1 &\in \left[r_1^-, r_1^+\right], \\ &\vdots \\ r_n &\in \left[r_n^-, r_n^+\right]. \end{aligned} \tag{B.31}$$

In the sequel we completely identify the vector space of real polynomials of degree less than or equal to n with $\mathbb{R}^{n+1}$. As a consequence we will indifferently talk about a polynomial of degree n as in B.29 or about an $(n+1)$-tuple as in B.30.

The *Kharitonov's polynomials* are built from two different even parts $K_{even,min}(s)$ and $K_{even,max}(s)$ and two different odd parts $K_{odd,min}(s)$ and $K_{odd,max}(s)$ defined as:

$$K_{even,min}(s) \triangleq r_0^- + r_2^+ s^2 + r_4^- s^4 + r_6^+ s^6 + r_8^- s^8 + \cdots, \tag{B.32}$$
$$K_{even,max}(s) \triangleq r_0^+ + r_2^- s^2 + r_4^+ s^4 + r_6^- s^6 + r_8^+ s^8 + \cdots, \tag{B.33}$$
$$K_{odd,min}(s) \triangleq r_1^- s + r_3^+ s^3 + r_5^- s^5 + r_7^+ s^7 + r_9^- s^9 + \cdots, \tag{B.34}$$
$$K_{odd,max}(s) \triangleq r_1^+ s + r_3^- s^3 + r_5^+ s^5 + r_7^- s^7 + r_9^+ s^9 + \cdots. \tag{B.35}$$

We have:

$$\begin{aligned} K_1(s) &= K_{even,min}(s) + K_{odd,min}(s), \\ K_2(s) &= K_{even,min}(s) + K_{odd,max}(s), \\ K_3(s) &= K_{even,max}(s) + K_{odd,min}(s), \\ K_4(s) &= K_{even,max}(s) + K_{odd,max}(s). \end{aligned} \tag{B.36}$$

The reason for the subscripts *min* and *max* is that for every polynomial in $\mathcal{K}$, for definition,

$$K_{even,min}(j\omega) = K_{min}^e(j\omega) \leq r^e(\omega) \leq K_{max}^e(j\omega) = K_{even,max}(j\omega), \tag{B.37}$$
$$\frac{K_{odd,min}(j\omega)}{j\omega} = K_{min}^o(j\omega) \leq r^o(\omega) \leq K_{max}^o(j\omega) = \frac{K_{odd,max}(j\omega)}{j\omega}. \tag{B.38}$$

The equations B.37 and B.38 are true if $\overline{\omega}$ is strictly positive.

Considering that:

$$K_4(s) = K_2(s) + K_3(s) - K_1(s), \tag{B.39}$$

there is a unique affine plane passing through the four *Kharitonov's polynomials*. We now define the *Kharitonov's plane* as the intersection of $\mathcal{K}$ with this affine plane.

An example is shown in figure B.1, and it can be defined analytically as the set of all polynomials of the form:

$$(1-\lambda) K_{even,min}(s) + \lambda K_{even,max}(s) + (1-\mu) K_{odd,min}(s) + \mu K_{odd,max}(s) \tag{B.40}$$

where:

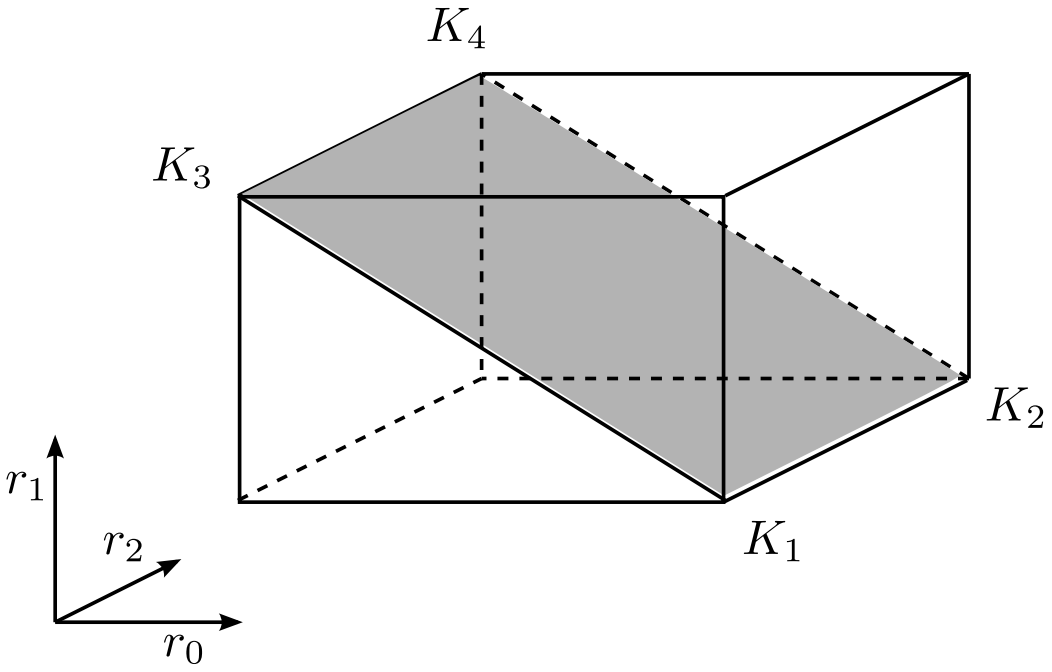

Figure B.1: *Kharitonov's plane* with $n = 2$.

$$\{\lambda, \mu\} \in [0, 1]\,. \tag{B.41}$$

Equivalently, the *Kharitonov's plane* can be defined as the set of all convex combinations of the four *Kharitonov's polynomials*.

Now let us prove that if an instability appears in the family of polynomials $\mathcal{K}$, then an instability must also appear in the Kharitonov plane.

Lemma 2 (Kharitonov's plane lemma)**.** *Suppose that there exists a polynomial in $\mathcal{K}$ with an unstable root, then there must also be an unstable polynomial in the* Kharitonov's plane*.*

Proof. There are two cases.

- Assume that $\mathcal{K}$ contains only unstable polynomials. In this case the *Kharitonov's plane* is also entirely unstable since it is included in $\mathcal{K}$.

- Suppose, on the contrary, that $\mathcal{K}$ contains at least one stable polynomial. In this case, due to the *continuity property* of the polynomials which is precisely explained in [7] or [11], there also exists a polynomial in $\mathcal{K}$ with a root at the origin or a pure imaginary root $j\overline{\omega}$ with $\overline{\omega}$ positive. The case of a polynomial having a root at the origin is easily taken into account because in this case we would necessarily have:

$$r_0^- \leq 0 \leq r_0^+ \tag{B.42}$$

and we could write for a precise value λ:

$$(1-\lambda)\, r_0^- + \lambda \leq r_0^+ = 0 \tag{B.43}$$

or equivalently:

$$(1-\lambda)\, K_{even,min}(0) + \lambda K_{even,max}(0) = 0 \tag{B.44}$$

Therefore, for this particular value of λ and for any value of μ, the polynomial

$$(1-\lambda)\, K_{even,min}(s) + \lambda K_{even,max}(s) + (1-\mu)\, K_{odd,min}(s) + \mu K_{odd,max}(s) \tag{B.45}$$

which indeed belongs to the *Kharitonov's plane* is also unstable.

Now, assume that a polynomial $p(\cdot)$ has a pure imaginary root $j\overline{\omega}$ where $\overline{\omega}$ is positive. This means that:

$$p^e(\overline{\omega}) = 0, \tag{B.46}$$
$$p^o(\overline{\omega}) = 0. \tag{B.47}$$

Let us define

$$p_1(s) = K_{even,min} + p_{odd}(s), \tag{B.48}$$
$$p_2(s) = K_{even,max} + p_{odd}(s). \tag{B.49}$$

Then, obviously,

$$p_1^e(\overline{\omega})\, p_2^o(\overline{\omega}) - p_2^e(\overline{\omega})\, p_1^o(\overline{\omega}) = p^o(\overline{\omega})\left[p_1^e(\overline{\omega}) - p_2^e(\overline{\omega})\right]. \tag{B.50}$$

and moreover, since B.46 we have by B.37:

$$p_1^e(\overline{\omega}) = K_{min}^e(\overline{\omega}) \leq 0 \leq K_{max}^e(\overline{\omega}) = p_2^e(\overline{\omega}). \tag{B.51}$$

Then, necessarily:

$$p_1^e(\overline{\omega})\, p_2^e(\overline{\omega}) \leq 0 \tag{B.52}$$

and since

$$p_1^0(\overline{\omega})\, p_2^0(\overline{\omega}) = [p^o(\overline{\omega})]^2 = 0, \tag{B.53}$$

we can, with B.50, apply the *introductory lemma* and conclude that there must necessarily be a real λ for which

$$p_\lambda(s) = p_{\lambda,even}(s) + p_{odd}(s) \tag{B.54}$$

where:

$$p_{\lambda,even}(s) = (1-\lambda) K_{even,min}(s) + \lambda K_{even,max}(s) \tag{B.55}$$

has $j\overline{\omega}$ as a root.

Starting now with $p_\lambda(s)$. we could carry out exactly the same reasoning and define:

$$p_{\lambda,1}(s) = p_{\lambda,even}(s) + K_{odd,min}(s), \tag{B.56}$$
$$p_{\lambda,2}(s) = p_{\lambda,even}(s) + K_{odd,max}(s). \tag{B.57}$$

We would then conclude to the existence of a real μ such that

$$\begin{aligned} p_{\lambda\mu}(s) = &[(1-\lambda) K_{even,min}(s) + \lambda K_{even,max}(s)] + \\ &+ [(1-\mu) K_{odd,min}(s) + \mu K_{odd,max}(s)] \end{aligned} \tag{B.58}$$

has $j\overline{\omega}$ among its roots. But $p_{\lambda\mu}(s)$ is clearly of the form B.40 and therefore belongs to the *Kharitonov's plane*.

□

In order to demonstrate the *Kharitonov's theorem* we will use an *auxiliary lemma* which has been proved, for example, in [4] as well as in [5] and says the following.

Lemma 3 (Auxiliary lemma)**.** *Let $r_1(s)$ and $r_2(s)$ be two stable polynomials having the same even part $r_{even}(s)$. Then:*

$$\lambda r_1(s) + (1-\lambda) r_2(s), \quad \forall \lambda \in [0,1]. \tag{B.59}$$

The same result is true, of course, if $r_1(s)$ and $r_2(s)$ have the same odd part.

We mention here as an aside, that this lemma (and consequently, the *Kharitonov's theorem*) can be proved without making use of the *Hermite-Bieler theorem*[1], but this is only of pure mathematical interest.

Let us now suppose that the four Kharitonov polynomials are stable.

Then we can apply three times the *auxiliary lemma* to the equations B.36. $K_1(s)$ and $K_2(s)$ are stable and therefore for any μ the polynomial

$$K_{even,min}(s) + [(1-\mu) K_{odd,min}(s) + \mu K_{odd,max}(s)] \tag{B.60}$$

is stable. Likewise $K_2(s)$ and $K_3(s)$ being stable, for any μ the polynomial

$$K_{even,max}(s) + [(1-\mu) K_{odd,min}(s) + \mu K_{odd,max}(s)] \tag{B.61}$$

is stable. Now fix any arbitrary value μ, the two polynomials in B.60 and B.61 are stable, and therefore for any λ the polynomial

$$\begin{aligned} &[(1-\lambda) K_{even,min}(s) + \lambda K_{even,max}(s)] + \\ &+ [(1-\mu) K_{odd,min}(s) + \mu K_{odd,max}(s)] \end{aligned} \tag{B.62}$$

is stable. Thus, since μ was arbitrary, the polynomial in B.62 is stable for any couple of values

$$\{\lambda, \mu\} \in [0,1] \times [0,1], \tag{B.63}$$

that is, the entire *Kharitonov's plane* is stable. Considering now the *Kharitonov's plane lemma* we can conclude immediatly that every polynomial in $\mathcal{K}$ has to be stable.

□

[1] See, for example, [4].

Bibliography

[1] Alligood, K. T., Sauer, T. D., Yorke, J. a., and Crawford, J. D. Chaos: An Introduction to Dynamical Systems. *Physics Today 50*, 11 (1997), 67.

[2] Avanzini, G. Bifurcation analysis of attitude dynamics in rigid spacecraft with switching control logics. *Journal of Guidance, Control, and Dynamics 24*, 5 (2001).

[3] Bergen, A. A note on Tsypkin's locus. *Automatic Control, IRE Transactions on*, 2 (1962), 78–80.

[4] Bia\las, S., and Garloff, J. Convex combinations of stable polynomials. *Journal of the Franklin Institute 319*, 3 (1985), 373–377.

[5] Bose, N. K. A system-theoretic approach to stability of sets of polynomials. *Contemporary mathematics 47* (1985), 25–34.

[6] Burton, R. L. Pulsed Plasma Thrusters. *Encyclopedia of Aerospace Engineering* (1998).

[7] Chapellat, H. *Geometric conditions for robust stability.* PhD thesis, Texas A & M University, 1987.

[8] Chapellat, H. An alternative proof of Kharitonov's theorem. *Automatic Control, IEEE 67*, 0 (1989), 448–450.

[9] Han, K. W. *Nonlinear control systems: some practical methods.* Academic Cultural Co., 1977.

[10] Landi, A. Lezioni di controllo di processi, 2008.

[11] Marden, M. *The geometry of the zeros of a polynomial in a complex variable.* American Mathematical Society, 1949.

[12] Mendel, J. Performance cost functions for a reaction-jet-controlled system during an on-off limit cycle. *Automatic Control, IEEE Transactions on*, 4 (1968), 362–368.

[13] Mendel, J. On-off limit-cycle controllers for reaction-jet-controlled systems. *Automatic Control, IEEE Transactions on x*, 3 (1970).

[14] Mesquita, A. Persistent motion and chaos in attitude control with switching actuators. *World Congress* (2005), 2–6.

[15] Mesquita, A. R., Kienitz, K. H., and Rempel, E. L. Robust limit cycle control in an attitude control system with switching-constrained actuators. *2008 47th IEEE Conference on Decision and Control* (2008), 1605–1610.

[16] Oliveira, N. Attitude controller design for a system using actuators with switching-time restrictions and delays. *Proceedings AIAA Guidance, Navigation, and*, August (2000), 4–12.

[17] Orrell, D. Visualizing bifurcations in high dimensional systems: the spectral bifurcation diagram. *INTERNATIONAL JOURNAL OF BIFURCATION AND* (2003), 24–29.

[18] Slotine, J., and Li, W. *Applied nonlinear control*. Prentice-Hall Englewood Cliffs, NJ, 1991.

[19] Tsypkin, I. *Relay control systems*. Cambridge Univ Pr, 1984.

[20] Velde, W. V. *Multiple-input describing functions and nonlinear system design*. New York: McGraw-Hill, 1968.